DEVELOPMENT OF PREDICTION MODELS FOR SKID RESISTANCE OF ASPHALT PAVEMENTS

A Thesis

Presented in Partial Fulfillment of the Requirements for the

Degree of Master of Science

with a

Major in Civil Engineering

in the

College of Graduate Studies

University of Idaho

by

Sand Aldagari

Major Professor: Emad Kassem, Ph.D.

Committee Members: Ahmed Abdel-Rahim, Ph.D.; Fouad Bayomy, Ph.D.

Department Administrator: Patricia J. S. Colberg, Ph.D.

January 2017

AUTHORIZATION TO SUBMIT THESIS

This thesis of Sand Aldagari, submitted for the degree of Master of Science with a major in Civil Engineering and titled "Development of Prediction Models for Skid Resistance of Asphalt Pavements" has been reviewed in final form. Permission, as indicated by the signatures and dates given below, is now granted to submit final copies to the College of Graduate Studies for Approval.

Major Professor: _____Date_____
Emad Kassem, Ph.D.

Committee Members: _____Date_____
Ahmed Abdel-Rahim, Ph.D.

_____ Date_____
Fouad Bayomy, Ph.D.

Department Administrator: _____ Date_____
Patricia Colberg, Ph.D.

ABSTRACT

Pavement skid resistance is one of the primary factors in highway safety. Pavements with adequate skid resistance reduce the number of crashes in wet conditions. The friction between pavement surface and vehicle tires is related to the macrotexture and microtexture of pavement surface. The macrotexture of asphalt pavement is dependent on aggregate gradation, while the microtexture is dependent on aggregate shape characteristics. Aggregates with angular shape and rough texture provide higher level of skid resistance compared to aggregates with smooth surface. In addition, pavement surfaces with high macrotexture provide higher skid resistance compared to those with low macrotexture. There were two main objectives of this study. The first object was to investigate and examine the surface and friction characteristics of various test sections of asphalt mixtures as well as seal coat surfaces. The test sections included different asphalt mixture types (e.g., dense graded, stone matrix asphalt, porous friction course), seal coat grades (Grade 1, Grade 2, and Grade 3), aggregate types (e.g., limestone, gravel, granite, sandstone), and the test sections were located in regions with different environmental conditions. The second objective was to develop a predictive model for skid resistance of seal coat surfaces and validate and revise an existing skid prediction model for asphalt pavements.

Field testing primarily included measurements of coefficient of friction using a dynamic friction tester, pavement surface texture using a circular texture meter, and skid number using a skid trailer. The measurements were conducted on the outer lane where pavement surfaces experience significant polishing rates because most of the trucks use that lane. The resistance of aggregate to polishing and abrasion was studied using laboratory test methods.

Several analytical models were developed to predict the friction and skid resistance of asphalt pavements and seal coat surfaces over their service life. These models incorporate parameters that describe aggregate resistance to abrasion and polishing, aggregate shape characteristics, aggregate gradation, and traffic level. These models were developed based on comprehensive field testing and aggregate laboratory characterization. Good correlations were found between the developed models and experimental data. The results demonstrated that aggregate and surface characteristics as well as traffic level have significant effect on skid resistance and rate of skid reduction. These models can be used during the mix design procedure to optimize the aggregate selection and aggregate gradation to produce mixtures with proper friction. In addition, these models can be incorporated in a Project Management System (PMS) at the network level to plan and program preventive maintenance activities to ensure that pavements have adequate skid resistance.

ACKNOWLEDGEMETS

In the name of God the most merciful, the most compassionate.

I would like to express my deepest gratitude and appreciation to my advisor, Dr. Emad Kassem, who has offered me a great opportunity to pursue my master's degree at the University of Idaho. I would not be able to finish this thesis without all his support, guidance, patience, and encouragement.

I would also like to thank my committee members: Dr. Ahmed Abdel-Rahim and Dr. Fouad Bayomy for their guidance, support and feedback throughout this study. I acknowledge the support and assistance from Dr. Arif Chowdhury of Texas A&M Transportation Institute for providing test data and guidance during the data analyses. I also would like to thank my colleague Mohammad Al-Assi for his help and guidance. I am thankful to Texas Department of Transportation (TxDOT) for sponsoring this research study which was executed by the Texas A&M Transportation Institute.

TABLE OF CONTENTS

AUTHORIZATION TO SUBMIT THESIS ii

ABSTRACT iii

ACKNOWLEDGEMETS v

TABLE OF CONTENTS vi

LIST OF TABLES ix

LIST OF FIGURES x

CHAPTER 1 - INTRODUCTION 1

1.1 Background 1

1.2 Problem Statement 2

1.3 Objectives 3

1.4 Research Tasks 4

1.5 Thesis Organization 6

CHAPTER 2 - LITERATURE REVIEW 7

2.1 Introduction 7

2.2 Definition of Skid Resistance 7

2.3 Pavement Surface Characteristics 8

2.4 Effects of Pavement Surface Characteristics on Skid Resistance 10

2.5 Asphalt Seal Coat Treatment 12

2.6 Aggregates Properties Affecting Pavement Friction 13

Hardness and Mineralogy 13

Polish Resistance 13

Abrasion Resistance 13

Angularity, Texture and Form 14

Soundness 15

2.7 Friction/Skid Resistance Measuring Devices 15

Locked Wheel Skid Trailer 15

Side Force Devices 16

Fixed Slip Devices 17
Variable Slip Devices 18
Dynamic Friction Tester 19
2.8 The International Friction Index (IFI) 19
2.9 Pavement Texture Measurements 20
CTMeter Device 20
Sand Patch Method 21
Stereo Photogrammetric Technique 22
2.10 Aggregate Resistance to Polishing 23
2.11 Effect of Pavement Deterioration on the Skid Resistance 24
2.12 Developing Skid Resistance Models 25
Masad et al. (2007) model 25
Masad et al. (2011) model 28
Zhong et al. (2012) model 34
Kassem et al. (2013) model 34
2.13 Summary 38
CHAPTER 3 – FIELD AND LABORATORY TESTING 39
3.1 Selection of the Field Sections 39
3.2 Frictional Characteristic Measurements 43
3.3 Aggregate Characterization 50
3.4 Aggregate Gradation Parameters 53
3.5 Skid Number Measurements 54
3.6 Summary 55
CHAPTER 4 - DATA ANALYSIS AND RESULTS FOR HOT MIX ASPHALT TEST SECTIONS 57
4.1 Analysis of Aggregate Gradation 57
4.2 Analysis of Aggregate Texture and Angularity 58
4.3 Development of Predictive Model for IFI 67
4.4 Analysis of Mean Profile Depth (MPD) 70
4.5 Skid Number Analysis 71

4.6 HMA Skid Resistance Model Sensitivity Analysis 74
Effect of Mixture Gradation 74
Effect of Traffic Level 75
Effect of Aggregate Type 76
4.7 SUMMARY 77
CHAPTER 5 - DATA ANALYSIS AND RESULTS FOR SEALCOAT TEST SECTIONS 79
5.1 Analysis of Aggregate Gradation 79
5.2 Analysis of Aggregate Texture and Angularity 80
5.3 Development Predictive Model for IFI for Seal Coat 87
5.4 Analysis of Mean Profile Depth (MPD) 89
5.5 Skid Number Analysis 90
5.6 Seal Coat Skid Resistance Model Sensitivity Analysis 93
Effect of Seal Coat Size 93
Effect of Traffic Level 94
Effect of Aggregate Type 94
5.7 SUMMARY 95
CHAPTER 6 – CONCLUSIONS AND RECOMMENDATIONS 96
6.1 Conclusions 96
6.2 Recommendations 97
References 99
Appendix A - Hot Mix Asphalt (HMA) 106
Appendix B – Sealcoat 118

LIST OF TABLES

Table 2-1 Classification of Pavement Texture (Henry 2000) 8

Table 2-2 Aggregate Texture Regression Coefficients 27

Table 3-1 HMA Test Sections 40

Table 3-2 Selected Sections for Seal Coat 42

Table 3-3 Aggregate Classification based on the SN 54

Table 4-1 Scale and Shape Parameters of the Weibull Distribution 60

Table 4-2 Regression Parameters of Aggregate Texture and Angularity 66

Table 4-3 Traffic Groups Based on TMF 73

Table 5-1 Scale and Shape Parameters of the Weibull Distribution 80

Table 5-2 Regression Parameters of Aggregate Texture and Angularity 86

Table 5-3 Traffic Groups Based on TMF 92

LIST OF FIGURES

Figure 2-1 Friction Force and Surface Characteristics (Noyce et al. 2005) 7

Figure 2-2 Schematic of Microtexture and Macrotexture (Henry 2000) 9

Figure 2-3 Key Mechanisms of Tire-pavement Friction (Hall et al. 2009) 10

Figure 2-4 Change in Pavement Friction with Speed (after Hogervorst 1974) 11

Figure 2-5 Effect of Microtexture/Macrotexture on Pavement Friction (Hall et al. 2006) 12

Figure 2-6 AIMS Aggregate shape characteristics 14

Figure 2-7 Locked-Wheel Skid Trailer 16

Figure 2-8 Side Force Device (Hall et al. 2009) 17

Figure 2-9 Fixed Slip Device (Gerthoffert et al. 2015) 18

Figure 2-10 Variable Slip Friction Testing Device (Gerthoffert et al. 2015) 18

Figure 2-11 Dynamic Friction Tester 19

Figure 2-12 CTMeter Device 21

Figure 2-13 Sand Patch Method (Sarsam et al. 2015) 22

Figure 2-14 3D Pavement Surface from Stereo Photogrammetric Technique (Mushairry et al. 2004) 23

Figure 2-15 AIMS texture index versus time in the Micro-Deval test 26

Figure 2-16 Laboratory Experiments in the TxDOT (Masad et al. 2011) 29

Figure 2-17 Aggregate Texture before and after Micro-Deval and Percent Change (Masad et al. 2011) 30

Figure 2-18 An example of IFI vs. polishing cycles (Kassem et al. 2013) 31

Figure 2-19 Steps Needed to Predict Skid Number SAAP in the TxDOT Project No.0-5627 33

Figure 2-20 Test Slabs Preparation and polishing (Kassem et al. 2013) 35

Figure 2-21 Texture Index and Weight Loss Results (Kassem et al. 2013) 36

Figure 2-22 AIMS System (Kassem et al. 2013) 36

Figure 2-23 Texture Index and Weight Loss Results (Kassem et al. 2013) 37

Figure 3-1 Layout of Measurement Section 44

Figure 3-2 Collecting Field Measurements 44

Figure 3-3 DFT Measurements for Seal Coat Test Section (IH-35-LRD-NP-COT-S_SealCoat) 45

Figure 3-4 DFT Measurements for Type-D Asphalt Mix Test Section (SH-36-HMA_TypeD) 45

Figure 3-5 Correlation between Mean Profile Depth (MPD) and Coefficient of Friction at 80 km/hr (DFT_{80}) for Seal Coat Test Sections 46

Figure 3-6 Correlation between IFI and Coefficient of Friction at 80 km/hr (DFT_{80}) for Seal Coat Test Sections 47

Figure 3-7 Correlation between Mean Profile Depth (MPD) and Coefficient of Friction at 80 km/hr (DFT80) for Hot Mix Asphalt Test Sections 47

Figure 3-8 Correlation between IFI and DFT80 for Hot Mix Asphalt Test Sections 48

Figure 3-9 Correlation between IFI and DFT80 for Hot Mix Asphalt and Seal Coat Test Sections and Pavement Surface Condition for Seal Coat Test Sections 49

Figure 3-10 Correlation between IFI and DFT80 for Hot Mix Asphalt and Seal Coat Test Sections and Pavement Surface Condition for Asphalt Mixture Test Sections 50

Figure 3-11 Procedure for Measuring Aggregate Texture and its Resistance to Polishing 52

Figure 3-12 Loss in Aggregate Texture and Angularity as a Result of Micro-Deval Abrasion and Polishing of Virgin Aggregates 53
Figure 3-13 Locked-Wheel Skid Trailer 55
Figure 4-1 Flow Chart of the Research Methodology 58
Figure 4-2 Weibull Distribution Function for Different Aggregate Sizes 61
Figure 4-3 Texture Indices of Sections in San Antonio 61
Figure 4-4 Angularity Indices of Sections in San Antonio 62
Figure 4-5 Regression Constants for Aggregate Texture 62
Figure 4-6 Regression Constants for Aggregate Angularity 63
Figure 4-7 Relationship between Predicted and Measured IFI 70
Figure 4-8 Relationship between Measured and Calculated MPD Values 71
Figure 4-9 Relationship between the measured and predicted SN 73
Figure 4-10 Measured Skid Numbers in terms of Traffic Level 74
Figure 4-11 Effect of Mixture Gradation on the Skid Number 75
Figure 4-12 Effect of AADT on the Skid Number 76
Figure 4-13 Effect of Aggregate Texture on the Skid Number 77
Figure 5-1 Weibull Distribution Function for Different Aggregate Sizes 80
Figure 5-2 Texture Indices of Sections in Odessa 82
Figure 5-3 Angularity Indices of Sections in Odessa 82
Figure 5-4 Regression Constants for Aggregate Texture 83
Figure 5-5 Regression Constants for Aggregate Angularity 83
Figure 5-6 Relationship between Predicted and Measured IFI 88
Figure 5-7 Relationship between Measured and Calculated MPD Values 90

Figure 5-8 Relationship between Measured and Predicted SN 91

Figure 5-9 Measured Skid Numbers at different Traffic Level 92

Figure 5-10 Effect of Seal Coat Aggregate Size on the Skid Number 93

Figure 5-11 Effect of AADT on the Skid Number 94

Figure 5-12 Effect of Aggregate Texture on the Skid Number 95

CHAPTER 1 - INTRODUCTION

1.1 Background

Traffic-related accidents are detrimental to U.S. economy. The National Highway Traffic Safety Administration (NHTSA 2004) indicated that the total cost due to traffic crashes was estimated at $242 billion in 2014. Traffic-related accidents occur due to three major factors including road conditions, driver behavior, and vehicle factors (Noyce et al. 2005). More than 6 million traffic collisions occurred in the United States, and the number of fatalities was 32,675, in addition to 2.338 million traffic-related injuries occurred in 2014 (NHTSA 2014). Previous research showed that 15 to 18 percent of total crashes occurred on wet pavements (Smith 1977; FHWA 1990). The crashes on wet pavements are related to inadequate pavement skid resistance leading to skidding of vehicles. Henry and Wambold (1992) found that good correlation between skid number and wet-pavement crashes when tested with smooth tires. The number of wet-pavement accidents can be greatly reduced by conducting frequent skid measurements in order to ensure an adequate level of skid resistance of pavements (Rizenbergs et al. 1972).

The friction between pavement surface and vehicle tires is related to the macrotexture and microtexture of pavement surface. The macrotexture of asphalt pavement is dependent on aggregate gradation, while the microtexture is dependent on aggregate shape characteristics (Masad et al. 2011; Kassem et al. 2012 and 2013). Aggregates with angular shape and rough texture provide higher level of skid resistance compared to aggregates with smooth surface (Kassem et al. 2012 and 2013). In addition, pavement surfaces with high macrotexture provide higher skid resistance compared to those with low macrotexture (Masad et al. 2011; Kassem et al. 2012 and 2013).

Henry (1986) studied the effect of vehicle speed on pavement friction. The results showed that skid resistance decreases with speed. Aggregates are polished with frequent traffic applications. Some aggregates become smoother than others resulting in low skid resistance. Shafii (2009) discussed the effect of rubber temperature on skid resistance of asphalt pavement. The results showed that the skid resistance decreases as the temperature of the rubber increases. Other factors that affect skid resistance including pavement surface grooving and bleeding. The skid resistance decreases with bleeding of asphalt binders on the surface (Sullivan 2005), while it is improved with surface grooving (Pasindu et al. 2010).

There are several studies attempted to develop prediction models for skid resistance of asphalt pavements. Ahammed and Tighe (2007) developed procedures to estimate skid resistance of concrete pavements as a function of concrete compressive strength, traffic level, and pavement texture. Kowalski (2007) developed a laboratory testing procedure to characterize pavement friction by determining the polishing rate and terminal friction value. Researchers at Texas A&M University developed prediction models for skid resistance of asphalt pavement (Masad et al. 2011; Kassem et al. 2012 and 2013). These models describe the skid resistance of asphalt pavements as a function of aggregate characteristics, mixture gradation, and traffic level. There is a need to validate and further develop these models with a wide range of pavement surface characteristics, aggregate properties, and traffic levels and environmental conditions.

1.2 Problem Statement

Pavement skid resistance is primarily a function of the surface texture, which includes both microtexture and macrotexture. Macrotexture is an overall asphalt mixture characteristic, which provides surface drainage paths for water to drain from the contact area

between the tire and pavement. Microtexture is primarily an aggregate surface characteristic that provides a rough surface which in turn disrupts the continuity of the water film and produces frictional resistance between the tire and pavement by creating intermolecular bonds. In the TxDOT research project 0-5627, the researchers (Masad et al. 2011) developed a method to predict asphalt pavement skid resistance based on inputs that describe aggregate texture before and after polishing, gradation of asphalt mixture, and traffic levels. This research study further validated the skid resistance prediction model for HMA at a wide range of conditions including asphalt mixture and aggregate types. In addition, this study developed a prediction model for skid resistance of seal coat surfaces.

Texas Department of Transportation sponsored a follow-up study 0-6746 at Texas A&M Transportation Institute to further investigate the results from previous research study 0-5627. The later study was undertaken to validate the previously developed prediction model for HMA surface and develop a new model for surface treated pavements. Dr. Arif Chowdhury served as principal investigator and Dr. Emad Kassem served as Co-PI on the research project 0-6746.

1.3 Objectives

The objective of this study were to:

1. Investigate and examine surface and friction characteristics of about 35 test sections of asphalt mixtures and 35 test sections of surface treated roads in Texas. The test sections covered a wide range of mixtures and aggregate types used in Texas.
2. Validate and revise the skid prediction model for HMA and develop a prediction model for skid resistance of seal coat surfaces.

1.4 Research Tasks

The above objectives were achieved by conducting the following tasks:

Task 1: Conduct literature search

A literature search was conducted to develop an up-to-date documentation of the following topics:

- Pavement surface characteristics that affect skid resistance
- Methods used to measure macrotexture and microtexture of asphalt pavements
- Test methods used to measure pavement friction
- Methods used to measure aggregate resistance to abrasion and polishing
- Attempts to predict friction or skid resistance of flexible pavements

Task 2: Design of experiment and selection of field test sections

The objective of Task 2 was to develop an experimental design to validate and revise the existing skid model for HMA pavements and expand the existing model or develop a new skid model for seal coat surfaces. Under this task, the researchers selected HMA and seal coat test sections for field testing. These test sections covered a wide range of asphalt mixture types, seal coat sizes, aggregate sources, traffic levels and environmental conditions.

Task 3: Conduct field and laboratory testing

Under this task, the measurements of pavement macrotexture and microtexture were collected on the selected sections using the circular texture meter (CTMeter) and dynamic friction tester (DFT). Also, the skid number was measured using a skid trailer. In the laboratory, the aggregate texture and angularity was quantified at different time durations of

polishing in the Micro-Deval test using the aggregate image measurement system (AIMS). Additionally, the information about the mix design of HMA and seal coat size was obtained.

Task 4: Refinement and validation of skid prediction model for HMA

Under this task, the skid prediction model for HMA developed by Masad et al. (2011) was revised to accommodate a wide range of conditions. The skid prediction model describes the skid resistance of asphalt pavements as a function of aggregate characteristics, mixture gradation, and traffic level. The aggregate texture and angularity were quantified using AIMS and parameters were developed to describe the resistance of aggregates to abrasion and polishing. Also parameters were developed to describe aggregate gradation. Statistical methods were used to develop a prediction model for skid number and the predicted values were compared to the measured ones in the field.

Task 5: Develop a skid prediction model for seal coat surfaces

Under this task, a skid prediction model was developed for seal coat surfaces. The skid resistance of seal coat depends on the same parameters as that of HMA including aggregate size, aggregate shape characteristics (angularity and texture), and traffic level. Three seal coat grades (Grade 3, Grade 4, and Grade 5) were used and examined in the seal coat test sections. Each grade stands for different aggregate size with Grade 3 being the coarsest. Similar to HMA, parameters were developed to describe aggregate shape characteristics and its resistance to abrasion and polishing. In addition, analytical tools were used to describe the macrotexture of the seal coat test sections. Statistical methods were used to develop a prediction skid model for skid number of seal coat and the predicted skid values were compared to the measured ones in the field.

Task 6: Documentation of findings

This task provided documentation of research efforts, results, and recommendations of this study.

1.5 Thesis Organization

Chapter 1 provides an introduction and background of the research project including: problem statement and objectives, research tasks, and thesis organization. Chapter 2 provides a literature review on the skid resistance including factors affecting skid resistance, pavement frictional surface characteristics, test methods used to measure pavement friction, previous attempts to predict friction or skid resistance of flexible pavements. Chapter 3 discusses the research plan and describes various tests conducted in the field and laboratory. Chapter 4 presents the model development of skid resistance of HMA based on the collected data from the field and laboratory. Chapter 5 presents the model development of skid resistance of seal coat surfaces. Finally, Chapter 6 summarizes the main findings of this study and provides recommendations for future studies. Appendices document the laboratory and field test results.

CHAPTER 2 - LITERATURE REVIEW

2.1 Introduction

Skid resistance is a key component in road safety. Skid resistance depends on several factors including pavement surface characteristics, tire material properties, environmental conditions. Several laboratory and field methods are used to characterize the parameters that affect skid resistance of asphalt pavements and determine skid level in the field (Kennedy et al. 1990). These methods and parameters are discussed in this section.

2.2 Definition of Skid Resistance

Pavement friction is the force that resists the relative motion between a vehicle tire and pavement surface. Skid resistance is an essential factor that prevents vehicles from sliding and reduces the stopping distance (Noyce et al. 2005). Figure 2-1 shows the friction force and the surface characteristics affecting skid resistance.

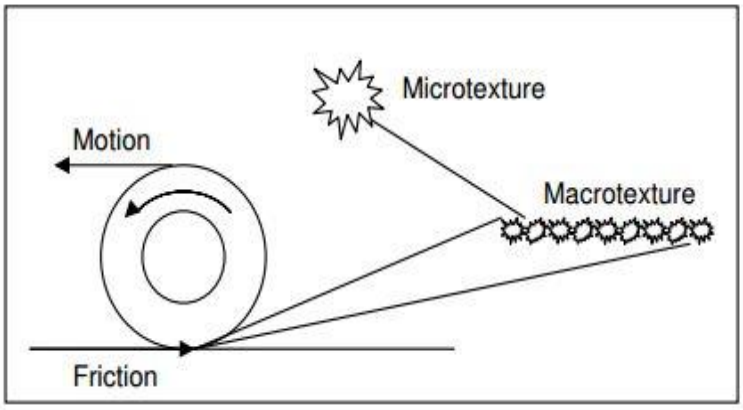

Figure 2-1 Friction Force and Surface Characteristics (Noyce et al. 2005)

Pavement skid resistance may slightly increase right after construction due to wearing of asphalt binders that coat the rocks at pavement surface. The skid decreases as the surface

aggregates get polished under traffic. The polishing action affects the microtexture and macrotexture of pavement surface (Flintsch et al. 2005; Forster 1989).

2.3 Pavement Surface Characteristics

Pavement texture and its friction is a key component of road safety (Mahone 1975). Skid resistance of asphalt pavements is affected by the macrotexture and microtexture of the pavement surface. In wet condition, water acts as a lubricant between the tires and pavement surface leading to reduced friction (Dahir 1979). Macrotexture of pavement is dependent on aggregate gradation, compaction level, and mixture design, while the microtexture is dependent on aggregate shape characteristics (Crouch et al. 1995). The texture is a property related to the surface that describes the interaction between the tires and pavement surface (Henry 2000). Texture is classified into several categories based on the wavelength as presented in Table 2-1.

Table 2-1 Classification of Pavement Texture (Henry 2000)

Texture Classification	Relative Wavelength
Microtexture	$\lambda < 0.5$ mm
Macrotexture	0.5 mm $< \lambda <$ 50 mm
Megatexture	50 mm $< \lambda <$ 500 mm
Roughness/Smoothness	500 mm $< \lambda <$ 50 m

Henry (2000) demonstrated the distinction between macrotexture and microtexture as shown in Figure 2-2. Macrotexture describes the irregularities of pavement surface. It is important in water drainage from pavement surface. In addition, it contributes to the hysteresis component of the friction (Dahir 1979). Pavement macrotexture is affected by the

nominal maximum aggregates size. Mixtures with nominal aggregate size of 9.5mm or 12.5mm provide a macrotexture below 0.5 mm (Wagner et al. 2004). Asphalt mixtures with coarse aggregate gradation usually have higher macrotexture compared with asphalt mixtures with fine aggregate gradation. Rough surface texture contributes to a high level of skid resistance; however, it may increase noise and vibration (Ivey et al. 1992). Microtexture is dependent on aggregate characteristics and contribute to skid resistance on both wet and dry conditions (Crouch et al. 1995; Dunford 2013; Flintsch et al. 2005).

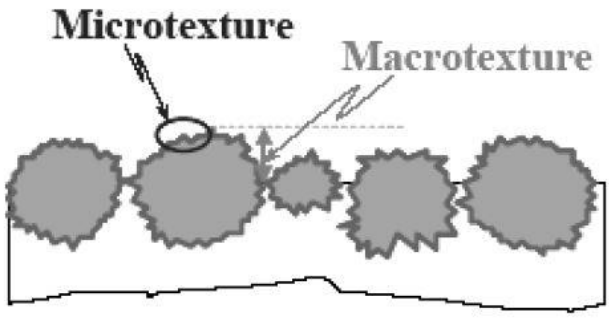

Figure 2-2 Schematic of Microtexture and Macrotexture (Henry 2000)

The megatexture is associated with the noise and rolling resistance and affected by pavement surface deformation such as potholes and ruts. The roughness is caused by the deformation due to traffic loading and has adverse effects on the ride and drainage quality (Dunford 2013). Megatexture and roughness adversely affect pavement ride quality while the macrotexture and microtexture are considered significant factors affecting skid resistance of asphalt pavements (Descornet 1989).

Skid resistance has two mechanisms; adhesion and hysteresis as shown in Figure 2-3. These two mechanisms are highly affected by pavement macrotexture and microtexture (Anupam et al. 2013). Adhesion is developed due to the direct contact between the tires and

pavement surface especially in areas with high local pressure (Cairney 1997). Pavement microtexture is significant to the adhesion component that originated from molecular bonds between stone and rubber. In addition, pavement macrotexture contributes to the hysteresis component of the friction (Ivey et al. 1992). Hysteresis is developed due to energy dissipation caused by the deformation of the tire rubber around bulges and depressions in the pavement surface (Cairney 1997).

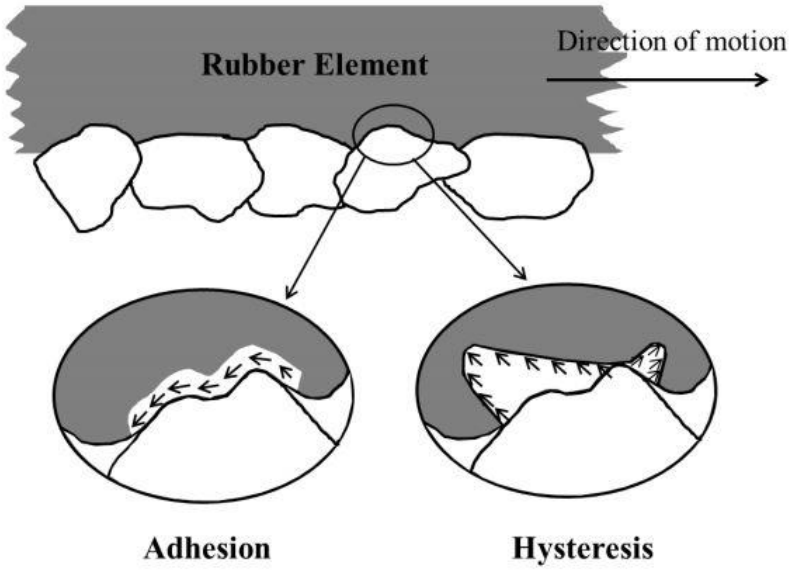

Figure 2-3 Key Mechanisms of Tire-pavement Friction (Hall et al. 2009)

2.4 Effects of Pavement Surface Characteristics on Skid Resistance

Adhesion and microtexture affect the skid resistance at all speeds, and they have prevalent influence at speeds below 30 mph. Hysteresis and macrotexture have little significance at low speeds; however, macrotexture is an essential factor for safety in wet conditions as speed increases (Galambos et al. 1977).

Hogervorst (1974) has shown that the reduction in skid resistance is associated with vehicle speed and it depends on pavement microtexture and macrotexture (Figure 2-4). The results showed that the skid resistance decreased with an increase in vehicle speed, and pavements with coarse and rough surface provided better skid resistance compared to the ones with fine and polished surface.

Road Surface		Surface Texture	
		macro	micro
A		coarse	rough
B		coarse	polished
C		fine	rough
D	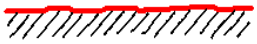	fine	polished

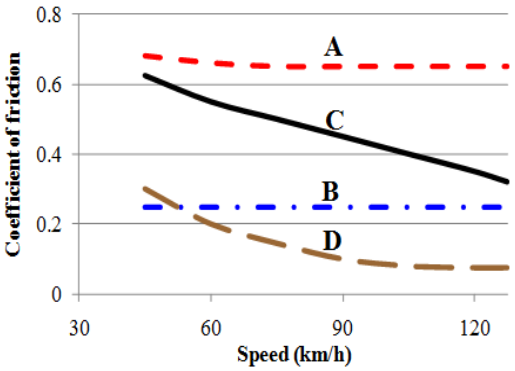

Figure 2-4 Change in Pavement Friction with Speed (after Hogervorst 1974)

Hall et al. (2009) indicated that microtexture locates the magnitude of skid resistance, while macrotexture controls the slope of the skid resistance reduction as the speed increases (Figure 2-5). Macrotexture affects the pavement friction at high speed by reducing the friction-speed slope, while it has little influence on friction at low speed. On the other hand, microtexture defines the level of friction (Hall et al., 2009; Rose and Gallaway, 1970; Gallaway et al., 1972).

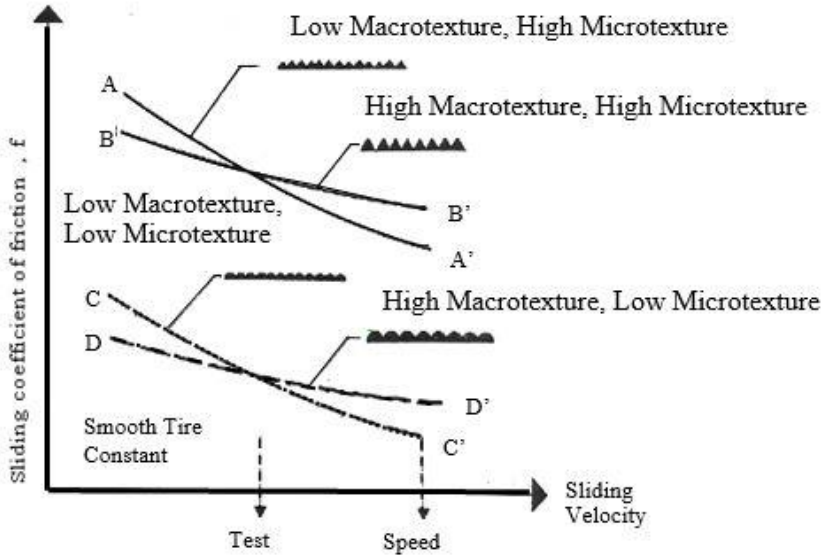

Figure 2-5 Effect of Microtexture/Macrotexture on Pavement Friction (Hall et al. 2006)

2.5 Asphalt Seal Coat Treatment

The seal coat or chip seal is widely used as preventive maintenance treatment and considered relatively inexpensive pavement surface treatment. It can be used effectively on roads with both high and low traffic levels (TxDOT 2003). Similar to hot mix asphalt (HMA) surfaces, the macrotexture and microtexture of seal coat surface have significant contributions to the skid resistance. The macrotexture of pavement surface is affected by the aggregate size and its embedment into the binder. Immoderate embedment may reduce the skid resistance of seal coat (Krugler 2012; Roque et al. 1991). In addition, aggregate polishing due to traffic reduces the skid resistance, and the rate of skid reduction depends on the aggregate shape characteristics (Masad et al. 2011; Razaei et al. 2011). The seal coat surface treatments (Grade 3 and Grade 4) provided higher skid resistance compared to asphalt concrete-surfaced pavements (Type C), but skid resistance of the surface treatments may decrease significantly once its macrotexture decreases (Masad et al. 2011).

2.6 Aggregates Properties Affecting Pavement Friction

This section discusses the aggregate properties that affect pavement friction.

Hardness and Mineralogy

The hardness of aggregate affects the aggregate resistance to wear and it can be measured using the hardness test. This test measures the resistance of aggregate surface to scratching on a scale from 1 to 10. Hardness values higher than 6 for hard minerals and 3 to 5 for soft minerals are recommended to ensure acceptable pavement frictional performance (Dahir et al. 1978).

Polish Resistance

This term refers to the ability of the aggregate to maintain its microtexture after subjected to repeated traffic loadings. The most common methods used to evaluate the polish resistance including polished stone value (PSV) and acid insoluble residue (AIR) (Hall et al. 2009). In PSV test, the aggregate is polished by accelerated polishing machine and then aggregate surface friction is measured using the British pendulum (Masad et al. 2007). The AIR test is performed to measure the noncarbonate ingredients of the aggregates, which contribute to aggregate resistance. Values of 30 to 35 for the PSV test, and 50 to 70% for the AIR test are recommended to ensure sufficient frictional resistance (Hall et al. 2009).

Abrasion Resistance

This terms refers to the ability of aggregate to resist mechanical degradation. The Micro-Deval and Los Angeles (LA) tests are used to evaluate the abrasion resistance of the aggregates (Hall et al. 2009). The Micro-Deval consists of a container with steel balls and the aggregate is polished with presence of water (Kassem et al. 2012). Also, the LA is used to

measure the coarse aggregate resistance to degradation by subjecting the aggregate in the LA machine (AASHTO T96). Values of percent losses less than 17 to 20 for the Micro-Deval test, and percent losses less than 35 to 45 for LA test are recommended to provide sufficient frictional resistance (Hall et al. 2009;).

Angularity, Texture and Form

Aggregate shape characteristics including angularity, texture, and form (Figure 2-6) are essential parameters in pavement skid resistance. The coarse and angular aggregates provide higher pavement friction compared to flat and elongated aggregates (Prowell et al. 2015). Also aggregate with rough surface provides higher friction compared to aggregate with smooth surface (Kassem et al. 2013). The AIMS is used to quantify aggregate shape characteristics (Masad et al. 2011). Also, there are other methods including laser-based aggregate analysis system, computer particle analyzer, multiple ratio shape analysis, VDG-40 Video grader that are used to perform the same function.

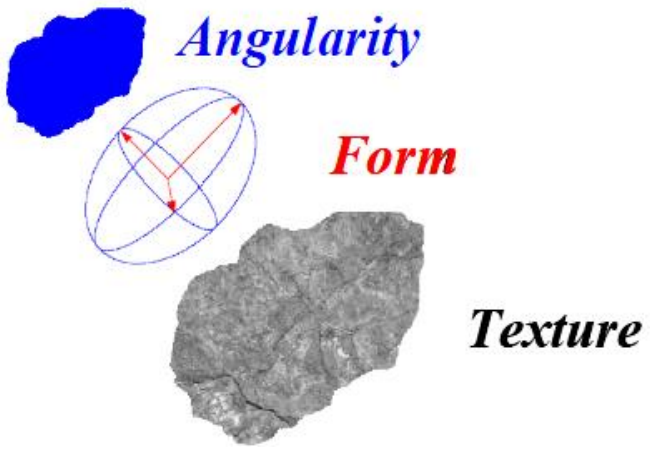

Figure 2-6 AIMS Aggregate shape characteristics

Soundness

Soundness of aggregates can be defined as the ability of aggregates to resist the degradation due to climatic and environmental factors such as thawing, freezing, wetting and drying. The soundness is quantified using the magnesium sulfate soundness test by quantifying the loss percentage of aggregate after cycles of hydration-dehydration. The loss percentages ranging from 10% to 20% are typical and provide sufficient frictional performance (Hall et al. 2009).

2.7 Friction/Skid Resistance Measuring Devices

There are several devices that are used to measure skid resistance in the field and some of them can be used in the field and laboratory. These devices rely on different measuring principles and some of them measure the peak friction while others measure values close to the peak friction (Henry 2000). This section discusses common devices used in measuring friction and skid resistance of pavements.

Locked Wheel Skid Trailer

The locked wheel is used to measure the pavement friction (Burchett et al. 1980). The coefficient of friction is measured by the locked wheel device and reported as a Skid Number (SN) (Gargett 1990). The SN is calculated using Eq. 2.1.

$$SN = (F / N) * 100 \quad (2.1)$$

where

SN = skid number

F = friction force

N = normal (vertical) load on the test tire

The skid trailer (Figure 2-7) is an appropriate method in terms of accuracy and safety. However, the data cannot be collected continuously in addition the skid trailer does not have the ability to measure the low friction accurately (Burchett et al. 1980). When using the skid trailer water is sprayed in front of the left wheel and the left wheel is locked while the truck is travelling at certain speed (e.g., 50 mph for Texas). The friction force that resists the rotation of the tire is measured (Masad et al. 2011).

Figure 2-7 Locked-Wheel Skid Trailer

Side Force Devices

Side force devices are used to measure the pavement side friction on runways and highways. Figure 2-8 shows an example of the side device. Similar to the skid trailer, a small amount of water is sprayed in front of the wheel, and the side force at 40 mph is recorded (Gargett 1990). The side force method is used to determine the ability of vehicles to maintain control especially in curves (Henry 2000).

Figure 2-8 Side Force Device (Hall et al. 2009)

Fixed Slip Devices

The fixed slip system is used to measure the friction between the tires and pavements, and anti-lock brakes are considered. Figure 2-9 shows a fixed slip device. This method is used essentially in the airport (Putov et al. 2016). The device can maintain at most 20 percent of firm slip, and the friction force between the surface and tire can be calculated after subjecting a vertical load to the tire. The preference of using the fixed slip device is that it can be operated continuously without excessive wear in the tires (Henry 2000).

Figure 2-9 Fixed Slip Device (Putov et al. 2016)

Variable Slip Devices

The variable slip device is another device that measures the frictional force when the tire is taken through a predetermined set of slip ratios (Figure 2-10). The result of dividing the longitudinal force by the vertical force is the slip friction number (SFN). The SFN is reported by using slip speeds between zero and the assigned speed (Henry 2000).

Figure 2-10 Variable Slip Friction Testing Device (Putov et al. 2016)

Dynamic Friction Tester

The dynamic Friction Tester (DFT) is used to measure the coefficient of friction. This device consists of a circular disk with three rubber pads (Figure 2-11). The circular disk rotates up to 100 km/hr. Once the disk reaches the specified speed, the disk is lowered to the pavement surface and the coefficient of friction is measured as the speed of the rotating disk gradually decreases (Saito et al. 1996 and Henry 1986). The pavement microtexture is quantified by the value of the coefficient of friction at 20 km/hr (DFT_{20}).

Figure 2-11 Dynamic Friction Tester

2.8 The International Friction Index (IFI)

The Permanent International Association of Road Congress (PIARC) developed a unified equation for the international friction index (IFI) to determine the surface friction of a pavement (PIARC 1995). It incorporates parameters that describe the microtexture and macrotexture of a pavement as presented in Eq. 2.2. The macrotexture is described by mean profile depth (MPD) measured by CTMeter while the microtexture is quantified by the coefficient of friction measured using DFT at 20 km/hr (DFT_{20}) (Wambold et al. 1995; Henry 2000).

$$IFI = 0.081 + 0.732 * DFT_{20} * \exp\left(\frac{-40}{S_p}\right) \quad (2.2)$$

$$S_p = 14.2 + 89.7MPD \quad (2.3)$$

where

IFI = international friction index

S_p= speed constant parameter

MPD = mean profile depth

2.9 Pavement Texture Measurements

There are several methods used for quantifying the macrotexture of asphalt pavements. These methods include the circular texture meter (CTMeter), sand patch method, outflow meter, in addition to laser-based (or electro-optic) technique (Hall et al. 2009).

CTMeter Device

This device is used to measure the mean profile depth (MPD) in the field and laboratory (Figure 2-12). This device has a charge-coupled device (CCD) laser displacement sensor attached to an arm mounted to the device. The arm rotates in a circle with a diameter of 28.4 cm. The laser sensor can collect about 1024 data points per round. The average MPD is calculated and reported according to ASTM E2157.

Figure 2-12 CTMeter Device

Sand Patch Method

The sand patch test is used to quantify the macrotexture of pavement surface by measuring the mean texture depth (MTD) in accordance with ASTM E1845. The sand patch method includes a brush for cleaning the surface, a cup and spreading tool to distribute the sand, and a scale tape (Figure 2-13). An amount of 100 grams of sand is used in each test. The sand sample should pass No.30 sieve and retained on No.50 sieve (Sarsam et al. 2015). The sand is spread in a circle on the pavement surface and the diameter of the circle is measured. The MTD is measured using Eq. 2.4 as a function of sand volume and diameter of sand patch (ASTM 2009).

$$MTD = \frac{4\ V}{3.14\ D^2} \qquad (2.4)$$

where

MTD: mean texture depth (mm).

D: average diameter of sand patch circle (cm)

V: sand volume (cm^3), (weight of sand / density of sand).

Figure 2-13 Sand Patch Method (Sarsam et al. 2015)

Stereo Photogrammetric Technique

This techniques is based on 3D measurement of pavement surface texture. The 3D images provide an indication of physical changes to pavement surface that cannot be accurately quantified using 2D profiles. The changes in the aggregate surface due to polishing process can be observed and quantified using the 3D measurements (Dunford 2013). Stereo photogrammetry relies on taking various images from different angles in order to estimate the 3D coordinates of a point. The close range photogrammetry is a version of stereo photogrammetry that has an ordinary camera to take various images from different angles to construct the 3D profile. Previous research demonstrated that this technique can be used to quantify the macrotexture, microtexture and megatexture (Mcquaid et al. 2014). Figure 2-14 shows the pavement 3D image obtained from stereo photogrammetric technique.

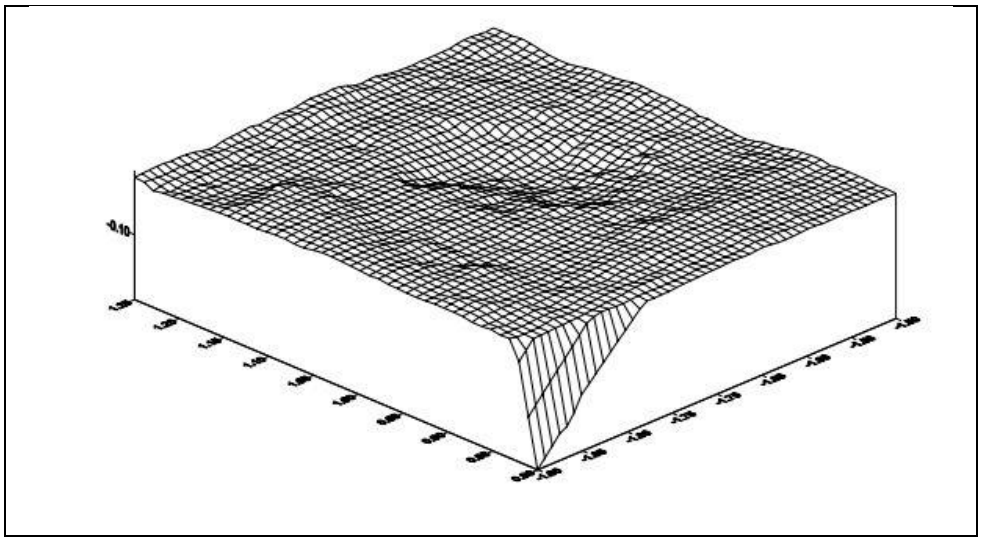

Figure 2-14 3D Pavement Surface from Stereo Photogrammetric Technique (Mushairry et al. 2004)

2.10 Aggregate Resistance to Polishing

Aggregates with good resistance to polishing retain their microtexture for a longer period of time compared to aggregates with poor resistance to polishing and abrasion. The LA is used to measure the coarse aggregate resistance to degradation (West et al. 2001; Fulop et al. 2000). Despite British pendulum test being widely used to predict the frictional properties of aggregates, the researchers indicated that this test has a high level of variability (Henry et al. 1979; Fwa et al. 2004).

The Micro-Deval polishing device was found to be a good alternative to the Los Angeles test (Prowell et al. 2005). The aggregates are typically polished in Micro-Deval for 105 min. and 180 min. (Al Rousan 2005). Another study (Mahmoud et al. 2007) recommended using the AIMS to measure the aggregate characteristics after subjecting the aggregates to polishing in the Micro-Deval test. Although there were some developments

regarding new tests, there was only slight progress in terms of developing models that can estimate the skid resistance of pavement (Mahmoud et al. 2007).

Polishing the pavement surface due to frequent traffic applications is the main cause of skid resistance reduction. Using aggregates with good resistance to polishing and abrasion provides pavements with higher friction (Kassem et al. 2013).

2.11 Effect of Pavement Deterioration on the Skid Resistance

Luis et al. (2010) conducted a study to evaluate the correlation between pavement roughness and skid resistance. A skid trailer was used to measure the skid number of different pavement test sections. These test sections were selected to have comparable surface characteristics in terms of macrotexture and microtexture but different levels of roughness. The analytical investigation demonstrated that sections with comparable surface characteristics but different roughness levels had different skid numbers. The researchers concluded that high level of roughness provides low skid numbers, in addition the roughness should be considered in pavement safety evaluation. Conversely, Fuentes (2009) studied the correlation between the international roughness index (IRI) and skid resistance and the results did not provide enough evidence on the effect of roughness on skid resistance.

The excessive binder in the mixture reduces the void content and causes bleeding. Bleeding is defined as excessive asphalt film on the road surface. The skid resistance decreases due to the loss of macrotexture and microtexture caused by bleeding and coating the aggregate particles with excessive asphalt binders. Surface treatments may increase the asphalt binder at the surface causing bleeding and hence reducing skid resistance (Kane et al. 2009).

2.12 Developing Skid Resistance Models

There are several attempts for developing prediction models for friction and skid resistance of asphalt pavements. This section discusses some of these attempts.

Masad et al. (2007) model

Masad et al. (2007) developed a new method to evaluate the change in the asphalt pavement skid resistance depending on aggregate texture, properties of mixtures, and environmental conditions. This method relies on the use Micro-Deval test and AIMS to evaluate the resistance of aggregate to polishing and abrasion. Aggregates retained on No. 4 sieve (4.75mm) were considered due to the significant effects of coarse aggregates on skid resistance compared to fine aggregates. The measurements of aggregate texture were obtained using AIMS at different time durations of polishing in the Micro-Deval (15, 30, 60, 75, 90, 105, and 180 min.) as shown in Figure 2-15. Figure 2-15 demonstrates the change in aggregate texture at three different levels (4, 5, and 6). Each level stands for different aggregate size.

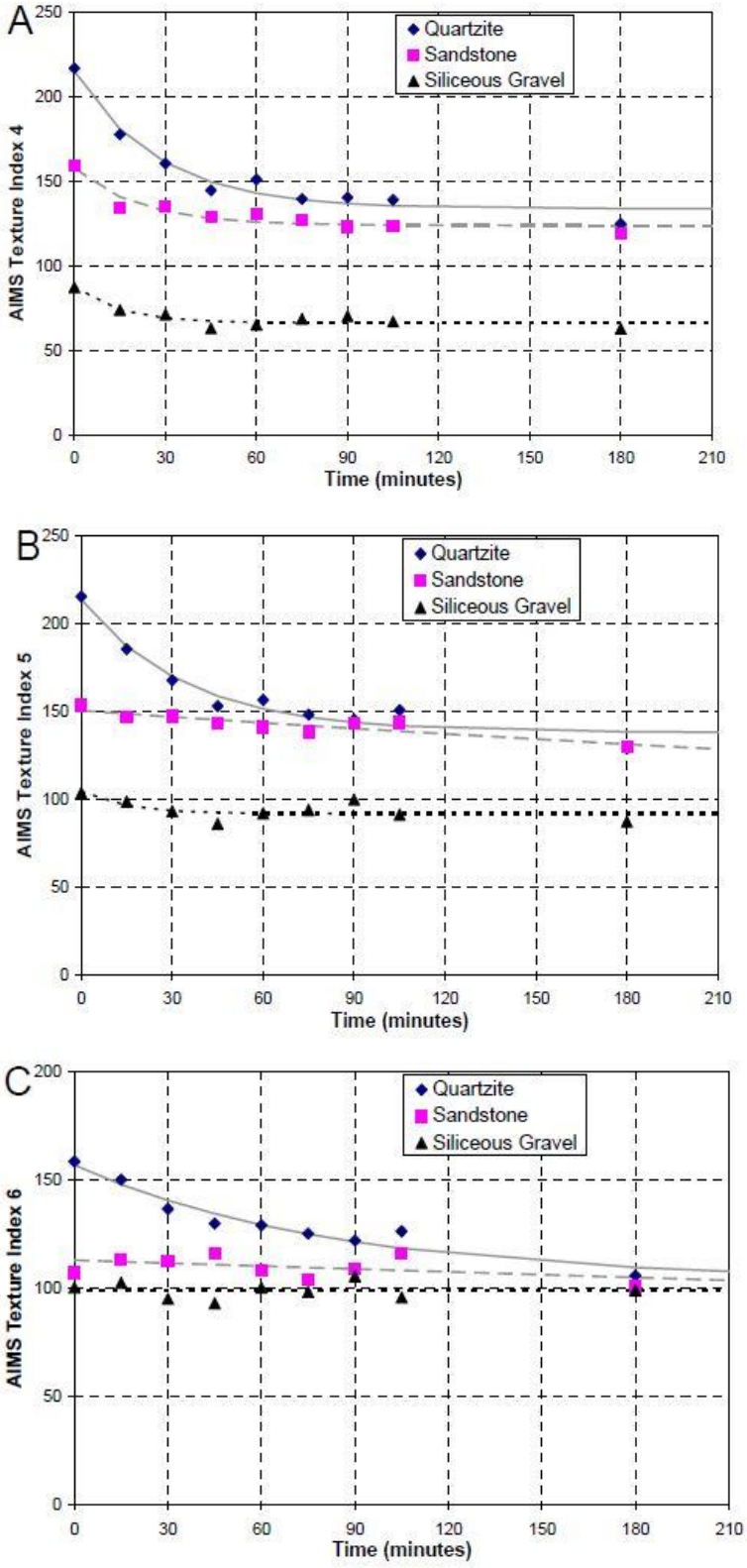

Figure 2-15 AIMS texture index versus time in the Micro-Deval test for A) texture level 4, B) texture level 5, and C) texture level 6

In the field, they examined nine pavement sections. These sections were selected to have different aggregate types (siliceous, sandstone, and quartzite) and mix design (CMHB-C, Superpave, and Type-C). The skid number was measured on the shoulder and on the outside lane. In the laboratory, test slabs were prepared using different aggregate types and different mixture types. The analysis of variance (ANOVA) was conducted at significance level of 0.05 to investigate the effect of both aggregate and mix type on the skid number. The results demonstrated that the aggregate type was significant factor (P-value < 0.05), while the mix type was not statistically significant (P-value = 0.089). The mix type was considered essential factor affecting the skid resistance; however, the mixes used in this study did not significantly contribute to skid resistance. The SPSS software was used to fit Eq. 2.5 in order to quantify the change in texture due to polishing in the Micro-Deval tests. Table 2-2 presents an example of the obtained regression coefficients.

$$\text{Texture}(t) = a + b \times \exp(-c \times t) \quad (2.5)$$

Table 2-2 Aggregate Texture Regression Coefficients

Aggregate	Texture Level	a	b	c
Siliceous Gravel	Level 4	66.19	21.04	0.06738
	Level 5	91.70	12.45	0.06687
	Level 6	49.38	49.54	0.00000
Sandstone	Level 4	123.70	33.69	0.04641
	Level 5	58.66	91.60	0.00130
	Level 6	0.21	112.77	0.00041
Quartzite	Level 4	133.54	81.17	0.03632
	Level 5	137.90	75.32	0.02875
	Level 6	103.67	53.18	0.01219

The results showed that aggregate type has significant effect on skid resistance. Gravel provided less skid resistance compared to sandstone and qurtize. Pavement sections

constructed with sandstone provided higher skid resistance compared to quartzite. The aggregate gradation was not found to have significant effect on skid resistance.

Masad et al. (2011) model

Masad et al. (2011) conducted a study that included measurements in the field and laboratory. In laboratory, several slabs with different asphalt mixtures and aggregate types were prepared and tested. Three mixture designs (Type C, Type D, and PFC) were evaluated. These mix designs were found to provide different frictional performance in the field. The mixtures were prepared and compacted in a special metal mold using a vibrator roller compactor as show in Figure 2-16a. The minimum slab size required to conduct the skid resistance measurements by the CTMeter and DFT was 17.75 in. by 17.75 in. The slabs were prepared to have a size of 60 inches by 26 inches. The researchers were able to evaluate the friction at three different locations on a single test slab (Figure 2-17b). A three-wheel polisher (Figure 2-16c) was used to polish the test slabs, and the measurements of the friction and mean profile depth were collected using the DFT and the CTMeter (Figure 2-16d) after different polishing cycles (5000, 10000, 20000, 35000, 50000, 75000, 100000). Similarly, British pendulum test and sand patch method were used in this study.

Aggregate texture and angularity were measured before and after different time intervals of polishing in the Micro-Deval. Figure 2-17 shows the change in the texture index before and after subjecting the aggregates to polishing and abrasion in the Micro-Deval. It shows that the selected aggregates provided different resistance to polishing. Effect of aggregate type on the pavement skid resistance was investigated among the prepared slabs. The results demonstrated high correlation between the aggregate properties and the mixture frictional characteristics. The aggregate characteristics affecting the skid resistance were the

British pendulum value, initial texture measured by AIMS, terminal texture after Micro-Deval measured by AIMS, and coarse-aggregate acid insolubility value.

(a) Walk-Behind Roller Compactor

(b) Laboratory Test Slabs

(c) NCAT Polisher

(d) DFT and CTMeter Measurements

Figure 2-16 Laboratory Experiments in the TxDOT (Masad et al. 2011)

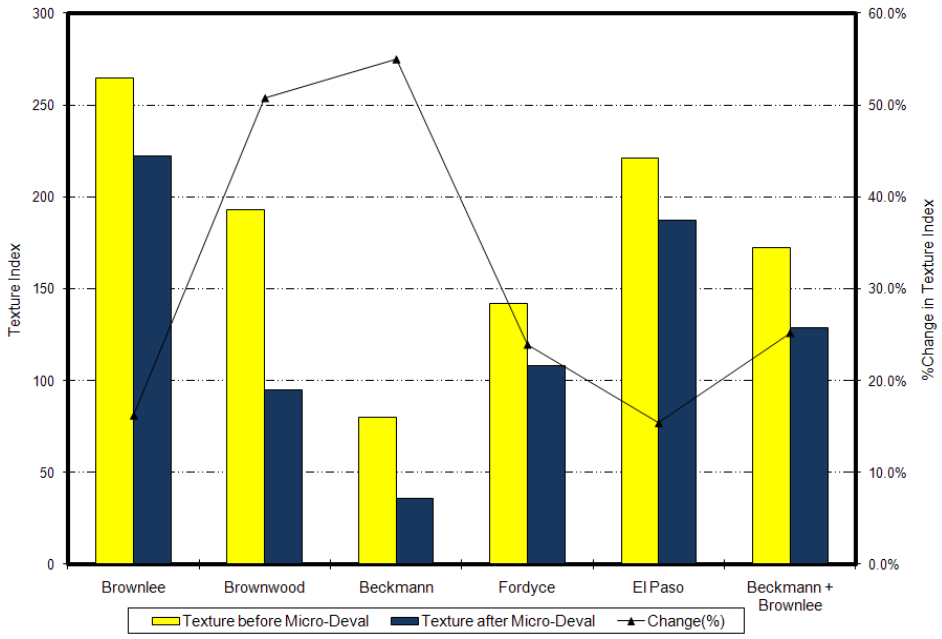

Figure 2-17 Aggregate Texture before and after Micro-Deval and Percent Change (Masad et al. 2011)

Masad et al. (2011) found that the change in the calculated IFI (Eq. 2.2) with the polishing cycles based on the MPD and DFT_{20} measurements can described by Eq. 2.6.

$$IFI\ (N) = a_{mix} + b_{mix} * e^{(-C_{mix}*N)} \quad (2.6)$$

where

a_{mix}: terminal IFI value for the mix

$a_{mix} + b_{mix}$: initial IFI value for the mix

c_{mix}: rate of change in IFI for the mix

N: number of polishing cycles in the laboratory

Figure 2-18 shows an example of the change in IFI with polishing cycles and the regression constants of Eq. 2.6. Based on laboratory stage, Masad et al. (2011) developed a model to predict the initial, terminal, and rate of change in IFI as a function of aggregate characteristics obtained from AIMS system and aggregate gradation parameters. This model

can be used to select the proper aggregate type to provide adequate skid resistance. Equations 2.7 to 2.9 represent the developed model.

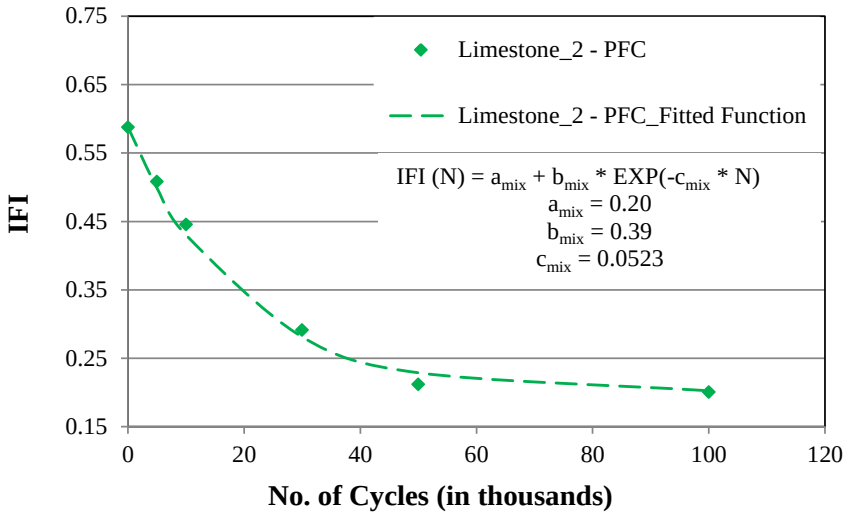

Figure 2-18 An example of IFI vs. polishing cycles (Kassem et al. 2013)

$$a_{mix} = \frac{18.422+\lambda}{118.936-0.0013(\text{AMD})^2} \quad (2.7)$$

$$a_{mix} + b_{mix} = 0.4984 * \ln\left(5.656 * 10^{-4}\left(a_{agg} + b_{agg}\right) + 5.846 * 10^{-2}\lambda - 4.985 * 10^{-2}k\right) + 0.8619 \quad (2.8)$$

$$C_{mix} = 0.765 * e^{\left(-7.297*\frac{10^{-2}}{C_{agg}}\right)} \quad (2.9)$$

where

a_{mix}: terminal IFI value for the mix

$a_{mix} + b_{mix}$: initial IFI value for the mix

c_{mix}: rate of change in IFI for the mix

AMD: aggregate texture after Micro-Deval

$a_{agg} + b_{agg}$: aggregate initial texture using texture model

c_{agg}: aggregate texture rate of change using texture model

k: shape factor of Weibull distribution used to describe aggregate gradation

λ: scale factor of Weibull distribution used to describe aggregate gradation.

The data collected in the laboratory were compared to skid values measured in the field for the same asphalt mixtures. Masad et al. (2011) developed a system to predict the skid number of asphalt mixtures as a function of traffic level. Input parameters required for this model included aggregate texture measured using AIMS before and after polishing in Micro-Deval, aggregate gradations, and traffic data. A computer program called skid analysis of asphalt pavements (SAAP), was developed to execute the steps needed to calculate the skid resistance of asphalt pavements as a function of time (or cumulative traffic). Figure 2-18 summarizes the steps needed to predict skid number according to Masad et al. (2011).

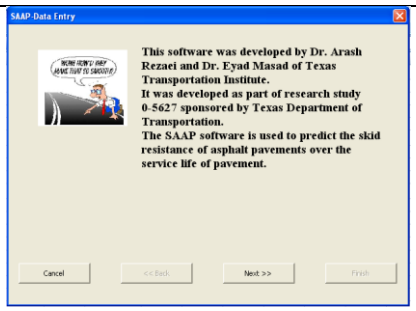

(1) Program interface

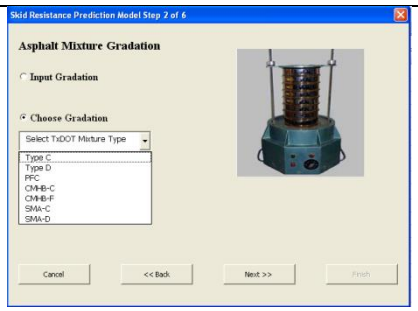

(2) Aggregate Gradation Input

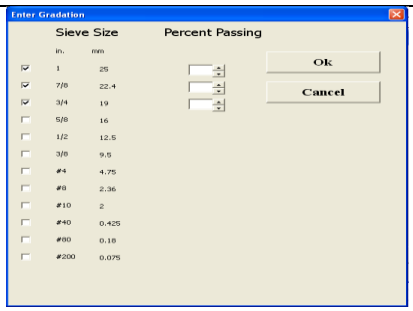

(3) Manual Aggregate Gradation

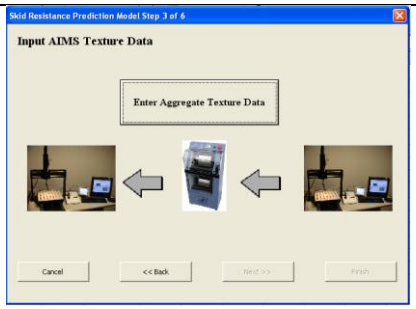

(4) AIMS Texture Data Input

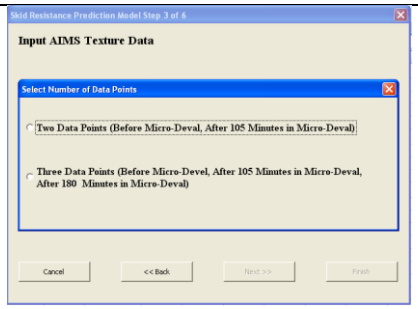

(5) Texture Data Points Select

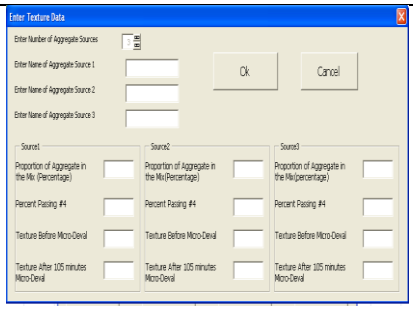

(6) Texture Measurement

(7) Input MPD Value

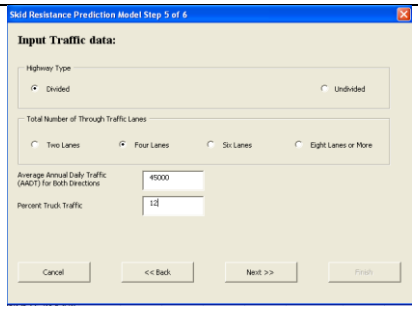

(8) Traffic Data Input

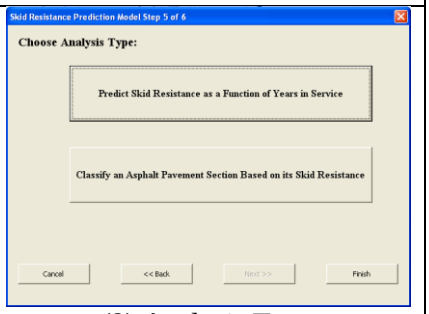

(9) Analysis Type

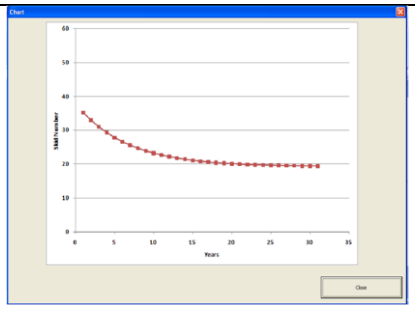

(10) Skid Number vs. Years

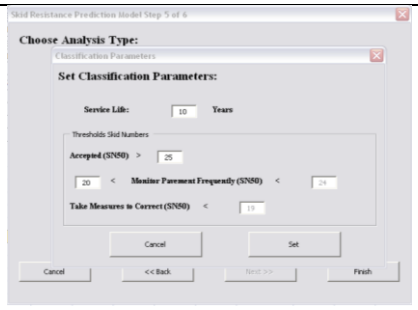

(11) Classification Setting

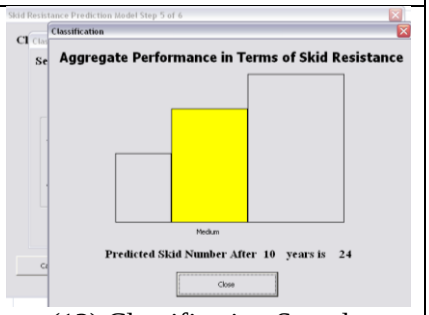

(12) Classification Sample

Figure 2-19 Steps Needed to Predict Skid Number SAAP in the TxDOT Project No.0-5627

Zhong et al. (2012) model

Zhong et al. (2012) developed a new model to estimate the skid resistance based on 12 mixtures with various mix types and aggregate sources. The aggregates included sandstone and siliceous limestone and four mix types were evaluated (19-mm Superpave level-II mix, 12.5-mm Superpave level 2 mix, SMA, OGPFC). The selection of the aggregates was based on the mixture construction in Louisiana. The Micro-Deval was used to polish the prepared slabs according to AASHTO T327-05. Also, the British pendulum number was measured according to AASHTO T278 and T279. Additionally, the macrotexture and microtexture of the prepared slabs were measured using the CTMeter and DTF after different polishing cycles. The model presented in Eq. 2.10 was developed as a function of the MPD and the DFT at 20 km/hr. The model estimates the friction number at 60 km/hr. The researchers also demonstrated that aggregates with low skid resistance can be blended with good quality aggregates in order to achieve adequate skid resistance.

$$F60 = 0.081 + 0.732\ DFN_{20} * \exp\frac{-40}{14.2+89.7MPD} \quad (2.10)$$

where

F60: friction number at 60 km/hr

MPD: mean profile depth

DFN_{20}: the friction at 20 km/hr

Kassem et al. (2013) model

Kassem et al. (2013) conducted a study to validate the IFI models developed by Masad et al. (2011). Squared-shaped slabs were prepared in the laboratory using three different types of aggregates (limestone 1, limestone 2, and sandstone) and four asphalt mixture designs (Type F, Type C, SMA, and PFC) were evaluated. A total number of 12

asphalt mixtures were prepared and two slabs of each mixture were tested. A total number of 24 slabs were tested in this study. The laboratory slabs were prepared using a linear kneading compactor (Figure 2-19a). The size (20 in. by 20 in.) of the prepared slabs were adequate for friction and mean profile depth measurements. A three-wheel polishing device was used to polish the test slabs at 5000, 10000, 30000, 50000, and 100000 cycles (Figure 2-20b).

Aggregate texture and angularity were measured using AIMS system at different time durations of polishing in the Micro-Deval. Figure 2-21 shows the percent weight loss of test aggregates. Sandstone had the highest texture index and lowest weight loss, while limestone 1 had the lowest texture index and highest percent weight loss. The AIMS (Figure 2-22) was used to measure the texture and angularity before and after polishing time durations of the Micro-Deval test.

(a) Preparing Slabs using Linear Kneading Compactor

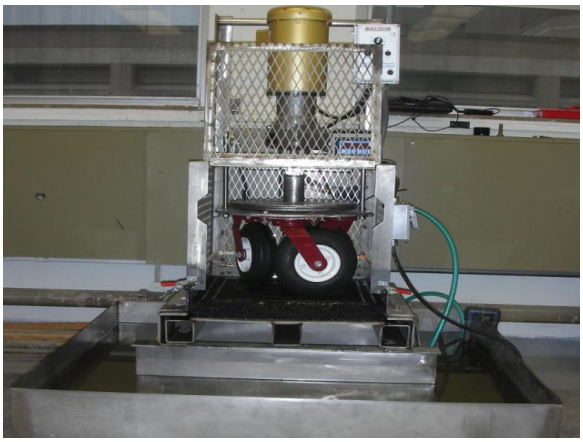

(b) Polishing Test Slabs using TTI polisher

Figure 2-20 Test Slabs Preparation and polishing (Kassem et al. 2013)

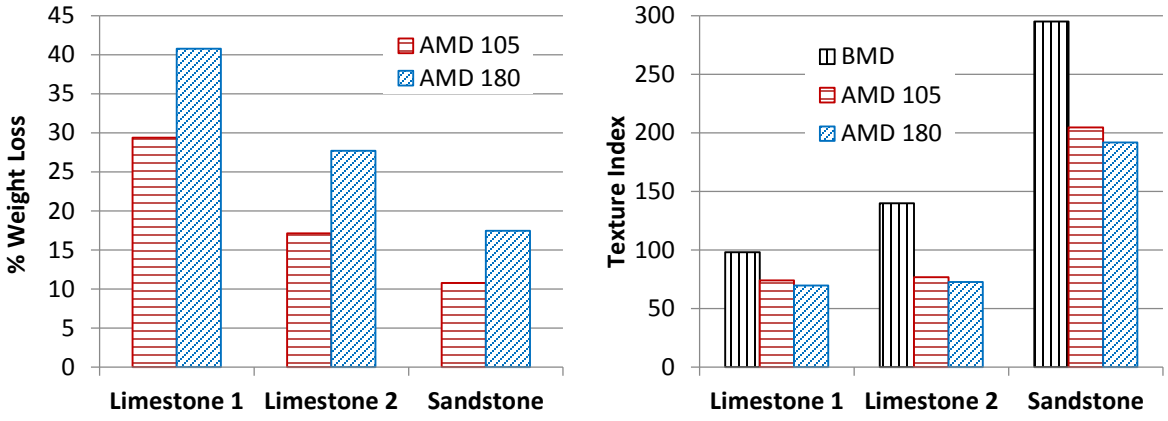

(a) Weight Loss of Micro-Deval Abrasion Test

(b) Texture Index Measured using AIMS

Figure 2-21 Texture Index and Weight Loss Results (Kassem et al. 2013)

Figure 2-22 AIMS System (Kassem et al. 2013)

The measurements of friction and macrotexture were conducted using the DFT and CTMeter after different polishing cycles. Then, the IFI was calculated based on the measured MPD and DFT at 20 km/hr. Figure 2-23 shows the IFI versus polishing cycles. The IFI of limestone 1 test slabs reached the terminal value after only 30,000 cycles while the sandstone reached the terminal value after 100,000 cycles. Also, the terminal IFI value of the sandstone is higher than the terminal value of limestone 1. The sandstone had rough texture with better

abrasion resistance compared to limestone 1. The findings also indicated that the coarse mixtures had better friction compared to fine mixtures. The results demonstrated high correlation between the measured and predicted IFI after considering aggregate texture and angularity indices in the developed model. Equations 2.11, 2.12 and 2.13 present the developed models.

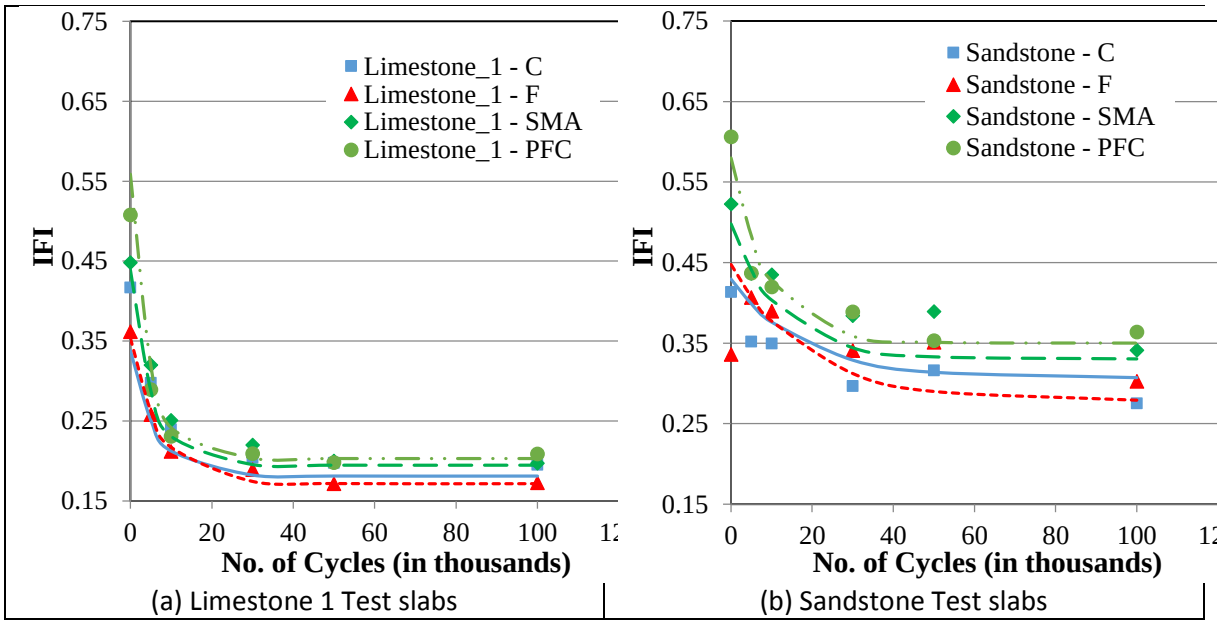

Figure 2-23 Texture Index and Weight Loss Results (Kassem et al. 2013)

$$a_{mix} = \frac{47.493+\lambda}{307.071-0.003(AMD)^2} \quad (2.11)$$

$$a_{mix} + b_{mix} = 0.308 * \ln\left(\frac{1.438*(a_{TX}+b_{TX})+46.893*\lambda+333.491*k}{2.420*(a_{GA}+b_{GA})}\right) + 1.008 \quad (2.12)$$

$$C_{mix} = 0.052 + 2.284 * 10^{-14} * e^{\left(\frac{0.523}{C_{TX}}\right)} + 2.008 * 10^{-47} * e^{\left(\frac{1.708}{C_{GA}}\right)} \quad (2.13)$$

where

a_{mix}: terminal IFI

$a_{mix} + b_{mix}$: initial IFI

C_{mix}: rate of change in IFI

λ, k: scale and shape parameters of Weibull distribution

AMD: the texture after 150 min. in Micro-Deval

a_{TX}, b_{TX}: regression constants for texture

a_{GA}, b_{GA}: regression constants for angularity

2.13 Summary

The skid resistance of pavement surface is affected by its surface texture properties. Providing adequate macrotexture and microtexture are essential requirements for pavement to ensure high skid resistance at all speeds. Skid resistance is mainly associated with aggregate characteristics and gradation. Additionally, recent studies showed that the Micro-Deval and AIMS are proper test methods for measuring the resistance of aggregates to abrasion and polishing. In order to improve the safety on highway pavements, the researchers have developed several models to predict the skid resistance as a function of aggregate characteristics, mix design and traffic level. These models need to be validated with additional data that cover a wide range of variables and parameters. In addition, these models should be extended to predict the skid resistance of surface treatments such as seal coat.

CHAPTER 3 – FIELD AND LABORATORY TESTING

The researchers measured the frictional characteristics and skid number on a number of HMA and seal coat test sections in Texas. All field measurements were collected by the researchers at the Texas A&M Transportation Institute (TTI). In addition, the aggregate shape characteristics were either measured in the laboratory or obtained from TxDOT database by the researchers. In this study, 35 test sections of HMA and 35 seal coat test sections were examined. Four seal coat test sections were excluded due to excessive bleeding. This chapter discusses the research plan and the field and laboratory testing.

3.1 Selection of the Field Sections

The researchers identified and selected 35 test sections of HMA and 35 test sections with seal coat. During the selection of test sections, the research team made an effort to include surfaces with wide varieties of mixture gradations, aggregate sources, and climatic zones of Texas. Focus was given to identify test sections with higher traffic levels so that the team can observe higher polishing within relatively short time. Another important criterion of test sections selection was to find existing sections with history of skid measurement under TxDOT's annual network-level pavement evaluation program. TxDOT does not collect the network-level skid data for all the roads every year. Typically, major highways (i.e., interstate highways) with higher traffic level are tested more frequently than other highways (i.e, farm-to-market roads). The annual skid testing frequency varies among different districts of TxDOT. Table 3-1 provides detailed information about the HMA test sections. This information includes the location of the test sections, section identification (ID), construction date, testing date, and number of lanes. The test sections of asphalt mixtures included different mixture type (SMA-C, SMA-D, SMA-F, CMHB-F, Type C, Type D, TOM, PFC,

CMHB-C, and CAM), aggregate type (Limestone, Gravel, Granite, Sandstone, Dolomite, Rhyolite, Traprock, and Quartzite), year of construction (2004 to 2013), and were distributed across Texas (ATL, AUS, BMT, BRY, ODA, SAT, YKM, HOU, LRD, PHR, and LFK districts of TxDOT). Table 3-2 provides the same information for the seal coat test sections. The test sections of seal coat included different grade type (Grade 3, Grade 4, and Grade 5), aggregates (Limestone, Gravel, Traprock, Sandstone, Dolomite, Rhyolite, LRA, and Lightweight), coating conditions (pre-coated and virgin), year of construction (2009 to 2013), and also were distributed across Texas (ATL, BMT, ODA, SAT, YKM, LRD, PHR, LFK, BRY).

Table 3-1 HMA Test Sections

District	Section ID	CTM DFT Test Date	Construction Date	Days between construction and field testing	Lane description
Atlanta	IH 30_ATL_SMA_	12/20/2013	7/1/2010	1268	Two lanes each way divided
	US 59_ATL_CMHB-F_FM 2792	12/18/2013	8/1/2005	3061	Two lanes each way divided
	US 59_ATL_TY D_TRM 310	12/18/2013	6/1/2011	931	Two lanes each way divided
	US 59_ATL_TY D_SHELBY CO LINE	12/18/2013	4/1/2011	992	Two lanes each way divided
	US 271_ATL_CMHB-F_CAMP	12/20/2013	6/1/2008	2028	Undivided, two lane each way with turn lane
Austin	IH 35 TOM Mix_AUS	8/28/2014	7/1/2011	1154	Three lanes each way, divided
	RM 3238_AUS_TOM	8/28/2014	7/1/2013	423	Undivided, one lane each way
	US71_AUS_TOM	8/27/2014	7/1/2013	422	Two lanes each way divided
Beaumont	IH10_BMT_SMA-D	9/30/2013	7/1/2009	1552	Two lanes each way divided
	SH 82_BMT_SMA-D	9/30/2013	4/1/2013	182	Undivided, two lane each way with turn lane
	SL 207_BMT_TY D	10/2/2013	5/1/2013	154	Undivided, one lane each way

	US 69_BMT_PFC	9/30/2013	9/1/2011	760	Two lanes each way divided
	US 90_BMT_SMA-D	9/30/2013	5/1/2013	152	Undivided, two lane each way with turn lane
Bryan	IH 45_BRY_TY C	10/2/2014	8/25/2008	2229	Two lanes each way divided
	IH 45_BRY_PFC	10/2/2014	8/17/2009	1872	Two lanes each way divided
	SH 6_BRY_NEW PFC	10/2/2014	9/28/2011	1100	Two lanes each way divided
	SH 6_BRY_OLD PFC	10/2/2014	6/21/2007	2660	Two lanes each way divided
Laredo	IH 35_LRD_SMA_WEBB	7/24/2013	6/1/2008	1879	Three lanes each way, divided
	IH 35_LRD_SMA-C_LASALLE	7/24/2013	6/1/2004	3340	Two lanes each way divided
Lufkin	US 59_LFK_PFC_Nacodoches	8/16/2013	6/1/2013	76	Two lanes each way divided
	SH 7_LFK_TY D_Houston	8/16/2013	5/1/2013	107	Undivided, one lane each way
Odessa	IH 20_ODA_SP-C_Martin	10/8/2013	9/1/2012	402	Two lanes each way divided
	IH 20_ODA_SP-D_Midland_2012	10/8/2013	6/1/2012	494	Two lanes each way divided
	IH 20_ODA_SP-D_Midland_2013	10/8/2013	6/1/2013	129	Two lanes each way divided
	US 385_ODA_CMHB-F	10/7/2013	10/1/2005	2928	Two lanes each way divided
	IH 20_ODA_PFC_2004	10/8/2013	6/1/2004	3416	Two lanes each way divided
San Antonio	IH 10_SAT_SMA-D_BEXAR	3/10/2014	4/1/2012	708	Two lanes each way divided
	IH 10_SAT_TY C_BEXAR	3/10/2014	3/1/2009	1835	Two lanes each way divided
	IH 37_SAT_PFC_BEXAR	3/10/2014	6/1/2013	282	Two lanes each way divided
YKM	IH 10_YKM_TY D_AUSTIN	5/23/2013	7/1/2011	692	Two lanes each way divided
	SH 36_YKM_TY D_AUSTIN	5/23/2013	7/1/2006	2518	Undivided, one lane each way
PHARR	US 77_PHR_TY D_Kennedy	2/20/2014	2/1/2013	384	Two lanes each way divided
	US 281_PHR_TY D_Hidalgo	2/20/2014	8/1/2011	934	Two lanes each way divided
Houston	SH 6 Bwp 2-1, Wp 2-1 Middle	6/20/2013	7/1/2005	2911	Two lanes each way divided
	SH 6 Bwp 2-1 Bottom	6/20/2013	7/1/2005	2911	Two lanes each way divided

Table 3-2 Selected Sections for Seal Coat

District	Section ID	CTM DFT Test Date	Construction Date	Days between construction and field testing
Pharr	US 77_PHR_GR3_Cameron	2/20/2014	5/1/2013	295
	US 281_PHR_GR3_Hidalgo	2/21/2014	5/1/2011	1027
	US 281_PHR_GR3_Brooke_TRM 752	2/21/2014	5/1/2011	1027
	US 281_PHR_GR3_Brooke_TRM 722	2/21/2014	9/1/2011	904
Dallas-FW	US 377_FTW_GR3_Hood	11/18/2014	7/1/2010	1601
	US 377_FTW_GR3_Tarrant	11/18/2014	7/1/2011	1236
	SH 199_FTW_GR3_Parker	11/18/2014	7/1/2010	1601
Brownwood	US 67_BWD_GR4_Coleman	10/9/2014	7/1/2010	1561
	US 67_BWD_GR4_Brown	10/9/2014	7/1/2011	1196
	US 183_BWD_GR4_Eastland	10/9/2014	7/1/2012	830
	US 377_BWD_GR4_Brown	10/9/2014	7/1/2012	830
San Antonio	US 90_SAT_GR4_Bexar	3/11/2014	6/1/2013	283
	FM 1518_GR3_Bexar	3/11/2014	6/1/2013	283
	SH 16_SAT_GR4_Atascosa_TRM 626	3/12/2014	6/1/2012	649
	SH 16_SAT_GR 4_Atascosa_TRM 642	3/12/2014	6/1/2012	649
YKM	SH 36_YKM_GR 3_Austin	5/23/2013	8/1/2008	1756
Lufkin	US 59_LFK_GR3_Angelina	8/5/2013	6/1/2010	1161
	US 69_LFK_GR4_Angelina	8/5/2013	6/1/2012	430
	US 287_LFK_GR4_Trinity	8/16/2013	6/1/2013	76
	FM 2213_LFK_GR5_San Augustine	8/26/2014	6/1/2012	816
	US 59_LFK_GR4_Shelby	8/26/2014	6/1/2012	816
Odessa	LP 338_ODA_GR4_Ector	10/7/2013	6/1/2012	493
	US 385_ODA_GR4_Crane	10/7/2013	6/1/2009	1589
	US 385_ODA_GR4_Ector	10/7/2013	6/1/2010	1224
Beaumont	SH 82_BMT_GR4_Jefferson	10/1/2013	9/1/2010	1126
	FM 365_BMT_GR4_Jefferson	10/1/2013	7/1/2013	92
	FM 105_BMT_GR4_Orange	10/2/2013	7/1/2013	93
Atlanta	US 80_ATL-GR4_Harrison	12/19/2013	6/1/2012	566
	US 59_ATL_GR3_Cass_RG_TRM238	12/19/2013	6/1/2013	201
	SH 77_ATL_GR4_Cass_TRM 745_SS	12/19/2013	6/1/2012	566
	SH 77_ATL_GR4_Cass_TRM 720_RG	12/19/2013	6/1/2013	201

3.2 Frictional Characteristic Measurements

Field testing primarily included measurements of friction using the dynamic friction tester (DFT), mean profile depth (MPD) using the circular texture meter (CTMeter), and skid number using the TxDOT's skid trailer. Figure 3-1 shows a layout of the test section used by the TTI researchers when taking CTMeter and DFT measurements in the field. The CTMeter device was used to measure the MPD, while the DFT was used to measure the coefficient of friction at different speeds (20, 40, 60, and 80 km/hr). During testing, the CTMeter and DFT devices were always positioned in the left wheel path of the outside lane. Six locations were tested in each section. Two locations were at the shoulder, and four locations were in the outer lane. Two DFT and six CTMeter readings were performed at each location. In some cases, where there was no shoulder, the researchers took CTMeter and DFT measurements between the wheel path to represent the initial skid values.

Figure 3-2 shows typical field operations at different locations and districts in Texas. Figure 3-3 shows an example of DFT measurements on a seal coat test section. One can notice, as expected, that shoulder had a higher coefficient of friction (Mu) compared to wheel path (WP), and between wheelpath (BWP). Note that the area between wheel paths also experience some polishing due vehicles lane change and wheel wandering. The coefficient of friction between wheel paths was close to the coefficient of friction at the shoulder. Figure 3-4 shows an example of DFT measurements for a Type-D asphalt mixture test section. The shoulder had higher friction value compared to wheel path as the later experienced frequent polishing under traffic.

Measurements of macrotexture and friction were conducted on the outer lane as the skid number was measured by the skid trailer at the outside lane (in case of multiple lanes)

on the left wheel path. Also, the outer lane experiences most polishing rates because most of the trucks and other vehicles use this lane.

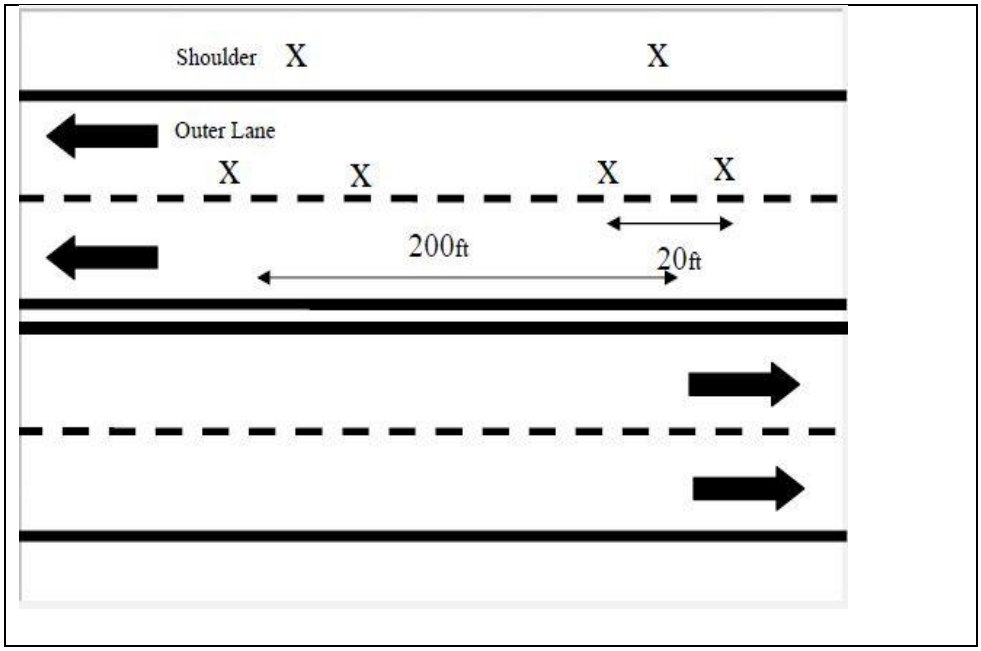

Figure 3-1 Layout of Measurement Section

Figure 3-2 Collecting Field Measurements

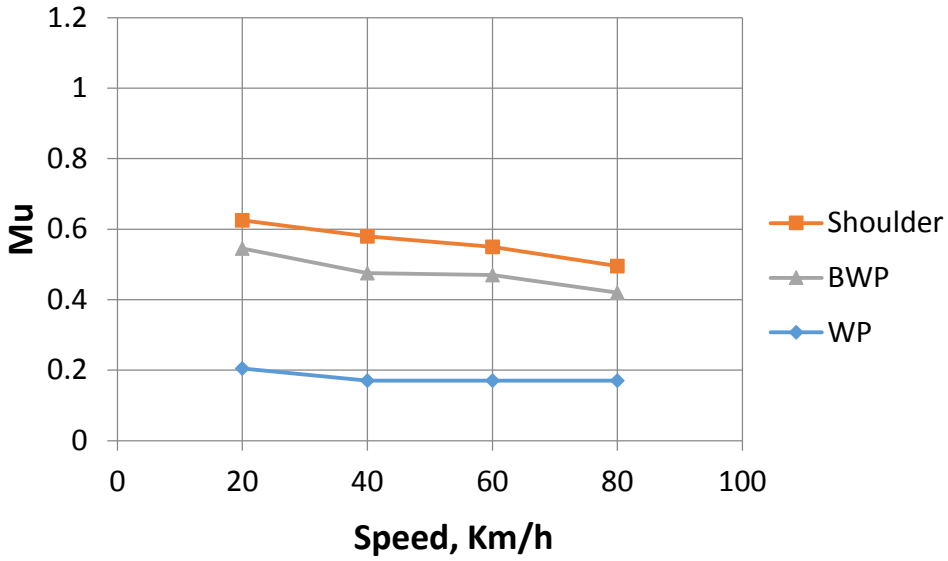

Figure 3-3 DFT Measurements for Seal Coat Test Section (IH-35-LRD-NP-COT-S_SealCoat)

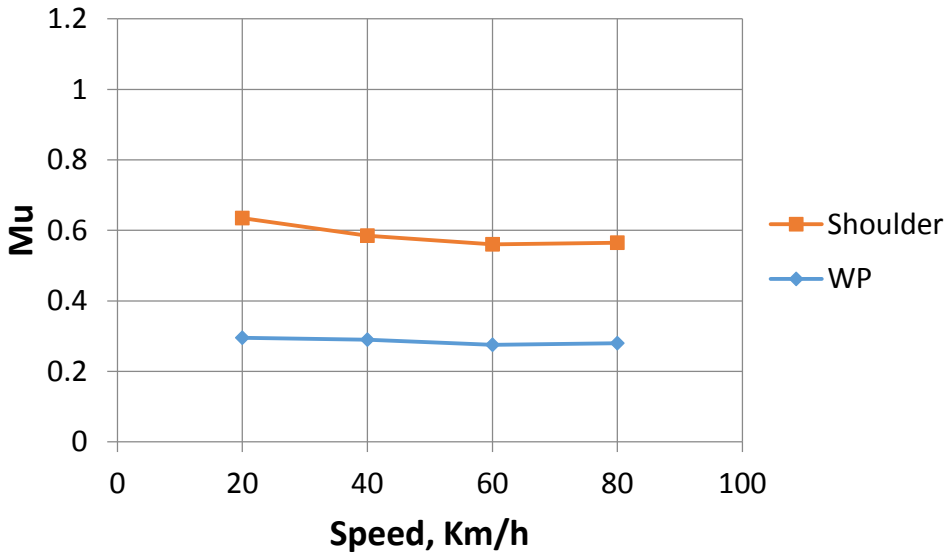

Figure 3-4 DFT Measurements for Type-D Asphalt Mix Test Section (SH-36-HMA_TypeD)

The results of the field testing on seal coat showed fair correlation between the mean profile depth (MPD) measured using the CTMeter and the coefficient of friction at 80 km/hr (DFT_{80}) measured using DFT as shown in Figure 3-5. This relationship demonstrates that

higher macrotexture (higher seal coat grade) would provide better friction. The researchers calculated the international friction index (IFI) using the mean profile depth and friction obtained from the field according to Equation 3.1.

$$IFI = 0.081 + 0.732 DFT_{20} \exp\left(\frac{-40}{S_p}\right) \quad (3.1)$$

$$S_p = 14.2 + 89.7 MPD \quad (3.2)$$

where

MPD = mean profile depth measured using the CTMeter

DFT_{20} = coefficient of friction at 20 km/hr measured using DFT

The researchers found good correlation between the IFI (Equation 3.1) and DFT_{80} measured using the DFT as presented in Figure 3-6.

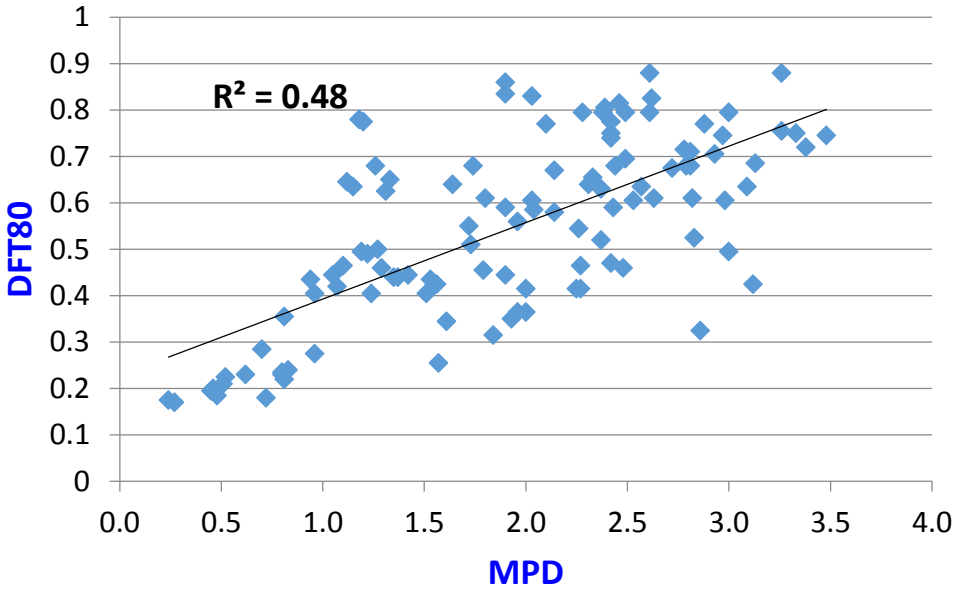

Figure 3-5 Correlation between Mean Profile Depth (MPD) and Coefficient of Friction at 80 km/hr (DFT_{80}) for Seal Coat Test Sections

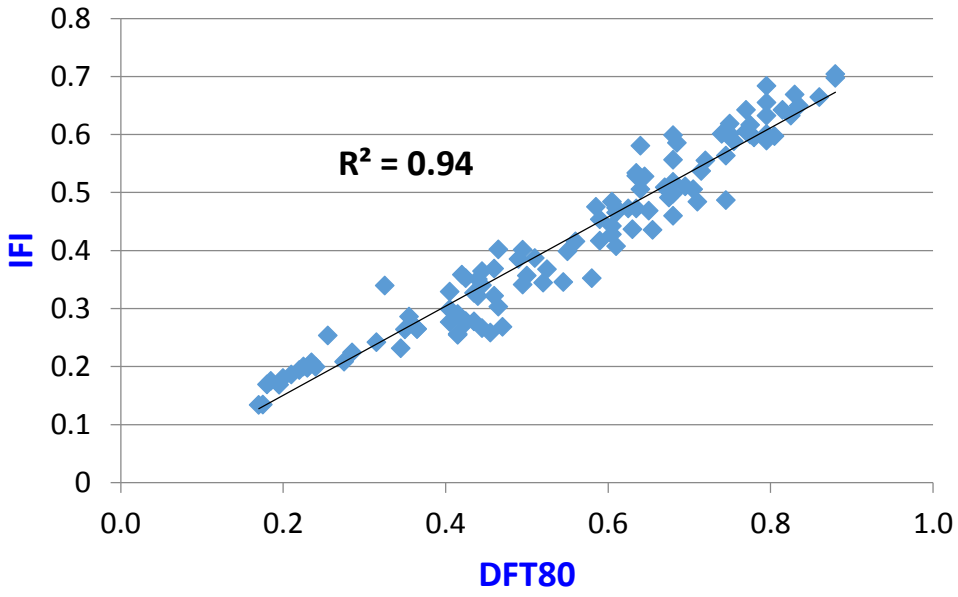

Figure 3-6 Correlation between IFI and Coefficient of Friction at 80 km/hr (DFT_{80}) for Seal Coat Test Sections

The results of the field testing on asphalt mixture test sections showed no correlation between MPD measured using CTMeter and DFT_{80} measured using DFT as shown in Figure 3-7. However, fair correlation was found between IFI and DFT80 as shown in Figure 3-8.

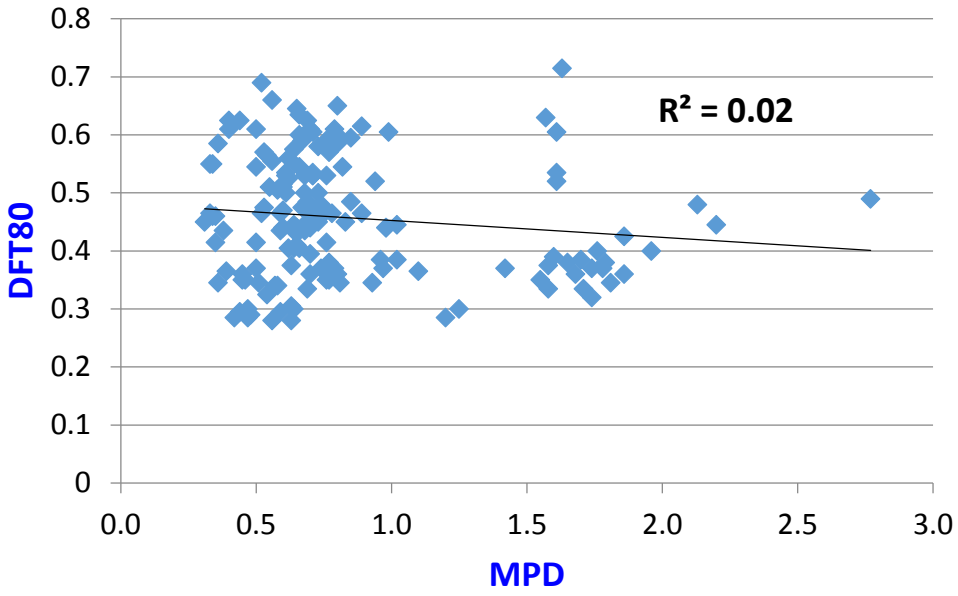

Figure 3-7 Correlation between Mean Profile Depth (MPD) and Coefficient of Friction at 80 km/hr (DFT80) for Hot Mix Asphalt Test Sections

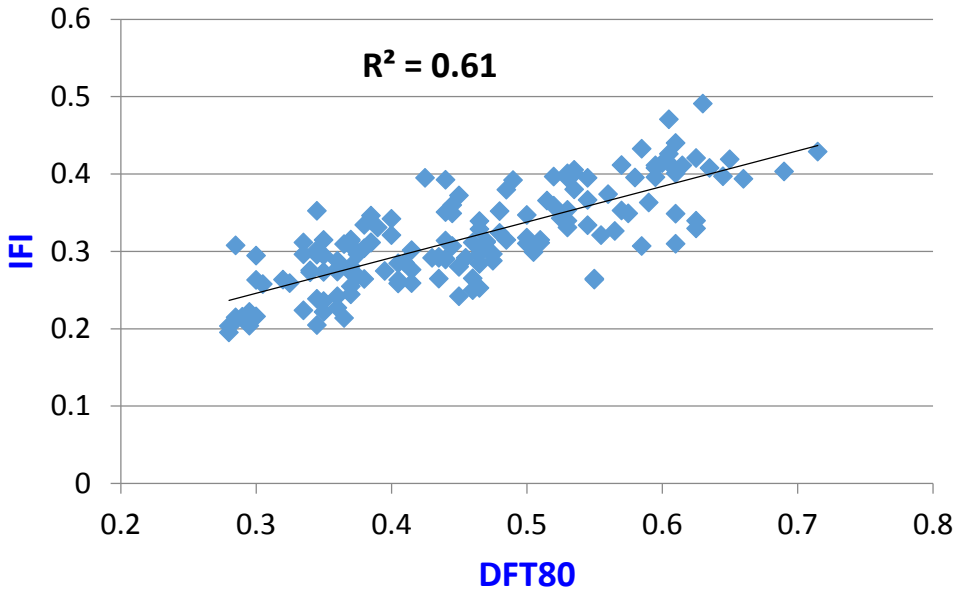

Figure 3-8 Correlation between IFI and DFT80 for Hot Mix Asphalt Test Sections

Fair correlation observed between IFI and DFT_{80} is expected since the IFI is a function of DFT_{20}; and DFT_{20} has typically good correlation with DFT_{80}. The main purpose of presenting Figures 3-6, 3-8, 3-9, and 3-10 was to demonstrate the range of values for both IFI and DFT_{80} for HMA and seal coat surfaces. Figure 3-9 shows the IFI versus DFT_{80} measured using DFT for some seal coat test sections (blue data points) and asphalt mixture test sections (red data points) examined in this project. It can be seen from Figure 3-9 that, in general, the seal coat had higher friction compared to asphalt mixtures. However, the seal coat had a wider range of friction values compared to asphalt mixture. Figure 3-10 shows the surface conditions of some of the examined asphalt mixture. The porous friction course (PFC) had higher macrotexture and friction compared to Type-D mixture.

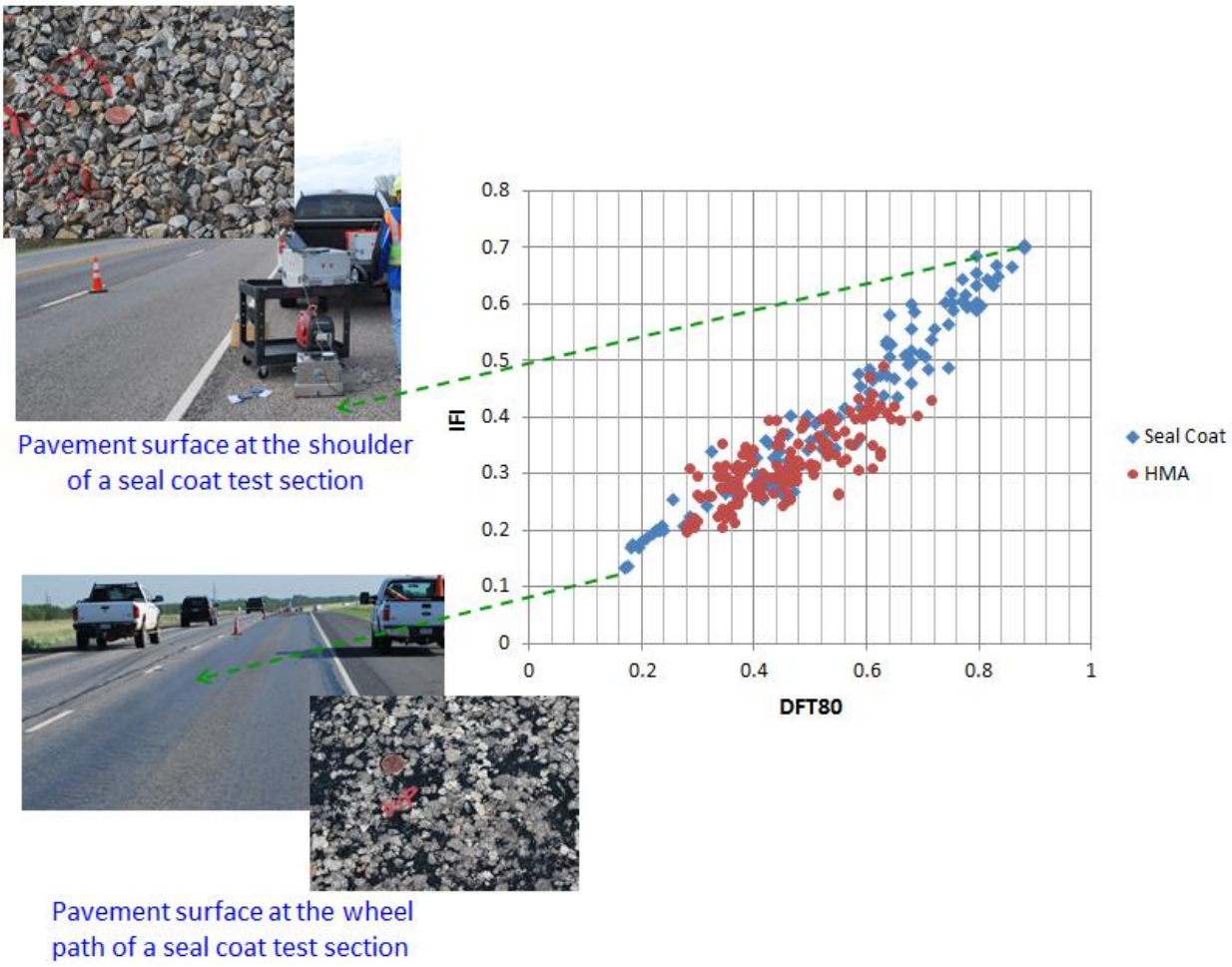

Figure 3-9 Correlation between IFI and DFT80 for Hot Mix Asphalt and Seal Coat Test Sections and Pavement Surface Condition for Seal Coat Test Sections

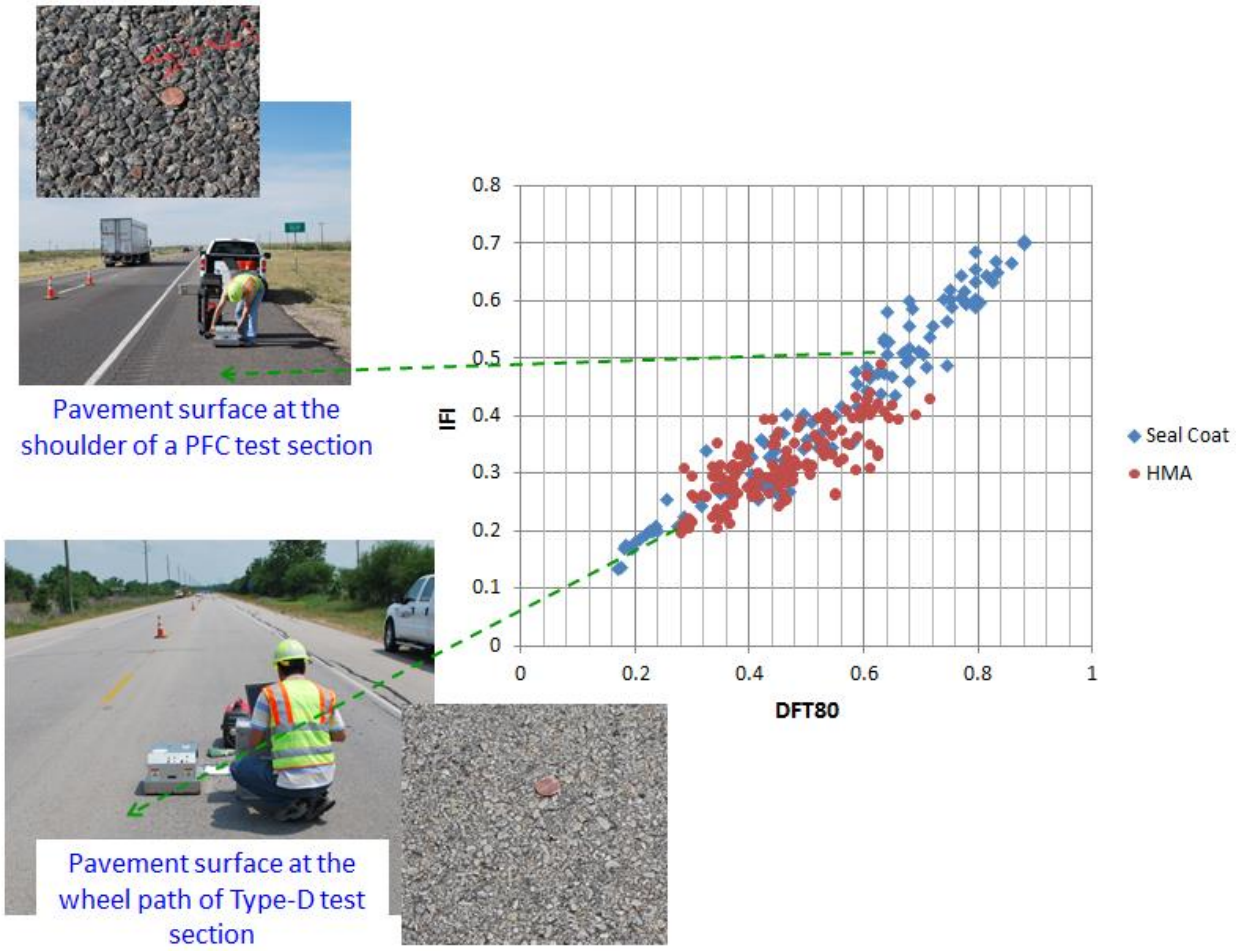

Figure 3-10 Correlation between IFI and DFT80 for Hot Mix Asphalt and Seal Coat Test Sections and Pavement Surface Condition for Asphalt Mixture Test Sections

3.3 Aggregate Characterization

Under this subtask, the researchers used the AIMS and Micro-Deval devices to measure aggregate's resistance to polishing and abrasion. The AIMS was used to quantify the aggregate's texture and angularity before and after polishing using the Micro-Deval apparatus. Figure 3-11 illustrates the procedure followed in this study for measuring aggregate texture and angularity and its resistance to polishing and abrasion. Both of the texture and angularity of aggregates decrease with the time of polishing in the Micro-Deval test. The loss of texture can be described using only three data points: texture measured

before the Micro-Deval test, after 105 min. and 180 min. of polishing in the Micro-Deval test. Figure 3-12 shows an example of loss in aggregate texture and angularity as a result of Micro-Deval abrasion and polishing of virgin aggregates.

Mahmoud et al. (2007) and Kassem et al. (2013) suggested using Eqs.3.3 and 3.4 to describe change in aggregate texture and angularity as a function of polishing time in Micro-Deval:

$$TX(t) = a_{TX} + b_{TX} * e^{(-C_{TX}*t)} \quad (3.3)$$

$$GA(t) = a_{GA} + b_{GA} * e^{(-C_{GA}*t)} \quad (3.4)$$

where

TX (t): change in texture as a function of time (min.)

$a_{TX}, b_{TX,}\ C_{TX}$: aggregate texture regression constants

t: polishing time in Micro-Deval

GA (t): change in angularity as a function of time (min.)

$a_{TX}, b_{TX,}\ C_{TX}$: aggregate angularity regression constants

t: polishing time in Micro-Deval

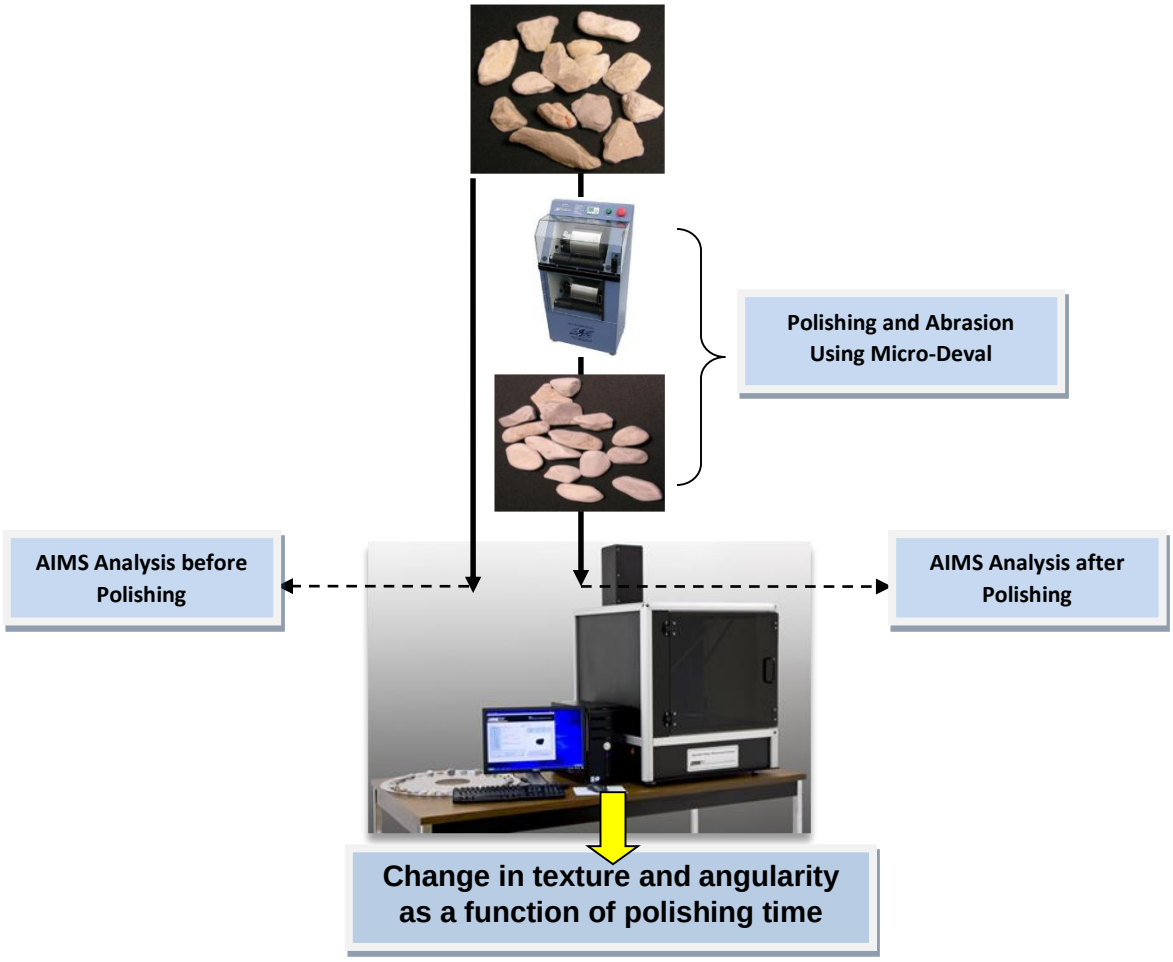

Figure 3-11 Procedure for Measuring Aggregate Texture and its Resistance to Polishing

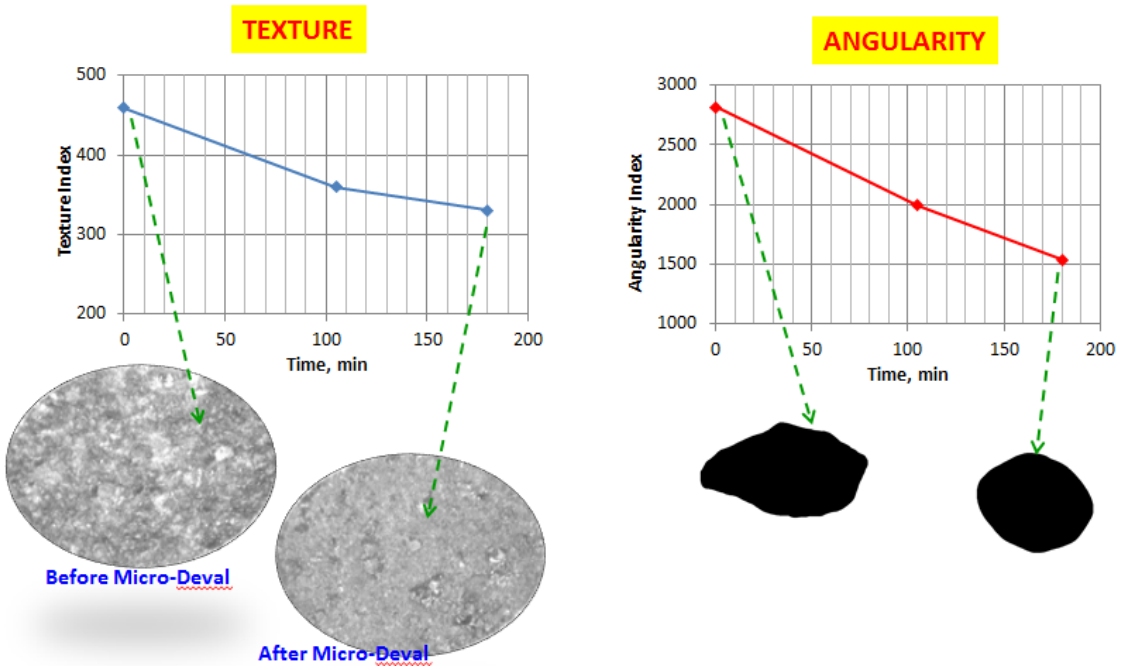

Figure 3-12 Loss in Aggregate Texture and Angularity as a Result of Micro-Deval Abrasion and Polishing of Virgin Aggregates

3.4 Aggregate Gradation Parameters

Masad et al. (2011) have indicated that aggregate gradation is a fundamental factor that affects skid resistance. Masad et al. (2011) and Kassem et al. (2013) used the cumulative two-parameter Weibull distribution (Eq. 3.5) to describe the aggregate gradation. The Weibull distribution function (Eq. 3.5) is used to fit the aggregate size distribution and both scale (λ) and shape (κ) parameters were used to quantify the aggregate gradation.

$$F(x, \lambda, \kappa) = 1 - e^{-(\frac{x}{\lambda})^{\kappa}} \quad (3.5)$$

where

x: aggregate size in millimeters

λ, κ: scale and shape parameters of Weibull distribution

3.5 Skid Number Measurements

Skid number data used in this study was obtained from two sources: TxDOT's annual network-level data collection, and TTI's project level measurement. Each year TxDOT periodically measures the skid number for all its highways although at different intervals for different highways. The research team obtained the data form TxDOT's Pavement Management Information System (PMIS) database. TxDOT PMIS database typically store the skid number data for each of the PMIS section which is typically 0.5 mile long. The length of test sections included in this study varied between two miles to little over 15 miles. TxDOT measures skid number using a skid trailer with a smooth tire according to ASTM E 274, "Standard Test Method for Skid Resistance of Paved Surfaces Using a Full-Scale Tire". The left tire is locked to measure the skid number at 50 mph (80 km/h). The skid number was measured at the outside lane (in case of multiple lanes) on the left wheel path. The pavement sections are typically classified after 5 years of service based on the measured skid number by a skid trailer at 50 mph as presented in Table 3-5.

Table 3-3 Aggregate Classification based on the SN

Aggregate Class	SN values
High	SN(50) > 30
Medium	21 > SN(50) > 29
Low	SN(50) < 20

The SN can be measured as a function of IFI and speed constant parameter according to Eq. 3.6 (ASTM E 274).

$$IFI = 0.045 + 0.925 \times 0.01 \times SN(50)e^{\frac{20}{S_P}} \quad (3.6)$$

where

SN(50): skid number measured by a smooth tire at 50 mph (80 km/h)

IFI: international friction index

S_p: speed constant parameter

Figure 3-13 shows measuring the skid number using the skid trailer. When using the skid trailer, water is sprayed in front of the left wheel and the left wheel is locked while the truck is travelling at certain speed (i.e., 50 mph in Texas). The friction force that resists the rotation of the tire is measured (Masad et al. 2011).

Figure 3-13 Locked-Wheel Skid Trailer

3.6 Summary

Chapter 3 discusses the research plan and selection of HMA and seal coat test sections. About 35 HMA and 35 seal coat test sections were selected which were distributed across Texas. These test sections were constructed using different materials and mix design and

subjected to different traffic levels. In the field, the researchers measured the surface frictional characteristics of the test sections using DFT and CTMeter, in addition a skid trailer was used to measure the skid number. In the laboratory, the researchers used methods to characterize the resistance of test aggregates to abrasion and polishing and quantify the aggregate shape characteristics (texture and angularity). These data were used for model developments as discussed in Chapters 4 and 5.

CHAPTER 4 - DATA ANALYSIS AND RESULTS FOR HOT MIX ASPHALT TEST SECTIONS

Researchers, in this study, developed skid prediction model for HMA and seal coat surfaces. The prediction models were basically developed using aggregate properties, field measurements, and traffic data. This chapter focuses on the development and validation of a prediction model for HMA pavements. Figure 4-1 shows the flowchart used for developing the predictive models for skid resistance of HMA and seal coat surfaces. This effort included laboratory measurements of aggregate shape characteristics and the resistance to abrasion and polishing. The researchers used relationships to describe the change in aggregate texture and angularity due to abrasion and polishing. They also used mathematical models to describe the aggregate gradations for asphalt mixture and seal coat. Statistical methods were used to develop prediction models for friction and skid resistance of HMA. Following subchapters describe how model parameters were obtained/measured and how they were used to develop the prediction models.

4.1 Analysis of Aggregate Gradation

The cumulative two-parameter Weibull distribution was used to describe the aggregate gradation as presented in Eq. 3.5. The MATLAB program was used to fit the Weibull function to aggregate size distribution. Figure 4-2 shows an example of Weibull functions for various aggregate gradations. The x-axis represents the aggregate size in millimeters, and y-axis represents the cumulative percent passing of the aggregate. The scale (λ) and shape parameters (κ) were calculated by fitting the aggregate gradation to the cumulative two-parameter Weibull distribution. Table 4-1 presents the scale (λ) and shape (κ) parameters for the aggregate gradations for all the mixtures used in this study for

developing the HMA skid prediction model. The λ parameter varied from 10.95 to 2.899, while the κ parameter varied from 4.30 to 0.69. The r-squared values for fitting Weibull function to the aggregate gradations were between 0.92 to 0.99. Higher values of λ were associated with coarser aggregate gradations as presented in Figure 4-2. The research team also calculated these two parameters to describe the shape factor for all common mixture gradations used in Texas. Typically, the aggregate gradations running through the middle of the bands (allowed by TxDOT), for given mixture type, was used to calculate the default shape parameters.

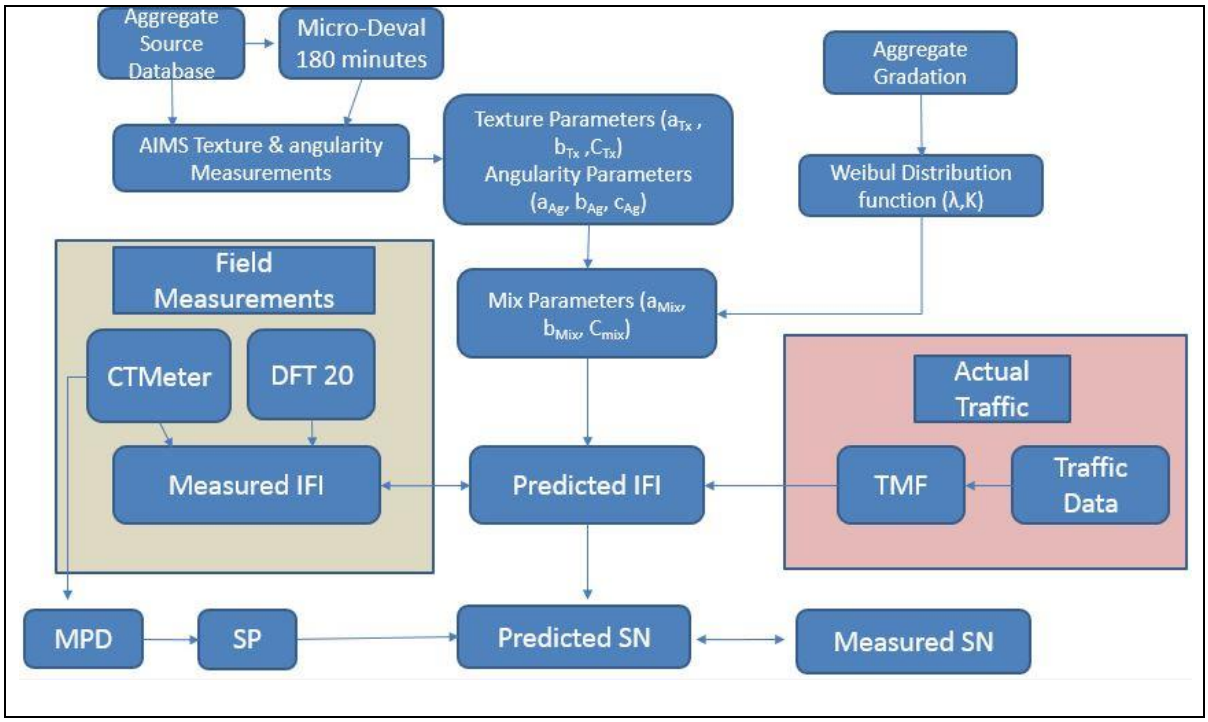

Figure 4-1 Flow Chart of the Research Methodology

4.2 Analysis of Aggregate Texture and Angularity

It should be noted that a total number of 56 different aggregate type/sources were examined this this study. The aggregate shape characteristics were measured using the AIMS

device at three different levels of polishing using the Micro-Deval device: before Micro-Deval (BMD) or without any polishing, after 105 min. of polishing (AMD105), and after 180 min. (AMD180). However, the common practice at TxDOT is to measure the aggregate shape/texture characteristics before and after the micro-Deval abrasion test (0 and 105 min.). The researchers considered both procedures when developing analytical models to describe the change in angularity and texture of aggregates due to abrasion and polishing. Figures 4-3 and 4-4 show examples of change in texture and angularity.

One can see that the loss of texture and angularity is significant after 105 min. of polishing in the Micro-Deval. After that polishing occurs at much slower rate. Equations 3.3 and 3.4 were used to describe the change in aggregate texture and angularity, respectively. Figures 4-5 and 4-6 show examples for the change in texture and angularity with the Micro-Deval polishing time. Figures 4-5 and 4-6 report the regression constants of Eq. 3.3 and 3.4 for the change in texture and angularity, respectively.

Table 4-1 Scale and Shape Parameters of the Weibull Distribution

State	Section ID	λ	k	R^2
Atlanta	IH 30_ATL_SMA_	5.47	1.03	0.94
	US 59_ATL_CMHB-F_FM 2792	5.20	1.11	0.96
	US 59_ATL_TY D_TRM 310	4.34	0.88	0.96
	US 59_ATL_TY D_SHELBY CO LINE	4.46	0.88	0.96
	US 271_ATL_CMHB-F_CAMP	5.20	1.21	0.95
Austin	IH 35 TOM Mix_AUS	4.96	1.44	0.97
	RM 3238_AUS_TOM	3.13	0.97	0.98
	US71_AUS_TOM	5.49	1.59	0.96
Beaumont	IH10_BMT_SMA-D	8.54	1.38	0.94
	SH 82_BMT_SMA-D	8.08	1.07	0.93
	SL 207_BMT_TY D	3.64	0.89	0.97
	US 69_BMT_PFC	10.26	2.45	0.99
	US 90_BMT_SMA-D	8.18	1.18	0.94
Bryan	IH 45_BRY_TY C	5.20	0.90	0.99
	IH 45_BRY_PFC	10.60	4.30	0.99
	SH 6_BRY_NEW PFC	10.95	3.23	0.99
	SH 6_BRY_OLD PFC	10.95	3.23	0.99
Laredo	IH 35_LRD_SMA_WEBB	7.96	1.57	0.96
	IH 35_LRD_SMA-C_LASALLE	9.82	1.56	0.95
Lufkin	US 59_LFK_PFC_Nacodoches	10.50	2.83	0.99
	SH 7_LFK_TY D_Houston	5.82	0.83	0.98
Odessa	IH 20_ODA_SP-C_Martin	5.10	1.03	0.98
	IH 20_ODA_SP-D_Midland_2012	4.76	0.99	0.98
	IH 20_ODA_SP-D_Midland_2013	4.79	0.97	0.97
	US 385_ODA_CMHB-F	5.39	1.65	0.98
	IH 20_ODA_PFC_2004	5.39	1.65	0.98
San Antonio	IH 10_SAT_SMA-D_BEXAR	9.37	1.41	0.92
	IH 10_SAT_TY C_BEXAR	5.10	0.73	0.97
	IH 37_SAT_PFC_BEXAR	10.51	2.99	0.99
YKM	IH 10_YKM_TY D_AUSTIN	3.96	0.85	0.96
	SH 36_YKM_TY D_AUSTIN	4.33	0.92	0.98
PHARR	US 77_PHR_TY D_Kennedy	3.96	0.79	0.98
	US 281_PHR_TY D_Hidalgo	3.81	0.77	0.97
Houston	SH 6 Bwp 2-1, Wp 2-1 Middle	4.85	0.93	0.98
	SH 6 Bwp 2-1 Bottom	2.89	0.69	0.96

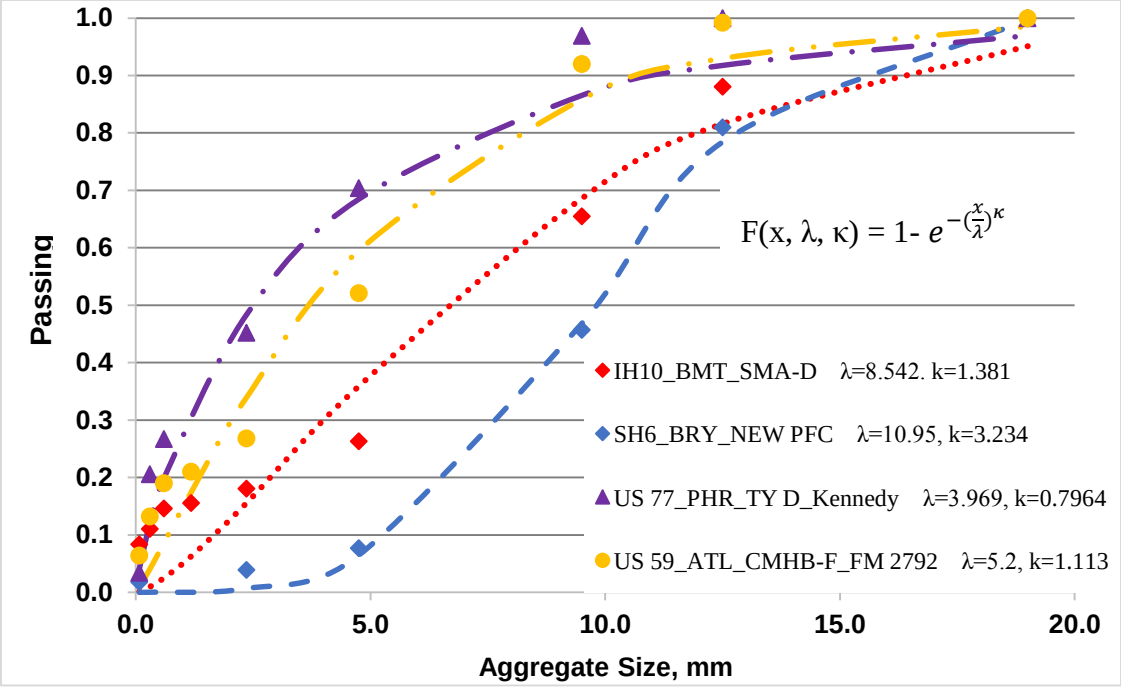

Figure 4-2 Weibull Distribution Function for Different Aggregate Sizes

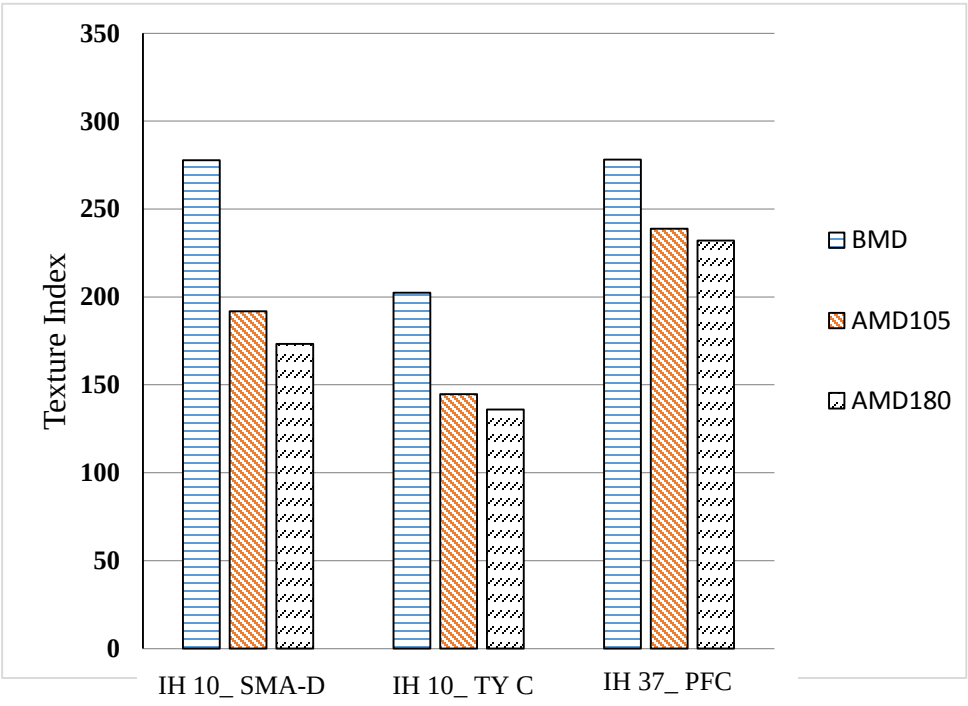

Figure 4-3 Texture Indices of Sections in San Antonio

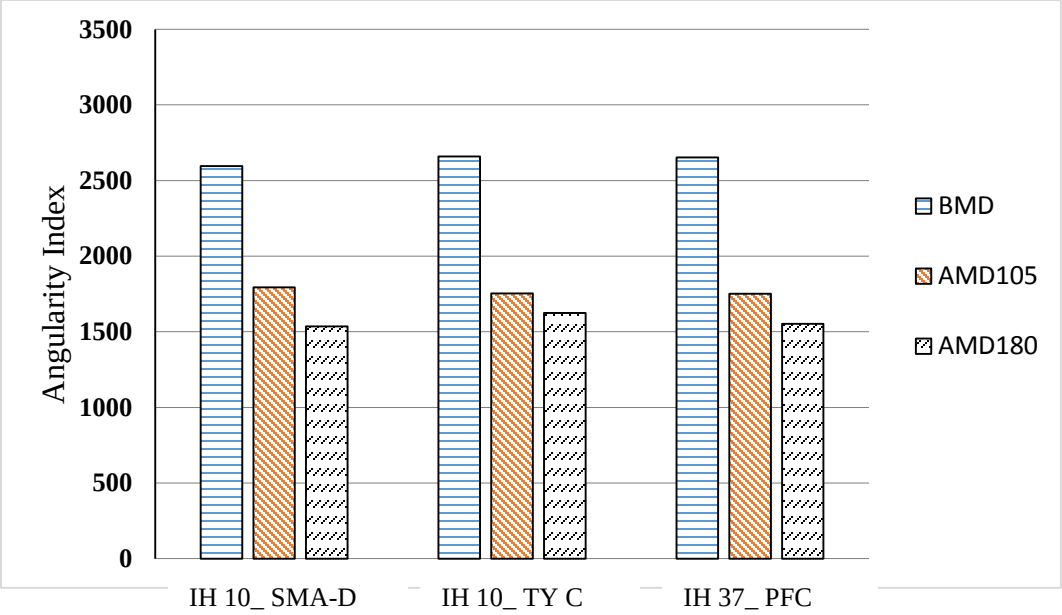

Figure 4-4 Angularity Indices of Sections in San Antonio

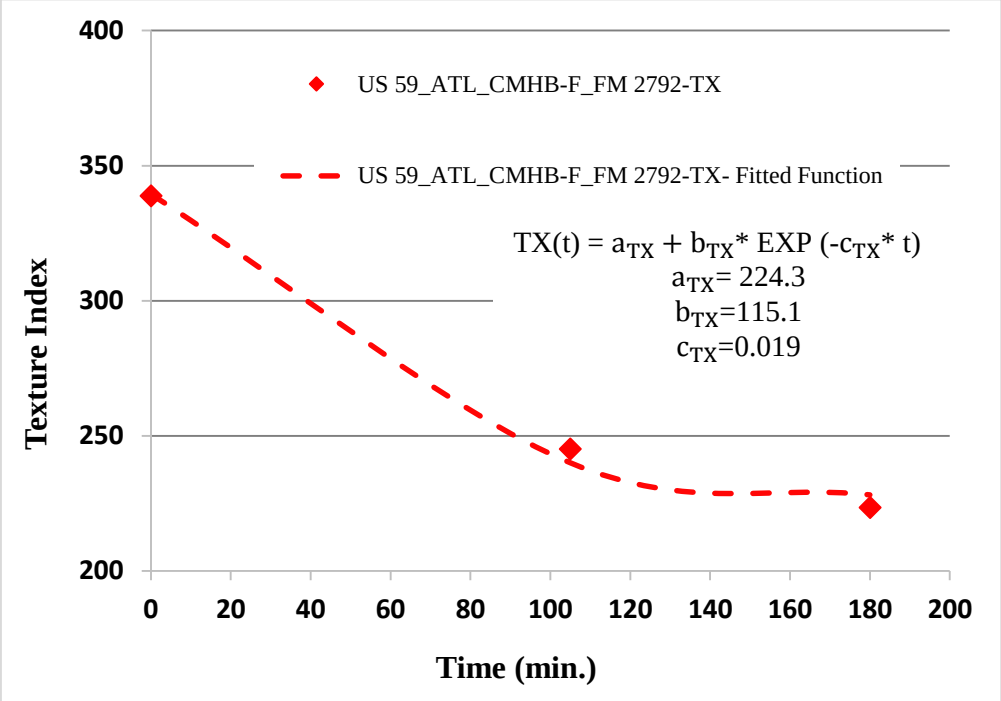

Figure 4-5 Regression Constants for Aggregate Texture

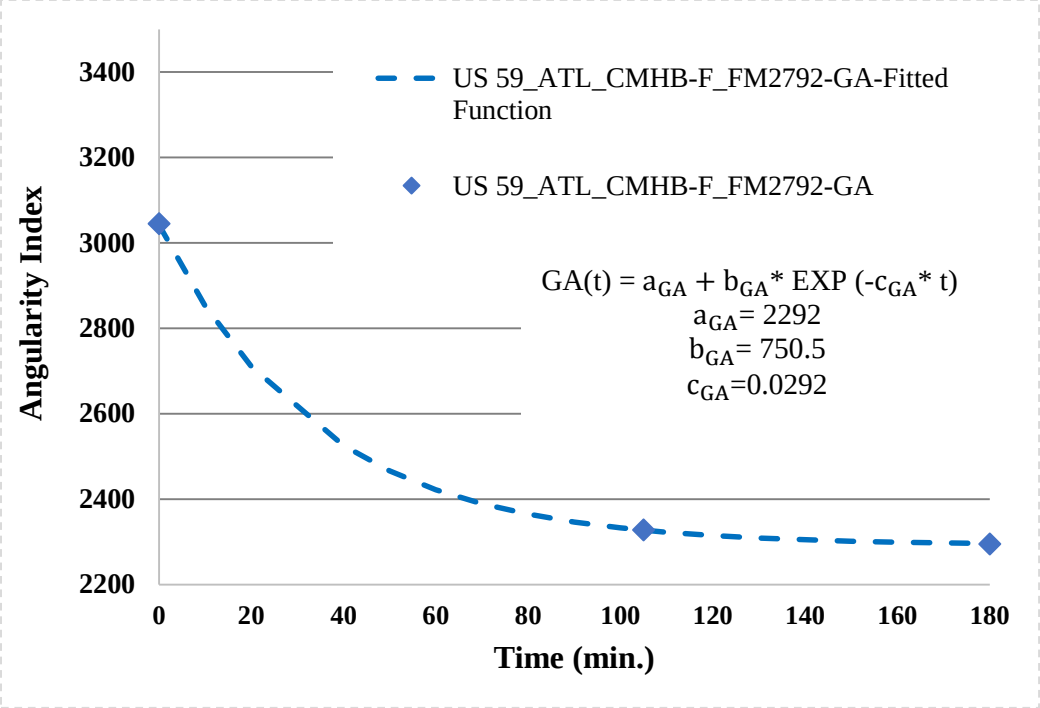

Figure 4-6 Regression Constants for Aggregate Angularity

Determining the regression constants in Eqs. 3.3 and 3.4 requires three points of texture or angularity indices. The researchers used nonlinear regression analysis to predict the regression constants in Eqs. 3.3 and 3.4 using only two points of texture or angularity indices (BMD and AMD105) which is the standard practice at TxDOT. Sixteen aggregates sources were used in the regression analysis to develop equations to predict initial measurements, terminal measurements, and rate of change of texture and angularity. The SPSS software was used for the regression analysis. Equations 4.1 through 4.5 determine the regression parameters for texture loss using two measurements; before micro-Deval (BMD) and after 105 min. of polishing in Micro-Deval (BMD105).

- Texture coefficients:

$$a_{TX} + b_{TX} = 0.999BMD + 0.438 \qquad (R^2 = 1) \qquad (4.1)$$

$$a_{TX} = 0.864\text{AMD} + 14.985 \qquad (R^2 = 0.949) \qquad (4.2)$$

$$c_{TX} = \frac{0.492+\text{TL}}{59.506-(7.106 \text{ x ARI})} \qquad (R^2 = 0.60) \qquad (4.3)$$

$$\text{TL} = \frac{\text{BMD}-\text{AMD}}{\text{AMD}} \qquad (4.4)$$

$$\text{ARI} = \frac{AMD/BMD}{1-(\frac{AMD}{BMD})^2} \qquad (4.5)$$

where

$a_{TX} + b_{TX}$: Initial texture index

a_{TX}: Terminal texture index

c_{TX}: Rate of change in texture

BMD, AMD: texture index before and after 105 min. polishing in Micro-Deval

TL, ARI: texture loss and aggregate roughness index respectively.

Equations 4.6 through 4.10 determine the regression parameters for angularity change based on two measurements; before micro-Deval (BMD) and after 105 min. of polishing in the Micro-Deval (BMD105).

- Angularity coefficients:

$$a_{GA} + b_{GA} = 0.999\text{BMD} + 2.646 \qquad (R^2 = 1) \qquad (4.6)$$

$$a_{GA} = 1.237\text{AMD} - 699.759 \qquad (R^2 = 0.95) \qquad (4.7)$$

$$c_{GA} = \frac{1.891+\text{TL}}{111.658+(1.081 \text{ x ARI})} \qquad (R^2 = 0.61) \qquad (4.8)$$

$$TL = \frac{BMD - AMD}{AMD} \quad (4.9)$$

$$ARI = \frac{AMD/BMD}{1-(\frac{AMD}{BMD})^2} \quad (4.10)$$

where

$a_{GA} + b_{GA}$: Initial angularity index

a_{GA}: Terminal angularity index

c_{GA}: Rate of change in angularity

BMD, AMD: angularity index before and after 105 min. polishing in Micro-Deval.

TL, ARI: Angularity loss and aggregate roughness index respectively.

Table 4-2 presents the regression coefficients of Eqs. 3.3 and 3.4 that describe the change in aggregate texture and angularity for all test aggregates evaluated in HMA tests sections.

Table 4-2 Regression Parameters of Aggregate Texture and Angularity

State	Section ID	Texture Parameters			Angularity Parameters		
		a_{TX}	b_{TX}	c_{TX}	a_{GA}	b_{GA}	c_{GA}
Atlanta	IH 30_ATL_SMA_	137.71	75.16	0.0200	2008	702.81	0.0190
	US 59_ATL_CMHB-F_FM 2792	224.32	115.12	0.0190	2292	750.52	0.0292
	US 59_ATL_TY D_TRM 310	218.13	122	0.0220	2267	786	0.0159
	US 59_ATL_TY D_SHELBY CO LINE	219.21	120.91	0.0190	2265	786.41	0.0159
	US 271_ATL_CMHB-F_CAMP	181.81	174.12	0.0175	1902	583.22	0.0273
Austin	IH 35 TOM Mix_AUS	226.45	103.27	0.0176	1565.35	1063.03	0.0206
	RM 3238_AUS_TOM	231.39	100.01	0.0173	1545.21	1104.08	0.0208
	US71_AUS_TOM	226.28	103.38	0.0176	1566.02	1061.67	0.0206
Beaumont	IH10_BMT_SMA-D	272.21	43.37	0.0180	2587.22	429.82	0.0175
	SH 82_BMT_SMA-D	241.11	136.72	0.0187	2586.64	503.47	0.0178
	SL 207_BMT_TY D	191.83	62.16	0.0230	1919	734	0.0296
	US 69_BMT_PFC	201.37	58.70	0.0172	2110.16	536.56	0.0179
	US 90_BMT_SMA-D	188.64	84.95	0.0177	1607.38	1029.71	0.0204
Bryan	IH 45_BRY_TY C	190.07	93.70	0.0181	1825.43	885.69	0.0195
	IH 45_BRY_PFC	129.29	64.01	0.0181	1307.11	1404.99	0.0227
	SH 6_BRY_NEW PFC	230.85	100.36	0.0168	1547.44	1099.53	0.0208
	SH 6_BRY_OLD PFC	230.85	100.36	0.0168	1547.44	1099.53	0.0208
Laredo	IH 35_LRD_SMA_WEBB	176.86	64.22	0.0175	1466.88	1254.77	0.0217
	IH 35_LRD_SMA-C_LASALLE	227.46	216.73	0.0171	1753.70	1118.91	0.0207
Lufkin	US 59_LFK_PFC_Nacodoches	231.84	115.82	0.0230	2300	786.20	0.0163
	SH 7_LFK_TY D_Houston	223.05	77.28	0.0170	2010.51	852.90	0.0193
Odessa	IH 20_ODA_SP-C_Martin	238.21	128.42	0.0190	1769	974.71	0.0179
	IH 20_ODA_SP-D_Midland_2012	219.52	122.51	0.0172	1706	1028	0.0167
	IH 20_ODA_SP-D_Midland_2013	226.11	116.22	0.0230	1706	1028	0.0167
	US 385_ODA_CMHB-F	282.19	145.36	0.0179	1774.20	993.70	0.0201
	IH 20_ODA_PFC_2004	282.19	145.36	0.0179	1774.20	993.70	0.0201
San Antonio	IH 10_SAT_SMA-D_BEXAR	172.96	105.33	0.0185	1252	1344	0.0207
	IH 10_SAT_TY C_BEXAR	133.52	68.87	0.0177	1576;	1083	0.0172
	IH 37_SAT_PFC_BEXAR	231.51	46.65	0.0178	1431	1223	0.0213
YKM	IH 10_YKM_TY D_AUSTIN	137.43	128.24	0.0180	1279	1374	0.0226
	SH 36_YKM_TY D_AUSTIN	66.84	51.81	0.0177	1558	1215	0.0277
PHARR	US 77_PHR_TY D_Kennedy	199.01	110.46	0.0188	2622.42	279.72	0.0166
	US 281_PHR_TY D_Hidalgo	177.10	121.52	0.0160	2615	189.83	0.0197
Houston	SH 6 Bwp 2-1, Wp 2-1 Middle	239.40	74.46	0.0172	2612.31	590.57	0.0182
	SH 6 Bwp 2-1 Bottom	239.41	74.46	0.0172	2612.31	590.57	0.0182

4.3 Development of Predictive Model for IFI

Masad et al. (2011) and Kassem et al. (2013) developed IFI prediction models. The parameters for the IFI model developed by Masad et al. (2011) (a_{mix}, $a_{mix} + b_{mix}$, and C_{mix}) presented in Eqs. 2.7 through 2.9 relied on factors that describe aggregate texture and its resistance to abrasion and polishing, aggregate gradation and number of polishing cycles in the laboratory. The parameters for the IFI model (a_{mix}, $a_{mix} + b_{mix}$, and C_{mix}) developed by Kassem et al. (2013), presented in Eqs. 2.11 through 2.13, used the same factors, in addition to factors that describe the aggregate angularity. Kassem et al. (2013) demonstrated the measured IFI (Eq. 2.2) and predicted IFI (Eq. 2.6) using the parameters presented in Eqs. 2.11 through 2.13, had better correlation when aggregate angularity is considered in addition to aggregate texture.

In this study, the models proposed by Kassem et al. (2013) were used and calibrated to fit the wide range of aggregates examined in this study. The model developed by Kassem et al. (2013) was based on limited number of aggregate types (soft limestone, intermediate limestone, and sandstone). The study herein evaluated about 56 different aggregate types. The researchers used the SPSS software in the IFI model development. Similar to Kassem et al. (2013), the IFI model include three analytical models for its parameters (a_{mix}, $a_{mix} + b_{mix}$, and C_{mix}). The a_{mix} presents the terminal IFI, the $a_{mix} + b_{mix}$ presents the initial IFI, while C_{mix} presents the rate of change of the IFI. Equations 4.11 through 4.13 show the modified models.

$$a_{mix} = \frac{49.3144 + \lambda}{351.289 - 0.00193(AMD)^2} \tag{4.11}$$

$$a_{mix} + b_{mix} = 0.33 * \ln\left(\frac{1.43757*(a_{TX}+b_{TX})+46.8933*\lambda+333.491*k}{2.42031*(a_{GA}+b_{GA})}\right) + 1.00801 \tag{4.12}$$

$$C_{mix} = 0.018 + 1.654C_{TX} + 1.346C_{GA} \quad (4.13)$$

where

a_{mix}: terminal IFI

$a_{mix} + b_{mix}$: initial IFI

C_{mix}: rate of change in IFI

λ, k: scale and shape parameters of Weibull distribution

AMD: the texture after 150 min. in Micro-Deval

a_{TX}, b_{TX}: regression constants for texture

a_{GA}, b_{GA}: regression constants for angularity

C_{TX}: rate of change in texture

C_{GA}: rate of change in angularity

It should be noted that Eq. 2.6 is a function of the number of polishing cycles in laboratory (N). Since the IFI models (Eqs. 4.11 to 4.13) were revised based on the traffic levels, a relationship developed by Masad et al. (2011) was used to convert the traffic level to corresponding number of polishing cycles (N). This relationship is presented in Eq. 4.14.

$$N = TMF \times 10^{\frac{1}{A+B \times c_{mix}+\frac{C}{c_{mix}}}} \quad (4.14)$$

where

N: number of polishing cycles in thousands

A, B and C: regression coefficients (-0.452, -58.95, 5.843 x 10^{-6}), respectively.

c_{mix}: rate change in IFI

TMF: Traffic Multiplication Factor

The Traffic Multiplication Factor (TMF) is calculated using Eq. 4.15

$$\text{TMF} = \frac{\text{Days between construction and field testing x adjusted traffic}}{1000} \quad (4.15)$$

The adjusted traffic is calculated using Eq. 4.16.

$$\text{Adjusted traffic} = \frac{AADTx\ (100-PTT)x\ DL_{AADT}}{100} + \frac{AADT\ x\ PTT\ \text{ x } DL_{truck}\ x\ 20}{100} \quad (4.16)$$

where

AADT: average annual daily traffic for each section

DL_{AADT}: design lane factor of AADT(depends on number of lanes and urban/rural condition)

DL_{truck}: design lane factor of trucks (depends on number of lanes and urban/rural condition)

PTT: Percent truck traffic

Figure 4-7 shows the correlation between the predicted and measured IFI. The data points in Figure 4-7 include the IFI measurements at the wheel path (WP) and at the shoulder or between the wheel path (BWP). Higher r-squared indicates higher correlations between the predicted and measured IFI.

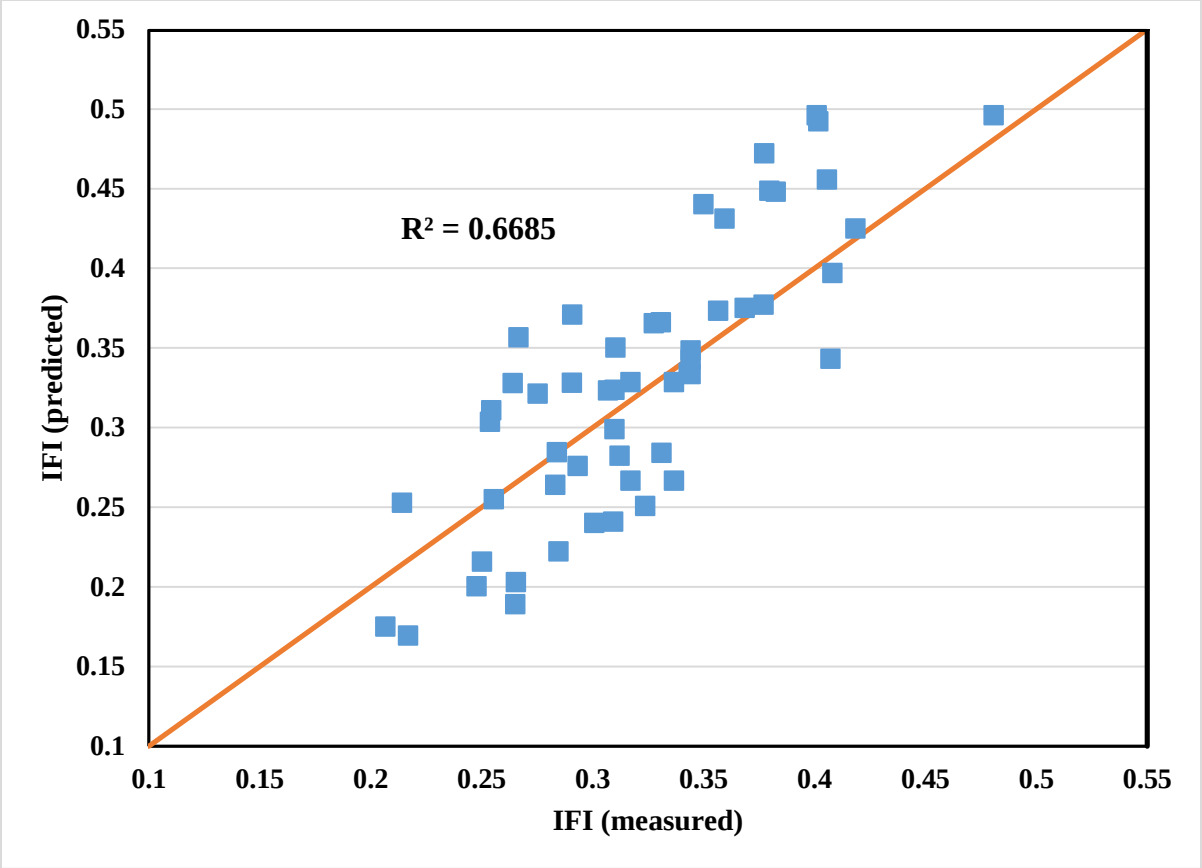

Figure 4-7 Relationship between Predicted and Measured IFI

4.4 Analysis of Mean Profile Depth (MPD)

The researchers also developed a predictive model for MPD as a function of aggregate gradation, polishing cycles (or traffic level). The purpose of this model was to predict MPD if such information is not available for a given mixture. Nonlinear regression was conducted using the SPSS software and the model is presented in Eq. 4.17. Figure 4-8 shows the correlation between the measured MPD and the predicted MPD (r-squared = 0.74). Equation 4.17 indicates that the MPD decreases with traffic and coarser mixture have higher MPD.

$$MPD = (\lambda/34.180) - (0.398/k) + (k^{0.416}) - 0.003N \quad (4.17)$$

where

λ, k: Weibull distribution parameters for aggregate gradation.

N: number of polishing cycles in thousands

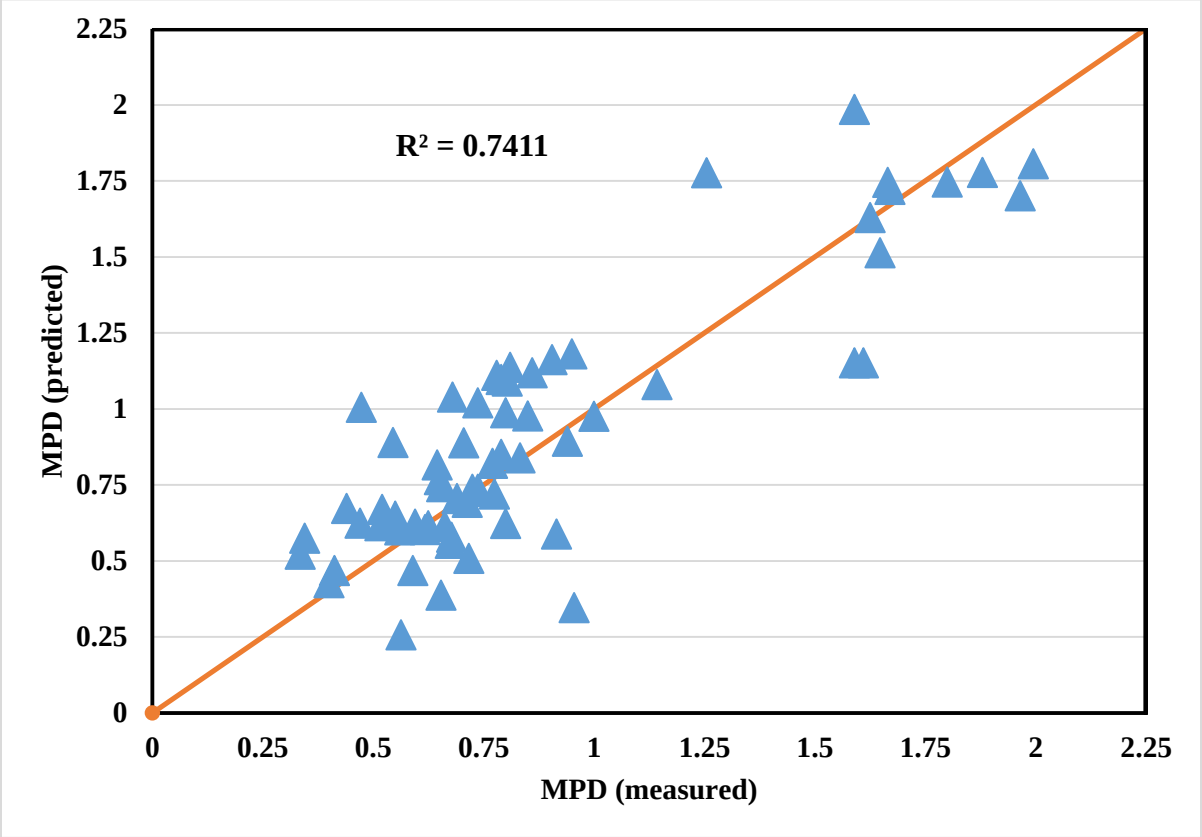

Figure 4-8 Relationship between Measured and Calculated MPD Values

4.5 Skid Number Analysis

The researchers used the developed IFI models (Eq. 2.6 and Eqs. 4.11 through 4.13) to predict skid number at 50 mph (SN[50]) using Eq. 3.6. Equation 4.18 presents a modified form of Eq. 3.6 to account for the difference between calculated and measured skid numbers in this study.

$$SN(50) = 1.97 + 200.4\ (IFI - 0.045)\ e^{\frac{-20}{S_p}} \quad (4.18)$$

where

IFI: predicted international friction index

S_p: speed constant parameter

The predicted SN(50) values calculated using Eq. 4.18 were compared to the SN measured in the field using a skid trailer at 50 mph. Figure 4-9 shows the correlation between the measured and predicted SN. Overall, a good correlation was found between the calculated and measured skid resistance. Although the r-squared has a value of 0.63, such correlation is considered good given the influence of other factors affecting skid resistance (e.g., geometry of roadway, climatic condition, construction quality, etc.). Construction quality can affect the surface characteristics in many ways such as segregation, bleeding of asphalt, and rough surface due to uneven paving. Asphalt bleeding can significantly reduce the skid number; however, it is associated with poor construction practice.

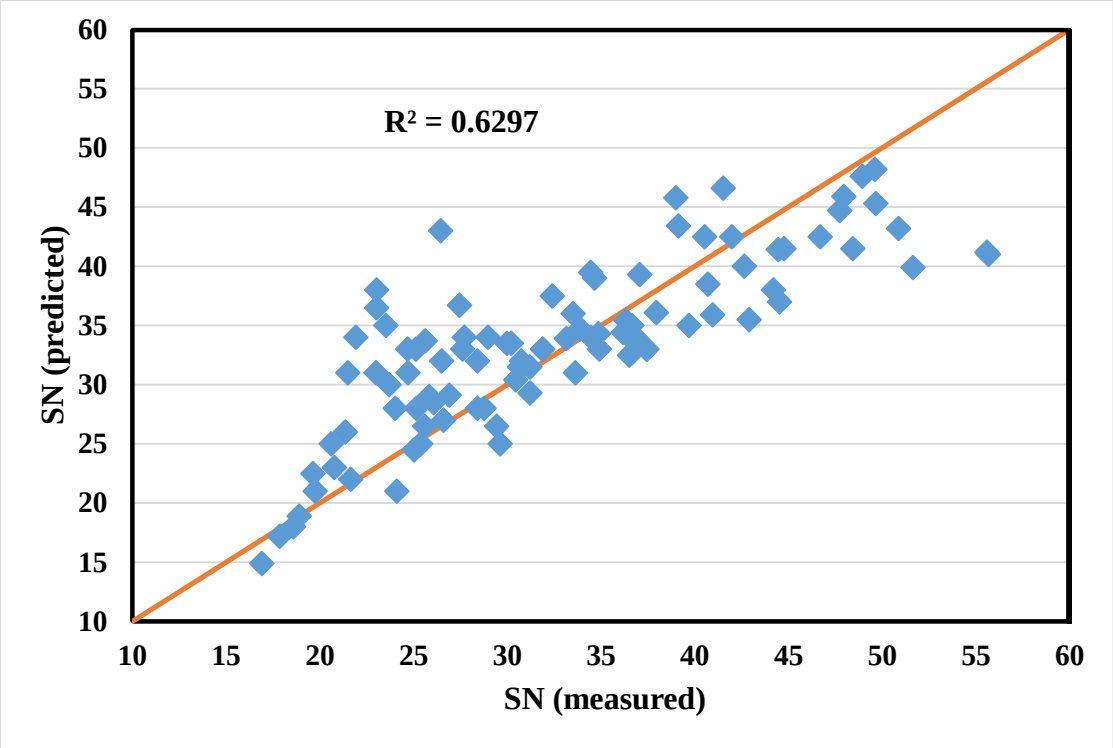

Figure 4-9 Relationship between the measured and predicted SN

The researchers further investigated the effect of the traffic level on the skid resistance. Traffic level is categorized in four groups as presented in Table 4-3. The Traffic level is expressed as TMF as presented in Eq. 4.15. Figure 4-10 shows the range of skid number values at different traffic level. In general, the SN decreased with the increase in the traffic level. Higher traffic level causes more polishing to the surface of asphalt pavements and thus reduces SN.

Table 4-3 Traffic Groups Based on TMF

Level	Traffic Multiplication Factor
Low	0 – 15,000
Medium	15,000 – 40,000
High	40,000 – 90,000
Very High	>90,000

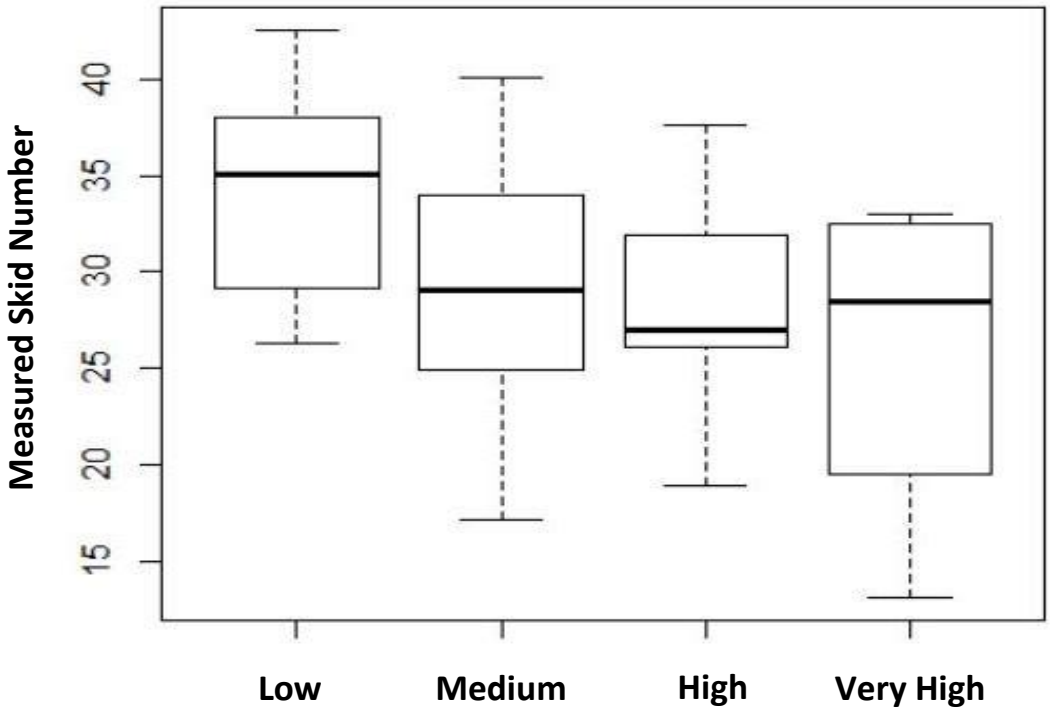

Figure 4-10 Measured Skid Numbers in terms of Traffic Level

4.6 HMA Skid Resistance Model Sensitivity Analysis

Under this section, the researchers examined the sensitivity of the HMA skid resistance model to various factors (e.g., aggregate gradation, type, and traffic level) that affect SN.

Effect of Mixture Gradation

Four mixtures with different aggregate gradations were evaluated; Type-C dense graded mixture, Type-D dense graded mixture (finer than Type-C), porous friction course (PFC), and stone matrix asphalt (SMA-C). The performance of these mixtures in terms of skid number was assessed using the developed model. All variables (e.g., traffic level, aggregate characteristics, etc.) were held constant and only the aggregate gradation was

varied. Figure 4-11 shows that the mixtures with coarse aggregate gradations (such as PFC and SMA-C) had higher skid numbers. The coarse aggregate gradation provides higher macrotexture and thus yields higher SN.

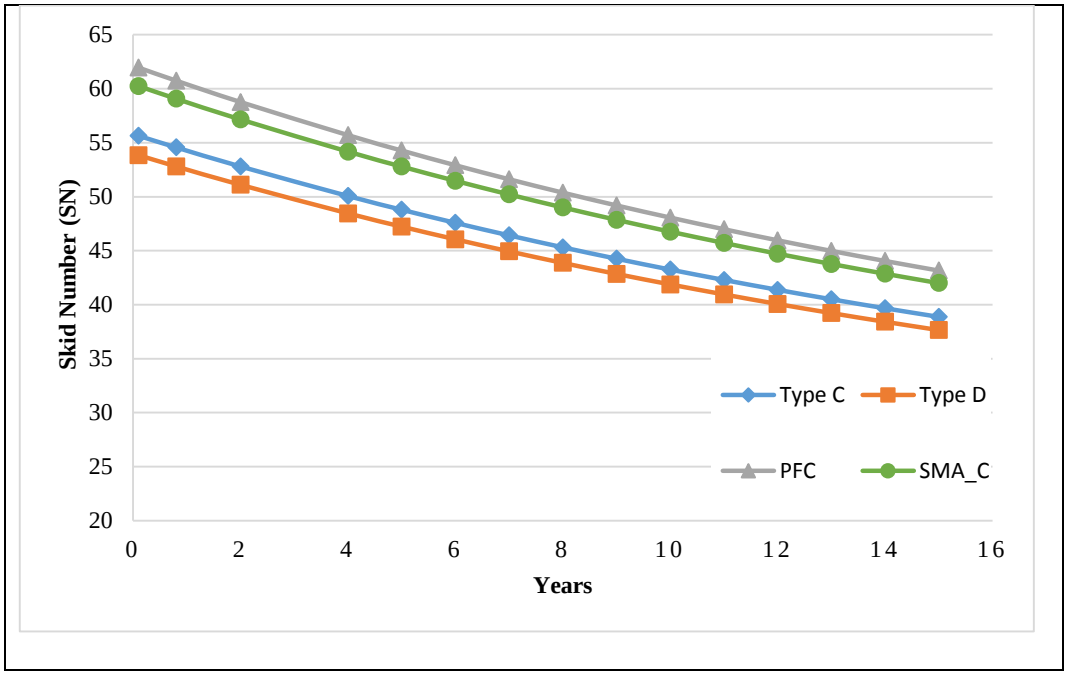

Figure 4-11 Effect of Mixture Gradation on the Skid Number

Effect of Traffic Level

Figure 4-12 shows the effect of different traffic levels or AADT on the skid resistance. The results showed that the skid number decreases with traffic level as expected; however, the SN had a steep slope or reduction at higher traffic levels. Pavement surface experiences most polishing at higher traffic levels which adversely affects the skid resistance.

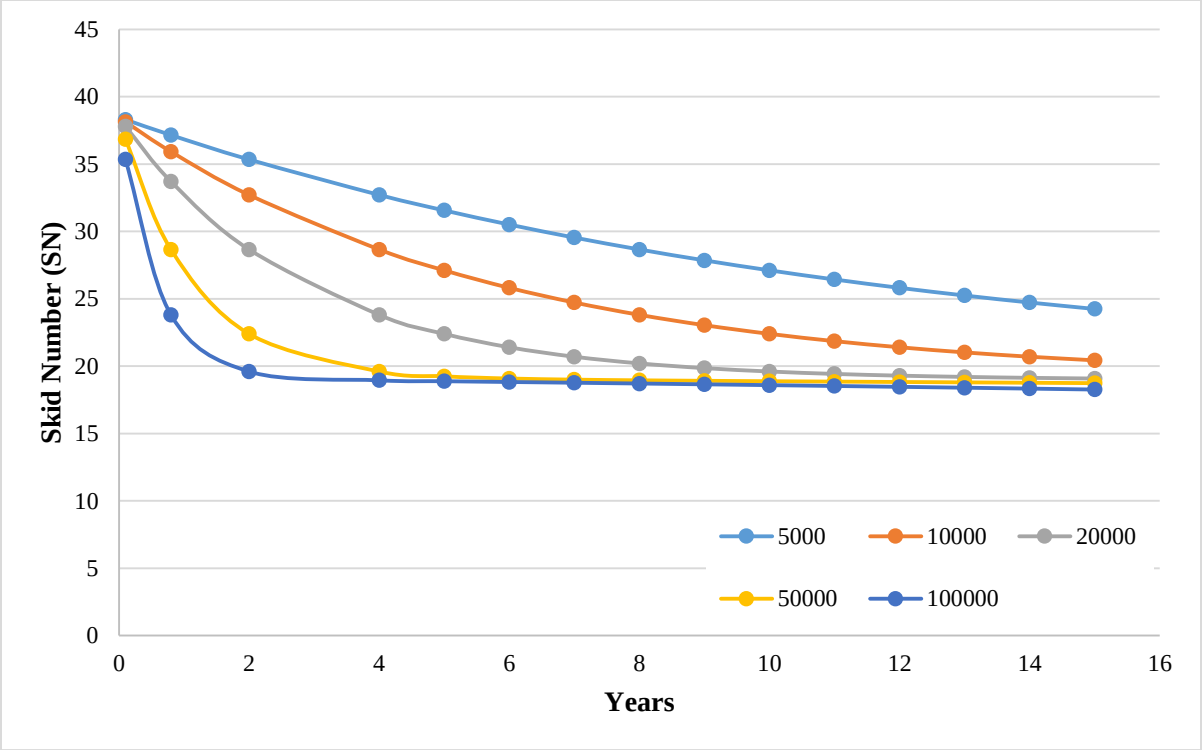

Figure 4-12 Effect of AADT on the Skid Number

Effect of Aggregate Type

Four different aggregate types (e.g. limestone, sandstone, dolomite, and different combinations) were examined. The traffic level and aggregate gradation were fixed. Figure 4-13 demonstrated that HMA mixtures prepared with aggregates with rough texture such as sandstone provide higher skid number and low rate of skid reduction compared to HMA mixtures with soft rock such as limestone. Thus it is recommended to use rough aggregates in asphalt pavements subjected to high traffic levels. Blending of aggregates with higher polishing resistance with local aggregate is recommended when transporting of good quality aggregate is prohibited by cost concern.

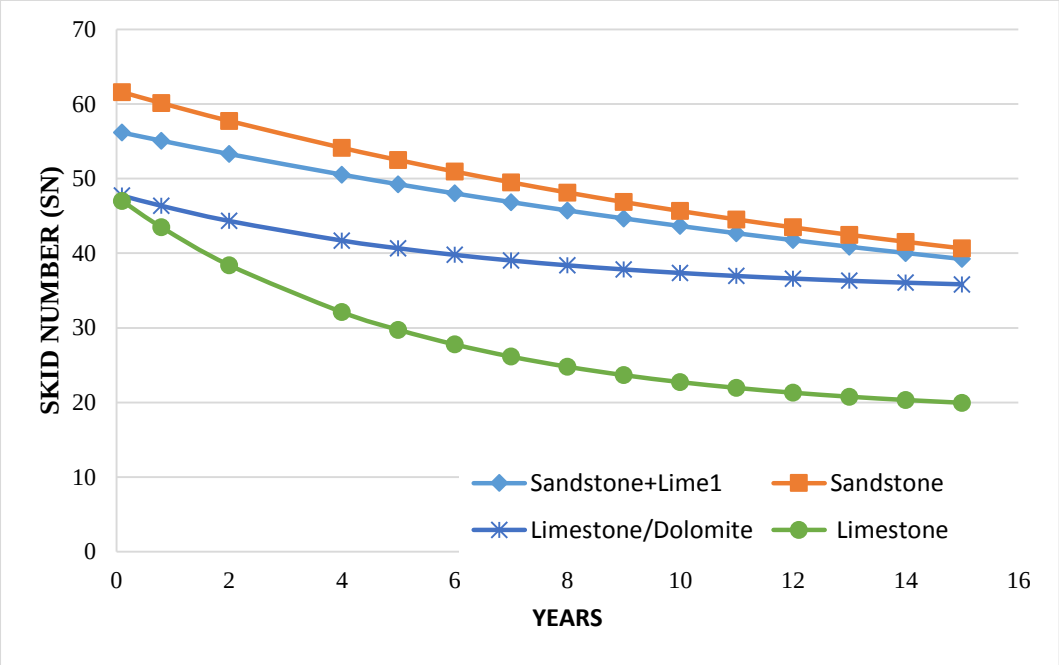

Figure 4-13 Effect of Aggregate Texture on the Skid Number

4.7 SUMMARY

This chapter discussed the steps followed by the researchers in analyzing the field and laboratory data and developing the IFI and SN models. The developed prediction model describes the skid resistance of asphalt pavements as a function of aggregate shape characteristics (texture and angularity), aggregate gradation, and aggregate resistance to polishing and abrasion, and traffic level. The major difference with this model to the one developed by Masad et al. (2011) is the inclusion of aggregate angularity parameter. A good correlation was observed between predicted and measured SN. In addition, different factors affecting the skid resistance were investigated. Coarse aggregate gradation with rough texture provided higher skid resistance compared to aggregate with fine gradation and smooth texture. Also, steep reduction in skid number was observed at higher traffic levels. Higher

truck traffic accelerated the polishing of pavement at even faster rate. The model is capable of predicting the skid resistance over roadway's service life.

CHAPTER 5 - DATA ANALYSIS AND RESULTS FOR SEALCOAT TEST SECTIONS

In this chapter, the researchers performed similar steps described in Chapter 4 to analyze the test results and develop a skid prediction model for the seal coat surface. Figure 4-1 shows a flowchart of key parameters examined and used in developing the predictive models of skid resistance of seal coat surfaces. The researchers developed mathematical indices to evaluate the aggregate resistance to abrasion and polishing and to describe the aggregate gradation. In addition, the researchers analyzed the field measurements and developed models to describe the international friction index (IFI) and skid number (SN).

5.1 Analysis of Aggregate Gradation

The cumulative two-parameter (λ, κ) Weibull distribution (Eq. 3.5) was used to describe the aggregate gradation used in seal coat test sections. There are three aggregate grades of seal coat (Grade 3, Grade 4, and Grade 5). Each grade stands for different aggregate size with Grade 3 being the coarsest. Similar to the HMA, the MATLAB program was used to fit the Weibull function to the gradation of seal coat aggregate sizes. The scale (λ) and shape parameters (κ) were calculated by fitting the aggregate gradation to the cumulative two-parameter Weibull distribution. Table 5-1 presents the scale (λ) and shape (κ) and parameters for the aggregate gradations examined for developing the seal coat skid prediction model. Figure 5-1 shows an example of aggregate gradation of three seal coat sizes. The x-axis represents the aggregate size in millimeters, and y-axis represents the cumulative percent passing of the aggregate. As one can see from Table 5-1 and Figure 5-1, the Weibull distribution function fits very well the aggregate gradation (r-squared = 0.99).

Table 5-1 Scale and Shape Parameters of the Weibull Distribution

Aggregate Grade	No. of sections	λ	κ	R^2
Grade 3	11	12.24	8.80	0.99
Grade 4	19	9.17	5.14	0.99
Grade 5	1	5.55	5.37	0.99

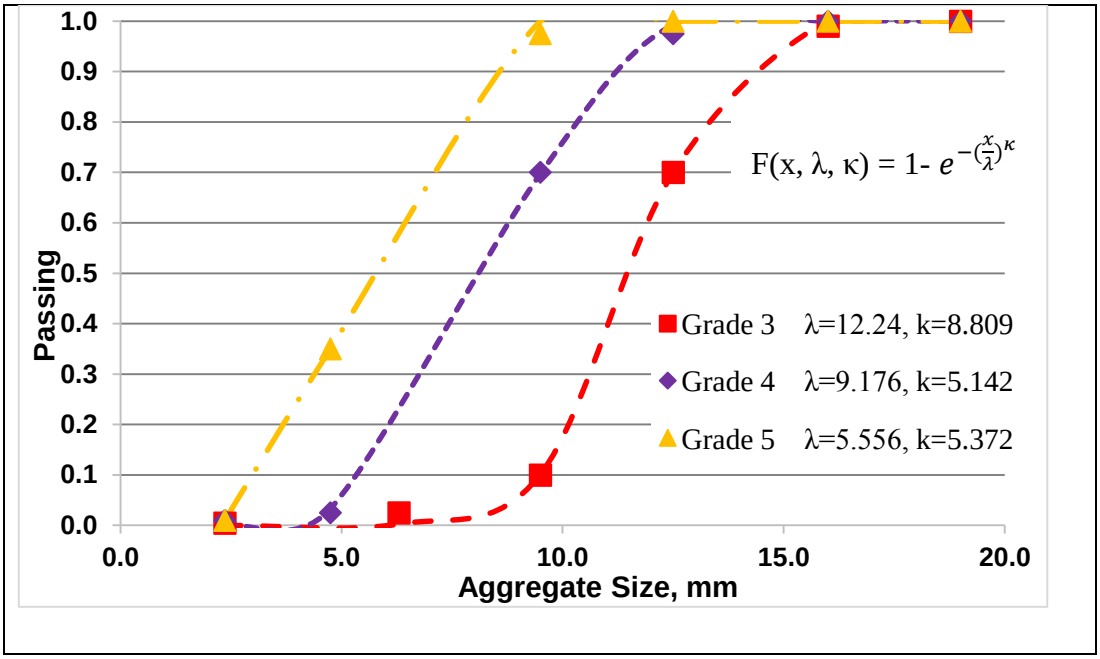

Figure 5-1 Weibull Distribution Function for Different Aggregate Sizes

5.2 Analysis of Aggregate Texture and Angularity

Similar procedure described in Section 4.2 was used in quantifying the aggregate shape characteristics. The AIMS was used to measure the texture and angularity before and after the Micro-Deval abrasion test. Figures 5-2 and 5-3 show examples of the change in texture and angularity of seal coat aggregates due to abrasion and polishing; before Micro-

Deval (BMD), 105 min. after polishing in the Micro-Deval (AMD105), and 180 min. after polishing in the Micro-Deval. Both texture and angularity decreased due to abrasion and polishing. As mentioned earlier, the current practice at TxDOT is to measure the aggregate shape characteristics before and after the micro-Deval abrasion test (0 and 105 min.). The researchers considered both procedures when developing analytical models to describe the change in angularity and texture of aggregates used in seal coat. Figures 5-4 and 5-5 show examples of the regression constants of the texture and angularity, respectively.

The researchers developed models to predict the regression constants in Eqs. 3.3 and 3.4 for the aggregates tested before and after 105 min. of polishing in the Micro-Deval (BMD and AMD105). A total number of 19 aggregates were used in the regression analysis to develop equations to predict initial measurements, terminal measurements, and rate of change of texture and angularity. Also, the SPSS software was used to conduct the regression analysis. Equations 5.1 through 5.10 determine the regression parameters for texture and angularity loss using two measurements; before micro-Deval (BMD) and after 105 min. of polishing in the Micro-Deval (BMD105). It should be noted that Eqs. 5.1 through 5.10 were developed based on the aggregates used in seal coat test sections evaluated in this study, while Eqs. 4.1 through 4.10 were developed based on the aggregates used in HMA test sections evaluated in this study. In the meantime, the researchers recommend measuring the texture and angularity at three different time durations of polishing in Micro-Deval for an accurate characterization.

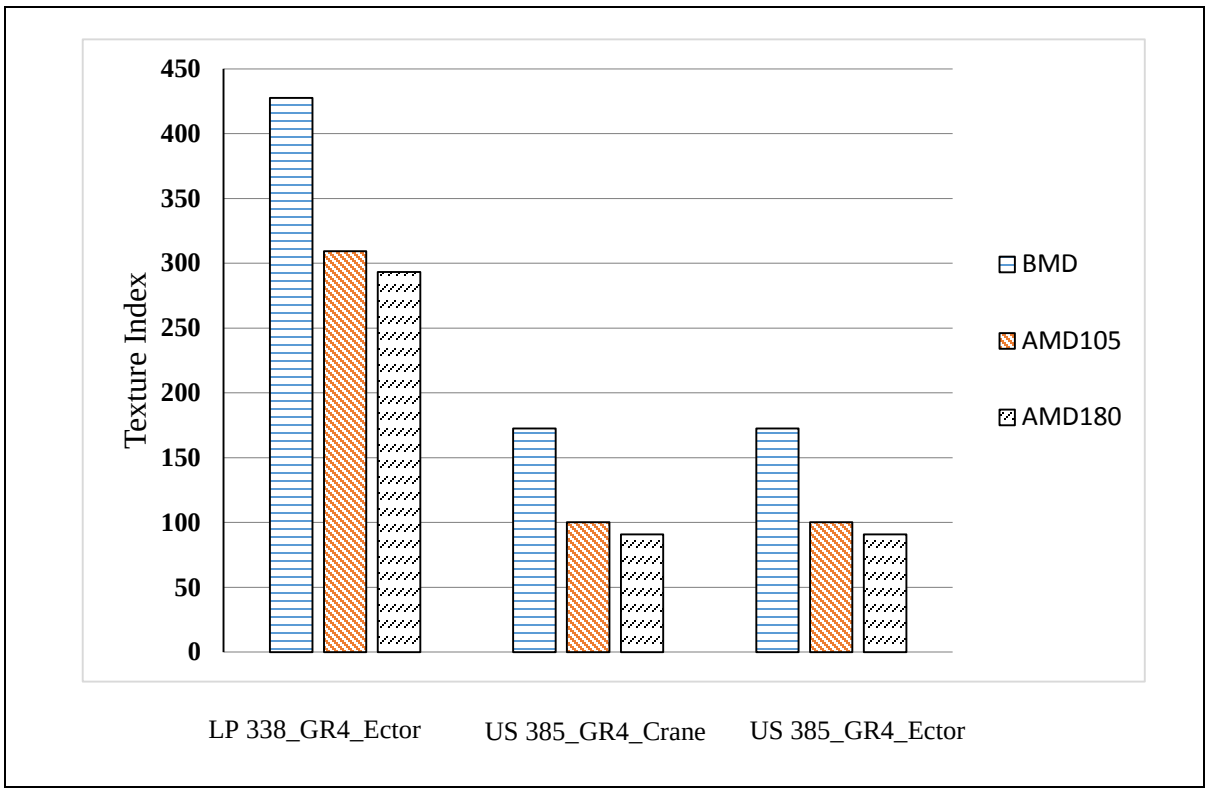

Figure 5-2 Texture Indices of Sections in Odessa

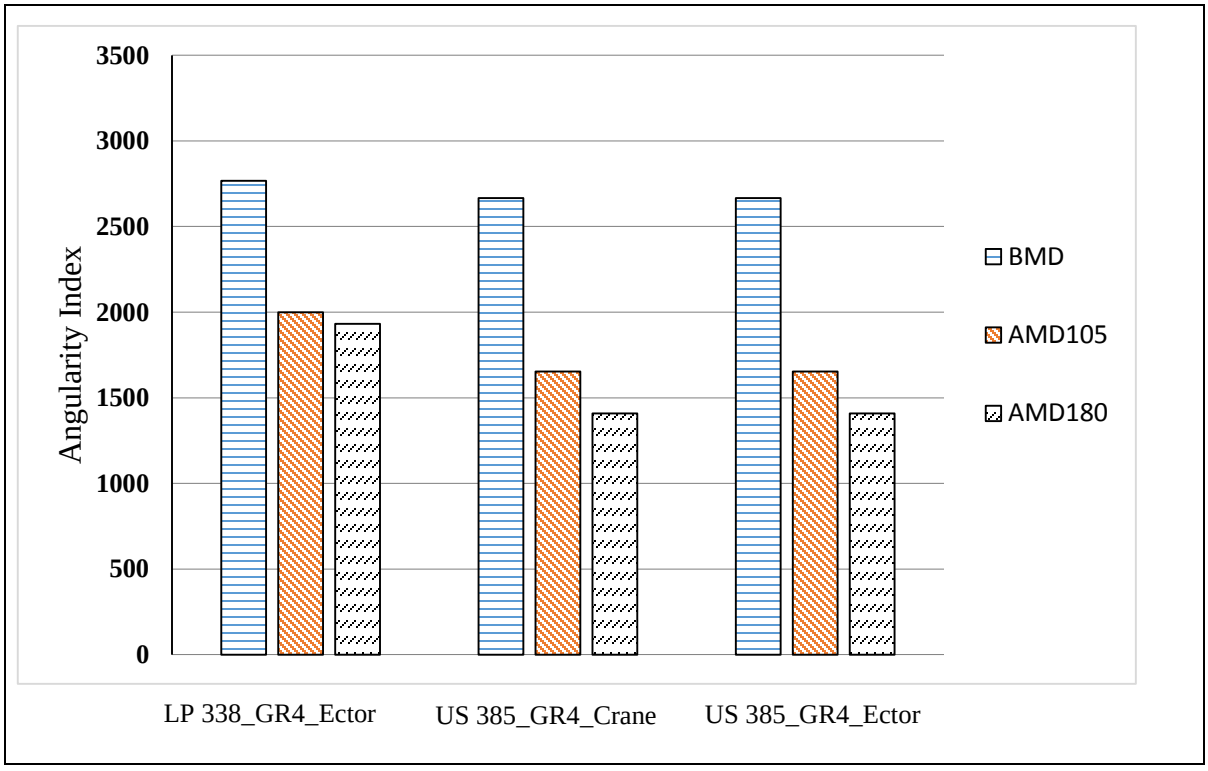

Figure 5-3 Angularity Indices of Sections in Odessa

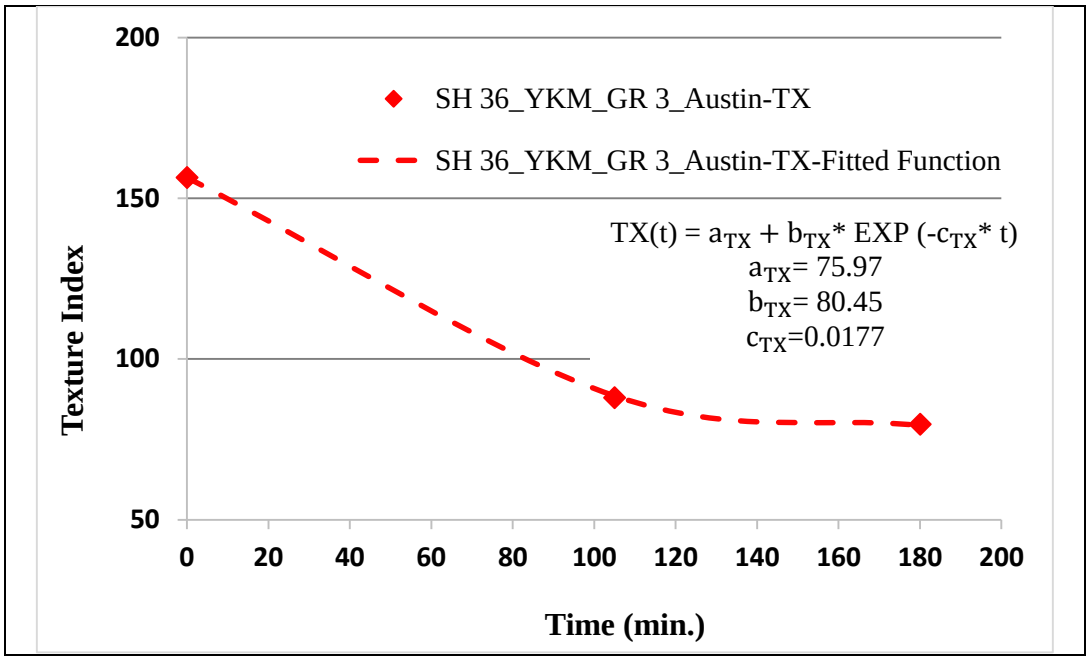

Figure 5-4 Regression Constants for Aggregate Texture

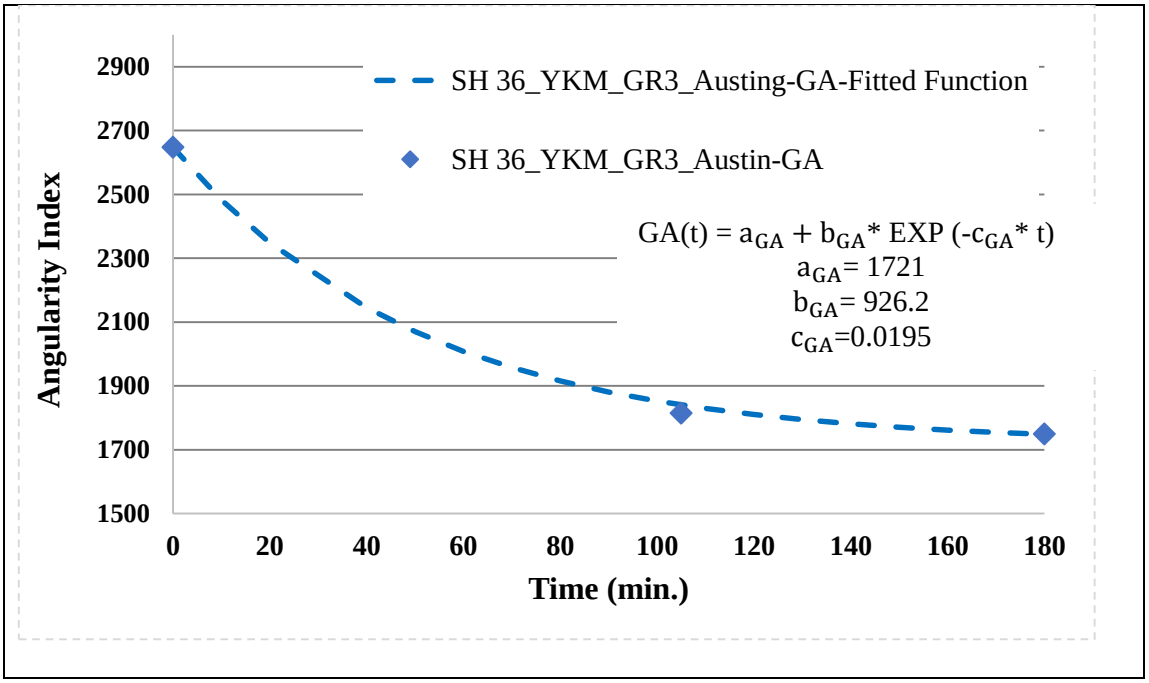

Figure 5-5 Regression Constants for Aggregate Angularity

- Texture model coefficients:

$$a_{TX} + b_{TX} = BMD + 0.134 \qquad (R^2 = 1) \qquad (5.1)$$

$$a_{TX} = 1.011AMD + 17.918 \qquad (R^2 = 0.95) \qquad (5.2)$$

$$c_{TX} = \frac{1.555+TL}{126.995-(18.174 \text{ x } ARI)} \qquad (R^2 = 0.58) \qquad (5.3)$$

$$TL = \frac{BMD-AMD}{AMD} \qquad (5.4)$$

$$ARI = \frac{AMD/BMD}{\sqrt{1-(\frac{AMD}{BMD})^2}} \qquad (5.5)$$

where

$a_{TX} + b_{TX}$: initial texture index

a_{TX}: terminal texture index

c_{TX}: rate of change in texture

BMD, AMD: texture index before and after 105 min. of polishing in Micro-Deval

TL, ARI: texture loss and aggregate roughness index, respectively

- Angularity model coefficients:

$$a_{GA} + b_{GA} = 0.994BMD + 21.084 \qquad (R^2 = 1) \qquad (5.6)$$

$$a_{GA} = 1.232AMD - 648.34 \qquad (R^2 = 0.94) \qquad (5.7)$$

$$c_{GA} = \frac{1.292+TL}{-9.77+(58.155 \text{ x } ARI)} \qquad (R^2 = 0.61) \qquad (5.8)$$

$$TL = \frac{BMD-AMD}{AMD} \qquad (5.9)$$

$$ARI = \frac{AMD/BMD}{1-(\frac{AMD}{BMD})^2} \quad (5.10)$$

where

$a_{GA} + b_{GA}$: initial angularity index

a_{GA}: terminal angularity index

c_{GA}: rate of change in angularity

BMD, AMD: angularity index before and after 105 min. of polishing in Micro-Deval.

TL, ARI: Angularity loss and aggregate roughness index, respectively

Table 5-2 summarizes the regression coefficients of aggregate texture and angularity evaluated in seal coat test sections.

Table 5-2 Regression Parameters of Aggregate Texture and Angularity

State	Section ID	Texture Parameters			Angularity Parameters		
		a_{TX}	b_{TX}	c_{TX}	a_{GA}	b_{GA}	c_{GA}
Pharr	US 77_PHR_GR3_Cameron	211.61	287.86	0.0278	1707	1223	0.0160
	US 281_PHR_GR3_Hidalgo	312.17	269.61	0.0204	1285.62	1309.54	0.0422
	US 281_PHR_GR3_Brooke_TRM 752	211.63	287.84	0.0278	1707	1223	0.0160
	US 281_PHR_GR3_Brooke_TRM 722	312.17	269.61	0.0204	1285.62	1309.54	0.0422
Dallas-FW	US 377_FTW_GR3_Hood	99.72	120.31	0.0195	1426	1253	0.0220
	US 377_FTW_GR3_Tarrant	99.72	120.31	0.0195	1426	1253	0.0220
	SH 199_FTW_GR3_Parker	99.35	95.90	0.0197	1379.59	1275.29	0.0388
Brownwood	US 67_BWD_GR4_Coleman	99.72	120.31	0.0195	1426	1253	0.0220
	US 67_BWD_GR4_Brown	99.72	120.31	0.0195	1426	1253	0.0220
	US 183_BWD_GR4_Eastland	113.72	135.62	0.0178	1484	1257	0.0204
	US 377_BWD_GR4_Brown	99.72	120.32	0.0195	1426	1253	0.0220
San Antonio	US 90_SAT_GR4_Bexar	81.15	66.65	0.0210	1883	780.87	0.0159
	FM 1518_GR3_Bexar	232	34.76	0.0296	1477	1188	0.0161
	SH 16_SAT_GR4_Atascosa_TRM 626	419.22	43.43	0.0168	1931	1213	0.1650
	SH 16_SAT_GR 4_Atascosa_TRM 642	312.17	269.61	0.0204	1285.62	1309.54	0.0422
YKM	SH 36_YKM_GR 3_Austin	75.97	80.45	0.0177	1721	926.22	0.0195
Lufkin	US 59_LFK_GR3_Angelina	433.34	125.42	0.0176	1955.98	1005.25	0.0225
	US 69_LFK_GR4_Angelina	221.09	62.57	0.0176	1011.73	972.41	0.0273
	US 287_LFK_GR4_Trinity	221.09	62.57	0.0176	1011.73	972.41	0.0273
	FM 2213_LFK_GR5_San Augustine	221.09	62.57	0.0176	1011.73	972.41	0.0273
	US 59_LFK_GR4_Shelby	232	34.76	0.0168	1477	1188	0.0167
Odessa	LP 338_ODA_GR4_Ector	287.64	139.91	0.0169	1916	851.62	0.0201
	US 385_ODA_GR4_Crane	86.28	86.17	0.0181	1348	1323	0.0215
	US 385_ODA_GR4_Ector	86.28	86.17	0.0181	1348	1323	0.0215
Beaumont	SH 82_BMT_GR4_Jefferson	221.09	62.57	0.0176	1011.73	972.41	0.0273
	FM 365_BMT_GR4_Jefferson	221.09	62.57	0.0176	1011.73	972.41	0.0273
	FM 105_BMT_GR4_Orange	221.09	62.57	0.0176	1011.73	972.41	0.0273
Atlanta	US 80_ATL-GR4_Harrison	221.09	62.57	0.0176	1011.73	972.41	0.0273
	US 59_ATL_GR3_Cass_RG_TRM238	156.93	34.44	0.0182	2208	483	0.0181
	SH 77_ATL_GR4_Cass_TRM 745_SS	150.62	93.79	0.0179	1726	855.24	0.0195
	SH 77_ATL_GR4_Cass_TRM 720_RG	115	51.46	0.0169	2313	589.66	0.0176

5.3 Development Predictive Model for IFI for Seal Coat

Similar to the IFI models developed for HMA in Section 4.3, IFI models were also developed for seal coat. These models used to describe parameters of IFI (a_{mix}, $a_{mix} + b_{mix}$, and C_{mix}) of Eq. 2.6. There are three models; one for initial IFI ($a_{mix} + b_{mix}$), one for terminal IFI (a_{mix}), and one for the rate of change in IFI (C_{mix}). These models incorporate parameters that describe aggregate gradation, aggregate shape characteristics (texture and angularity) and its resistance to abrasion and polishing. These models provide good correlation between predicted IFI (Eq. 2.6) and measured IFI (Eq. 2.2). These models are presented in Eqs. 5.11 through 5.13. Equation 4.14 was used to convert the traffic level to corresponding number of polishing cycles (N) since Eq. 2.6 is a function of number of polishing cycles in the laboratory (N).

$$a_{mix} = \frac{40.493 + \lambda}{330 - 0.0011(AMD)^2} \tag{5.11}$$

$$a_{mix} + b_{mix} = 0.4 * \ln\left(\frac{1.43757*(a_{TX}+b_{TX})+46.8933*\lambda+3343.491*k}{2.02031*(a_{GA}+b_{GA})}\right) \tag{5.12}$$

$$C_{mix} = 2.654C_{TX} + 1.5C_{GA} \tag{5.13}$$

where

a_{mix}: terminal IFI

$a_{mix} + b_{mix}$: initial IFI

C_{mix}: rate of change in IFI

λ, k: scale and shape parameters of Weibull distribution

AMD: the texture after 150 min. in Micro-Deval

a_{TX}, b_{TX}: regression constants for texture

a_{GA}, b_{GA}: regression constants for angularity

C_{TX}: rate of change in texture

C_{GA}: rate of change in angularity

Figure 5-6 shows the correlation between the predicted and measured IFI. The data points in Figure 5-6 include the IFI measurements at the wheel path (WP) and at the shoulder or between the wheel path (BWP). Good correlation was found between the predicted IFI and measured IFI (r-squared of 0.68). Such correlation is considered fair since other factors may contribute to the change in skid resistance of seal coat over time. Such factors may include bleeding, raveling, etc.

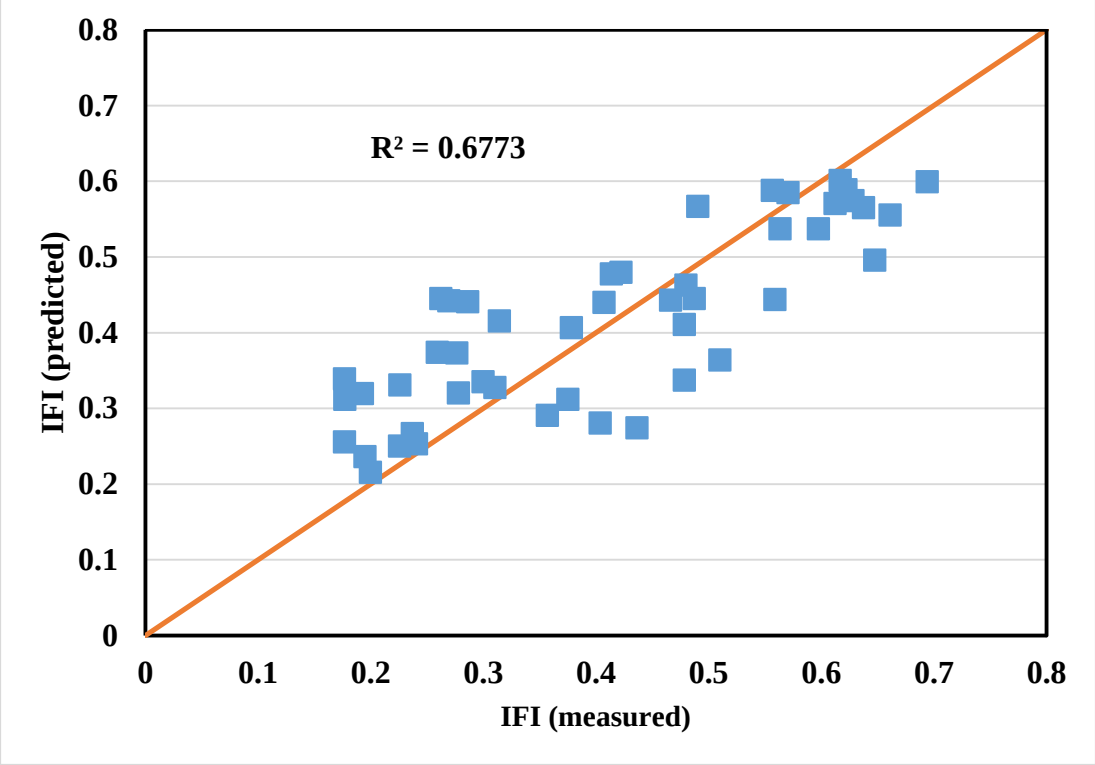

Figure 5-6 Relationship between Predicted and Measured IFI

5.4 Analysis of Mean Profile Depth (MPD)

The researchers also developed a predictive model for MPD as a function of seal coat size and polishing cycles. The purpose of this model was to predict MPD of seal coat surfaces if such information is not available. Nonlinear regression was conducted using the SPSS software and the model is presented in Eq. 5.14. Figure 5-7 shows the correlation between the measured MPD and the predicted MPD (r-squared = 0.53). Such correlation is considered fair given the wide range of seal coat sizes used in the field. Equation 5.14 demonstrated that MPD decreases with traffic and coarser seal coat has higher MPD.

$$MPD = (\lambda/5.403) + (3.491/k) + (k^{0.104}) + N^{-0.47} - 2.594 \quad (5.14)$$

where

λ, k: Weibull distribution parameters for aggregate gradation

N: number of polishing cycles in thousands

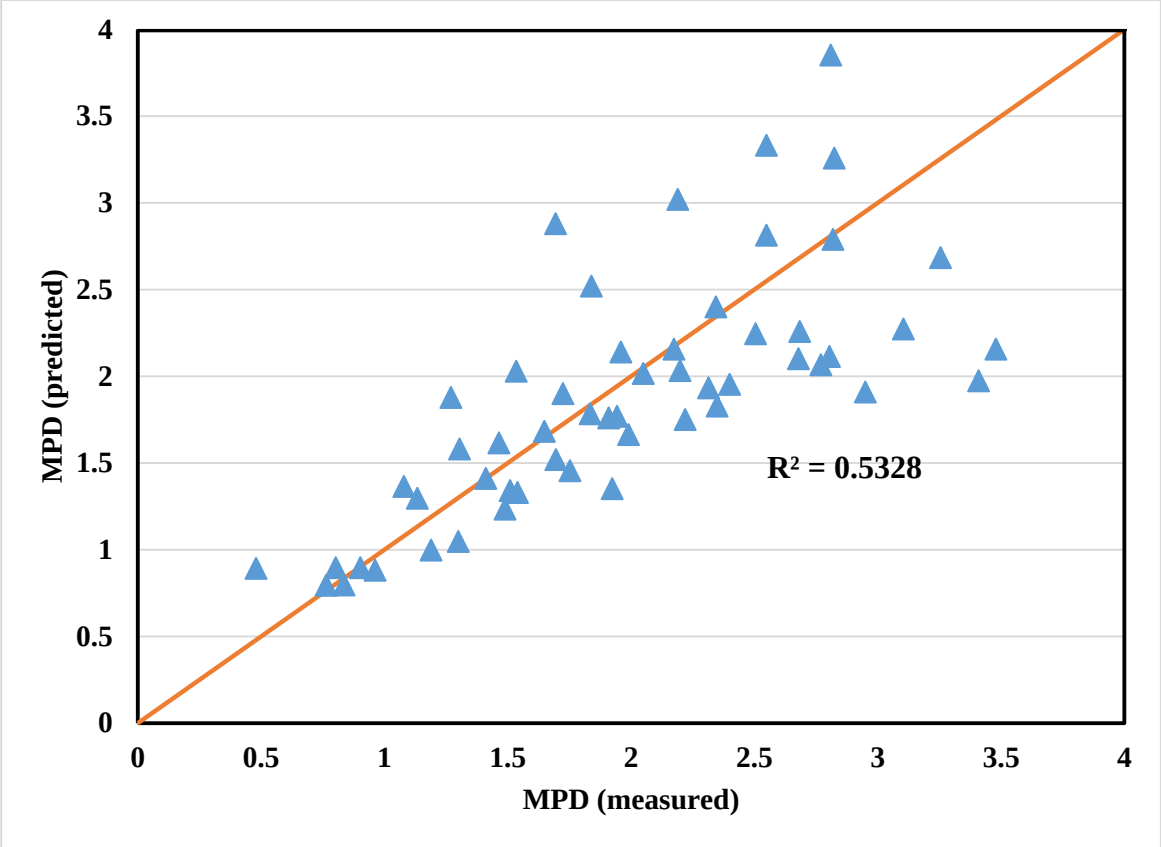

Figure 5-7 Relationship between Measured and Calculated MPD Values

5.5 Skid Number Analysis

The researchers used the developed IFI models (Eq. 2.6 and Eqs. 5.11 through 5.13) to predict the skid number at 50 mph (SN[50]) using Eq. 3.6. Equation 5.15 presents a modified form of Eq. 3.6 to account for the difference between calculated and measured skid numbers of seal coat test sections evaluated in this study.

$$SN(50) = 2.39 + 243.4\,(IFI - 0.045)\,e^{\frac{-20}{S_p}} \quad (5.15)$$

where

IFI: predicted international friction index

S_p: speed constant parameter

The predicted SN(50) values calculated using Eq. 5.15 were compared to the SN measured in the field using a skid trailer at 50 mph. Figure 5-8 shows the relationship between the measured SN values in the field the predicted SN using Eq. 5.15. Fair relationship was found (r-squared = 0.58). Such correlation is considered good for the seal coat surfaces since the skid performance of seal coat is highly affected by the quality of construction. For examples, the researchers noticed that a number of test sections had bleeding.

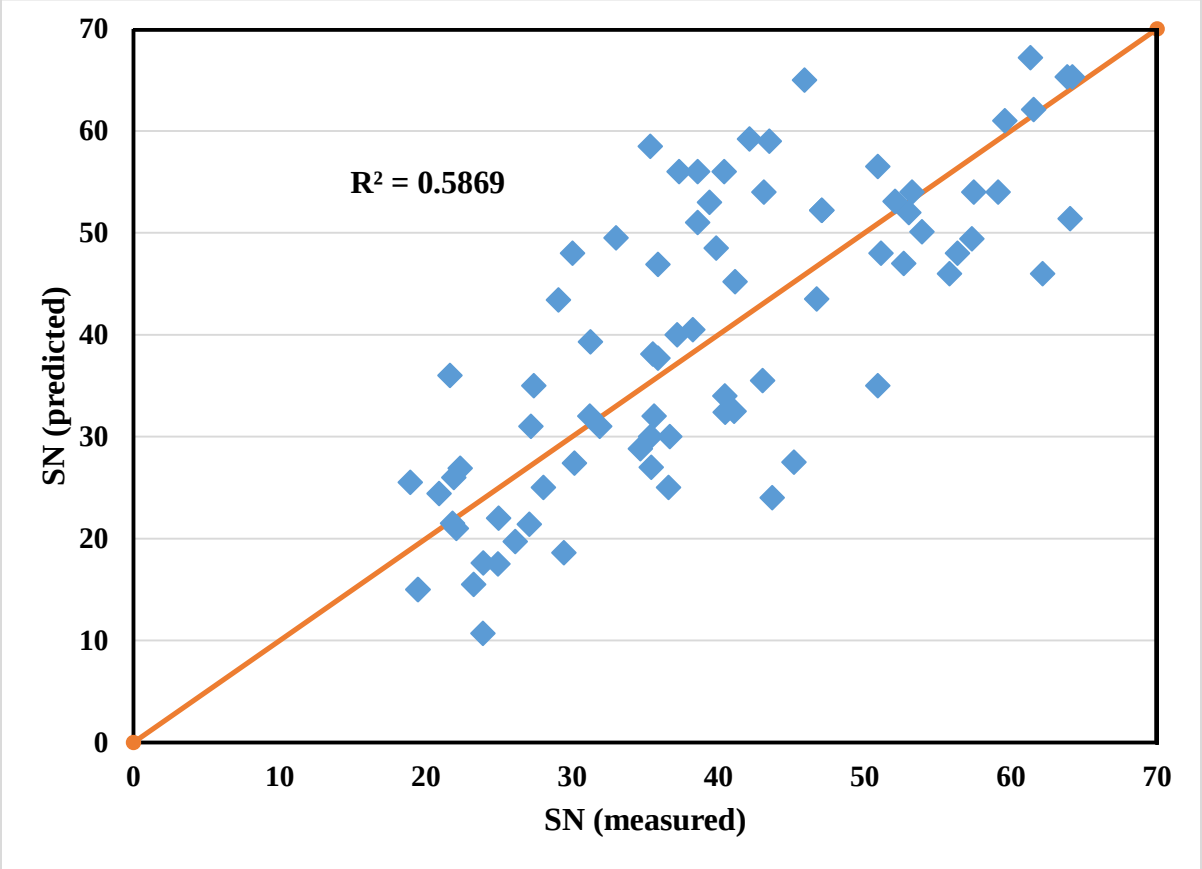

Figure 5-8 Relationship between Measured and Predicted SN

The researchers investigated the effect of the traffic level on the skid resistance of seal coat test sections. The traffic level is categorized in four groups as presented in Table 5-

3. The Traffic level is expressed as TMF as presented in Eq. 4.15. Figure 5-9 shows the range of skid number values for seal coat test sections at different traffic level. Seal coat test sections that experience low traffic level had higher SN and in general the SN decreases with the increase of traffic level. Higher traffic level causes more polishing and steep skid reduction.

Table 5-3 Traffic Groups Based on TMF

Level	Traffic Multiplication Factor
Low	0 – 5,000
Medium	5,000 – 20,000
High	20,000 – 40,000
Very High	>40,000

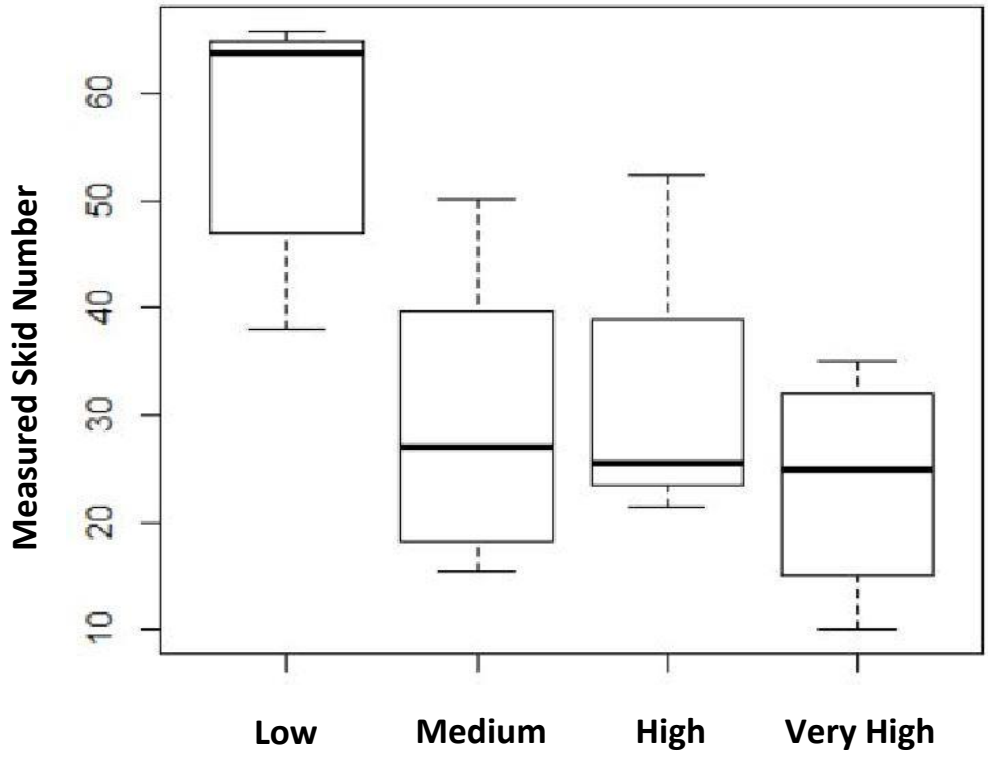

Figure 5-9 Measured Skid Numbers at different Traffic Level

5.6 Seal Coat Skid Resistance Model Sensitivity Analysis

The researchers examined the sensitivity of the seal coat skid resistance model to various factors (e.g., seal coat size, aggregate type, and traffic level) that affect SN.

Effect of Seal Coat Size

Three different sizes of seal coat were examined (Grade 3, Grade 4, and Grade 5). All variables (e.g., traffic level, aggregate characteristics, etc.) were held constant and only the seal coat aggregate size was varied. Figure 5-10 shows the SN with time for the three different seal coat grades. As expected the Grade 3 had higher SN compared to Grade 4 and Grade 5. Grade 3 provides higher macrotexture and thus yields higher SN compared to the other grades.

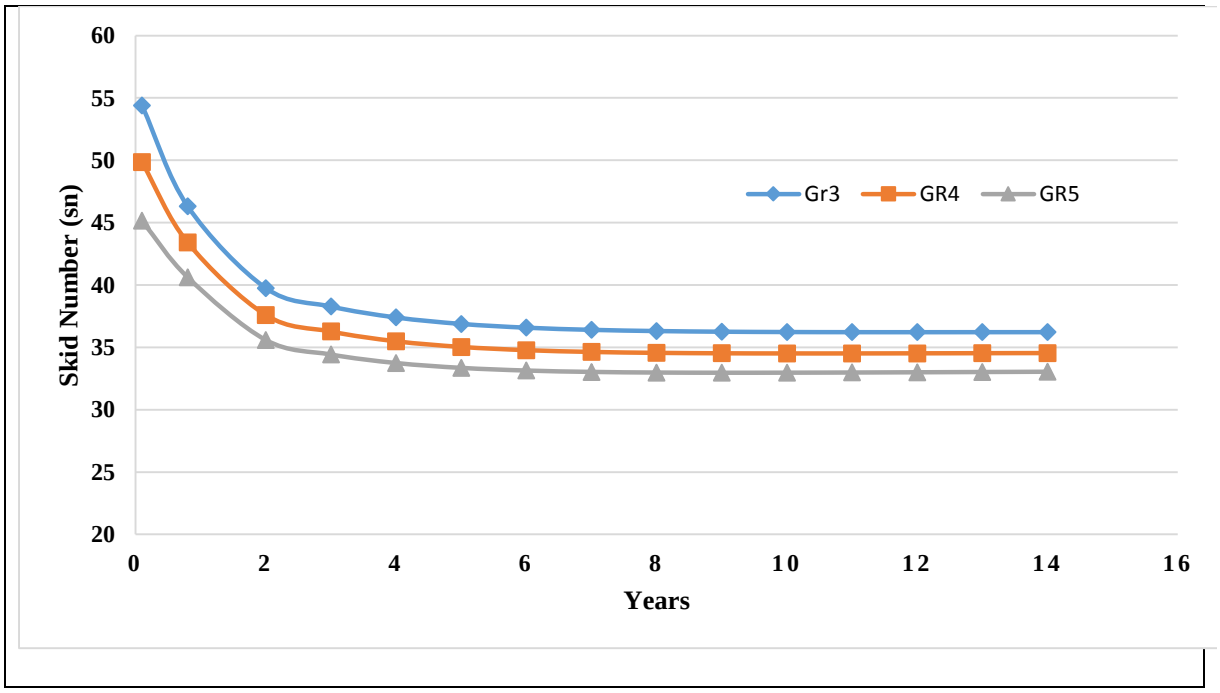

Figure 5-10 Effect of Seal Coat Aggregate Size on the Skid Number

Effect of Traffic Level

Figure 5-11 shows the effect of different traffic levels on skid resistance of seal coat. The results demonstrated that the SN decreases as the traffic increases. Higher traffic level is associated with steep reduction in SN since it causes significant polishing in a relatively short time.

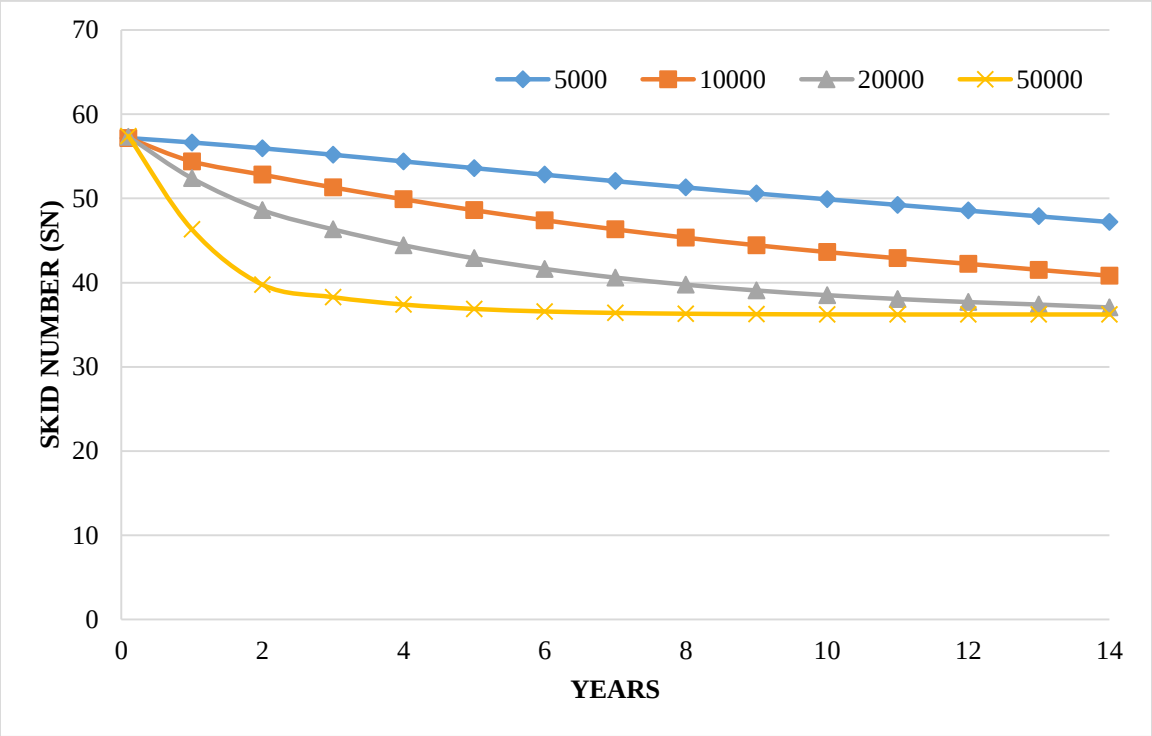

Figure 5-11 Effect of AADT on the Skid Number

Effect of Aggregate Type

Four different aggregate types/sources (e.g. limestone 1 and limestone 2, sandstone, igneous rock) were examined. Other variables including the traffic level and aggregate gradation were held constant. Figure 5-12 demonstrated that seal coat constructed with rough aggregates such as sandstone, that had better resistance to abrasion and polishing, provides

higher skid number and low rate of skid reduction compared to seal coat surfaces constructed with relatively softer rocks (e.g., limestone 1).

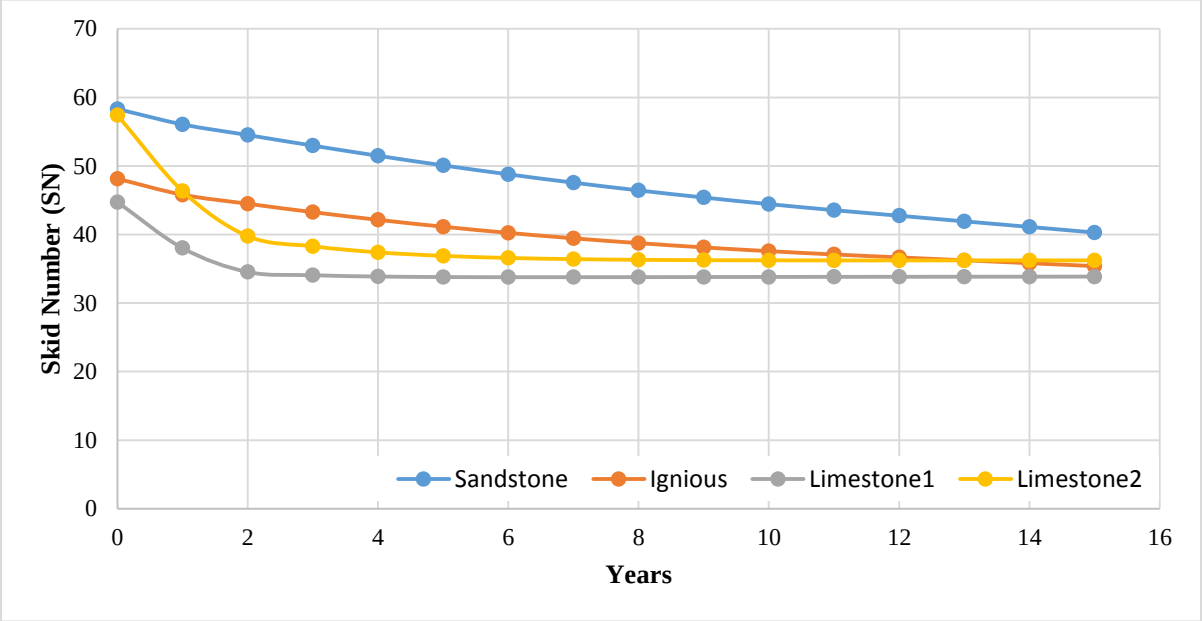

Figure 5-12 Effect of Aggregate Texture on the Skid Number

5.7 SUMMARY

This chapter discussed the development of the IFI and SN models for seal coat. The developed prediction model describes the skid resistance of seal coat as a function of seal coat aggregate size (gradation), aggregate shape characteristics (texture and angularity) and its resistance to polishing and abrasion, and traffic level. A fair correlation was found between predicted and measured SN. In addition, different factors affecting the skid resistance of seal coat were investigated. Grade 3 was found to yield higher MPD and SN compared to other grades. Seal coat constructed with rough aggregates had higher SN compared to seal coat with smooth aggregates. Also, higher traffic level caused steep reduction in skid resistance of seal coat. The model is capable of predicting the skid resistance of seal coat over its service life.

CHAPTER 6 – CONCLUSIONS AND RECOMMENDATIONS

6.1 Conclusions

Skid resistance is a key component in road safety. In this study, the researchers developed prediction models for the international friction index (IFI) and skid number (SN) for flexible pavements with asphalt mixture and seal coat as surface course. These models were developed based on comprehensive testing program in the field and laboratory. Field testing included measurements of coefficient of friction using DFT, MPD using CTMeter, skid number using a skid trailer. In the laboratory, the researchers used test methods to quantify the aggregate resistance to abrasion and polishing, in addition to measurements of aggregate texture and angularity using the AIMS apparatus. Statistical methods were used to develop the prediction models for friction and SN for HMA and seal coat. The main findings of this study can be summarized below.

- The results showed good correlations between the developed models and experimental measurements.
- The developed skid prediction model for HMA incorporate parameters that describe aggregate shape characteristics (texture and angularity), aggregate gradation, aggregate resistance to polishing and abrasion, and traffic level.
- The skid prediction model for seal coat incorporates parameters that describe seal coat aggregate gradation, aggregate shape characteristics (texture and angularity), aggregate resistance to polishing and abrasion, and traffic level.
- The model results demonstrated that aggregate and surface characteristics as well as traffic level to have significant effect on skid resistance and rate of skid reduction.

- Higher traffic level caused steep reduction in skid number due to the significant surface polishing in a short time.
- Asphalt mixtures prepared with coarse aggregate gradations had higher macrotexture and high skid resistance compared to asphalt mixtures with fine aggregate gradations.
- Asphalt mixtures prepared with aggregates with rough surface had higher skid resistance compared to asphalt mixtures with smooth aggregates.
- Seal coat Grade 3 was found to yield higher MPD and skid number compared to other grades.
- The AIMS and Micro-Deval tests were found to be proper tools to evaluate the aggregate shape characteristics and its resistance to abrasion and polishing.
- The models are capable of predicting the skid resistance of HMA and seal coat over their service life.

6.2 Recommendations

Based on the findings of this study, following recommendations are made for implementations and future research.

- These models can be incorporated in a Pavement Management System (PMS) at the network level to plan and program preventive maintenance activities to ensure that pavements have adequate skid resistance.
- These models can be used during mix design procedure to optimize the aggregate selection and aggregate gradation to produce mixtures with adequate friction.
- The skid value of seal coat sections depend highly on the quality of design and construction. Asphalt bleeding can drastically reduce the skid resistance on seal coat

surface regardless of the quality of aggregate. More sections of seal coat should be included in future study.

- It is recommended to validate the skid prediction models for both HMA and seal coat with more field measurements; especially to apply them on conditions different from Texas. Such measurements shall cover more asphalt mixture types, aggregate type and sources, aggregate combinations, traffic levels, and different climatic conditions.
- These prediction models were developed with data obtained from skid testing with smooth tires at 50 mph. In order to apply these models at different conditions, models should be calibrated for local test conditions (i.e., ribbed tire and /or different test speed).
- State DOTs can build their aggregate texture and angularity database under their aggregate quality monitoring program. Mixture designer can use such database in conjunction with skid prediction models to determine the future skid resistance of the intended mixture under traffic.

References

AASHTO (2002). AASHTO Designation TP 58-00: Standard Test Method for Resistance of Coarse Aggregate to Degradation by Abrasion in the Micro-Deval Apparatus. AASHTO Provisional Standards, American Association of State Highway and Transportation Officials, Washington, D.C.

Al Rousan, T. M. (2005). Characterization of aggregate shape properties using a computer automated system (Doctoral dissertation, Texas A&M University).

ASTM, Annual Book of ASTM Standards, Vol. 04.03, American Society for Testing and Materials, West Conshohocken, PA, 2006.

Ahammed, A. M., and Tighe, S. L. (2007). Evaluation of Concrete Pavements Surface Friction Using LTPP Data: Preliminary Analysis and Texture Performance Models. In Transportation Research Board 86th Annual Meeting (No. 07-0727).

Burchett J. L and R. L. Rizenbergs (1980) "Seasonal Variations in the Skid Resistance of Pavements in Kentucky." Transportation Research Record, No. 788.

Cairney, P. (1997). Skid Resistance and Crashes: a review of the literature (No. ARR 311).

Crouch, L., J. Gothard, G. Head, and W. Goodwin (1995). Evaluation of Textural Retention of Pavement Surface Aggregates. Transportation Research Record 1486, Transportation Research Board, Washington, D.C.

Descornet, G. (1989). A criterion for optimizing surface characteristics. Transportation Research Record, (1215).

Dunford, A. (2013). Friction and the texture of aggregate particles used in the road surface course (Doctoral dissertation, University of Nottingham).

Dahir, S. H., and Henry, J. J. (1978). Alternatives for the optimization of aggregate and pavement properties related to friction and wear resistance (No. FHWA-RD-78-209 Final Rpt.).

FHWA, 1990. Nationwide personal transportation survey, NPTS databook, FHWA – Report FHWA-PL-94-010, Federal Highway Administration, U.S. Department of Transportation, Washington, DC.

Fülöp, I. A., Bogardi, I., Gulyas, A., and Csicsely-Tarpay, M. (2000). Use of friction and texture in pavement performance modeling. Journal of Transportation Engineering, 126(3).

Flintsch, G. W., McGhee, K. K., and de Leon, E. (2005). Field validation of macrotexture-based hot mix asphalt segregation detection methods. Journal of the Association of Asphalt Paving Technologists.

Forster, S. W. (1989). Pavement microtexture and its relation to skid resistance. Transportation Research Record, (1215).

Fwa, T. F., Choo, Y. S., and Liu, Y. (2004). Effect of surface macrotexture on skid resistance measurements by the British Pendulum Test. Journal of Testing and Evaluation, 32(4).

Fuentes, L. G. (2009). Investigation of the factors influencing skid resistance and the international friction index (Doctoral dissertation, University of South Florida).Luis, Manjriker Gunaratne, and Daniel Hess. "Evaluation of the effect of pavement roughness on skid resistance." Journal of Transportation Engineering 136.7 (2010).

Gargett, T. (1990). The Introduction of a Skidding-Resistance Policy in Great Britain.

Henry, J. J. (2000). NCHRP Synthesis of Highway Practice 291: Evaluation of Pavement Friction Characteristics. Transportation Research Board, National Research Council, Washington, D.C.

Henry, J. J., and Dahir, S. H. (1979). Effects of Textures and the Aggregates that Produce them on the Performance of Bituminous Surfaces. Transportation Research Record.

Henry, J.J. (1986). Tire Wet-Pavement Traction Measurement: A State-of-the-Art Review. ASTM Special Technical Publication 929: The Tire Pavement Interface. ASTM, Philadelphia.

Hogervorst, D. (1974). Some properties of crushed stone for road surfaces. Bulletin of the International Association of Engineering Geology-Bulletin de l'Association Internationally de Géologie de l'Ingénieur, 10(1).

Hall, J. W., Smith, K. L., Titus-Glover, L., Wambold, J. C., Yager, T. J., & Rado, Z. (2009). Guide for pavement friction. NCHRP Project.

Henry, J.J. and Wambold, J.C. (1992). Use of Smooth-Treaded Test Tire in Evaluating Skid Resistance. Transportation Research Record 1348, Transportation Research Board, National Research Council, Washington, D.C.

Ivey, D. L., D. L. Bullard, J. R. Lock, and L. I. Griffin III (1992). Texas Skid Initiated Accident Reduction Program: Final Report. Report 910-1F, TTI: 2-18-89/910, TX-92/910-1F, Texas Department of Transportation.

Kassem, E., Awed, A., Masad, E., and Little, D. (2013). Development of Predictive Model for Skid Loss of Asphalt Pavements. Transportation Research Record: Journal of the Transportation Research Board, (2372).

Kassem, E., Masad, E., Awed, A., and Little, D. (2012). Laboratory Evaluation of Friction Loss and Compactability of Asphalt Mixtures (No. SWUTC/12/476660-00025-1).

Kennedy, C.K., Young, A.E., and Butler, I.C. (1990). Measurement of Skidding Resistance and Surface Texture and the Use of Results in the United Kingdom.

Kowalski, K. J. (2007). Influence of mixture composition on the noise and frictional characteristics of flexible pavements. ProQuest.

Kane, M., Scharnigg, K., Conter, M., Roe, P., and Schwalbe, G. (2009). Report on different parameters influencing skid resistance, rolling resistance and noise emissions. TYROSAFE Deliverable D.

Krugler, P. E., Freeman, T. J., Wirth, J. E., Wikander, J. P., Estakhri, C. K., and Wimsatt, A. J. (2012). Performance Comparison of Various Seal Coat Grades Used in Texas (No. FHWA/TX-12/0-6496-1).

Mahmoud, E., and Masad, E. (2007). Experimental methods for the evaluation of aggregate resistance to polishing, abrasion, and breakage. Journal of Materials in Civil Engineering, 19(11).

Masad, E., Rezaei, A., Chowdhury, A., and Freeman, T. J. (2010). Field evaluation of asphalt mixture skid resistance and its relationship to aggregate characteristics (No. 0-5627-3). Texas Transportation Institute.

Mahone, D. C. (1975). An Evaluation of the Effects of Tread Depth, Pavement Texture, and Water Film Thickness on Skid Number-Speed Gradients. Virginia Highway and Transportation Research Council, Charlottesville, VA.

Masad, E., Luce, A., Mahmoud, E., and Chowdhury, A. (2007). Relationship of Aggregate Texture to Asphalt Pavement Skid Resistance Using Image Analysis of Aggregate Shape. Final Report for Highway IDEA Project.

Mustaffar, M., bin Che Puan, O., and Chai, L. T. (2004, August). Application of Digital Photogrammetry to Quantification of Road Surface Distresses. In 6 the Malaysian Road Conference.

McQuaid, G., Millar, P., and Woodward, D. (2014). A comparison of techniques to determine surface texture data. In Civil Engineering Research in Ireland Conference, Belfast, Ireland.

National Highway Traffic Safety Administration (NHTSA) (2004). Traffic Safety Facts 2014 – A Compilation of Motor Vehicle Crash Data from the Fatality Analysis Reporting System and the General Estimates System.

Noyce, D. A., Bahia, H. U., Yambo, J. M., and Kim, G. (2005). Incorporating Road Safety into Pavement Management: Maximizing Asphalt Pavement Surface Friction for Road Safety Improvements. Draft Literature Review and State Surveys, Midwest Regional University Transportation Center (UMTRI), Madison, Wisconsin.

Putov, V. V., Putov, A. V., Stotckaia, A. D., Sheludko, V. N., and Ignatiev, K. V. (2016). The measurement method of runway frictional properties correlated with the braking performance of aircraft. In Soft Computing and Measurements (SCM), 2016 XIX IEEE International Conference. IEEE.

Prowell, B. D., Zhang, J., and Brown, E. R. (2005). Aggregate properties and the performance of superpave-designed hot mix asphalt (No. 539). Transportation Research Board.

Rose, J. G., Gallaway, B. M., and Hankins, K. D. (1970). Macrotexture Measurement and Related Skid Resistance at Speeds from 20 to 60 Miles per Hour. Highway Research Record.

Rizenbergs, R.L., Burchett, J.L. and Napier, C.T., 1972. Skid resistance of pavements. Report No.KYHPR-64-24, Part II. Lexington, KY: Kentucky Department of Highways.

Roque, R., Anderson, D., and Thompson, M. (1991). Effect of material, design, and construction variables on seal-coat performance. Transportation research record, (1300).

Rezaei, A., Masad, E., and Chowdhury, A. (2011). Development of a model for asphalt pavement skid resistance based on aggregate characteristics and gradation. Journal of transportation engineering, 137(12).

Shafii, M. A. (2009). Skid resistance and the effect of temperature (Doctoral dissertation, Universiti Teknologi Malaysia).

Sullivan, B. W. (2005, May). Development of a fundamental skid resistance asphalt mix design procedure. In Proceedings, International Conference on Surface Friction, Christchurch, New Zealand.

Saito, K., Horiguchi, T., Kasahara, A., Abe, H., and Henry, J.J. (1996). Development of Portable Tester for Measuring Skid Resistance and Its Speed Dependency on Pavement Surfaces. Transportation Research Record 1536, Transportation Research Board, National Research Council, Washington, D.C.

Smith, H. A. (1977). Pavement contributions to wet-weather skidding accident reduction. Transportation research record, 622.

Sarsam, S. I., and Al Shareef, H. N. (2015). Assessment of texture and skid variables at pavement surface.

Wagner, C., Studdard, J., and Gardiner, M. S. (2004). Evaluation of hot mix asphalt macro- and microtexture. Journal of Testing and Evaluation, 32(1).

Wu, Z., King, B., Abadie, C., and Zhang, Z. (2012). Development of design procedure to predict asphalt pavement skid resistance. Transportation Research Record: Journal of the Transportation Research Board, (2306).

Wambold, J.C., Antle, C.E., Henry, J.J., and Rado, Z. (1995). International PIARC Experiment to Compare and Harmonize Texture and Skid Resistance Measurements: Final Report.

West, T., Choi, J., Bruner, D., Park, H., and Cho, K. (2001). Evaluation of dolomite and related aggregates used in bituminous overlays for Indiana pavements. Transportation Research Record: Journal of the Transportation Research Board, (1757).

Appendix A - Hot Mix Asphalt (HMA)

Table A-1 Sieve Size Analysis

Section ID	Sieve Size, Cumulative Passing %								
	No.200	No.50	No.30	No.16	No.8	No.4	(3/8)"	(1/2)"	(3/4)"
IH 30_ATL_SMA_	8.1	15.9	18	21.1	27.8	49.5	86.3	100	-
US 59_ATL_CMHB-F_FM 2792	6.4	13.2	19	21	26.8	52.1	92	99.2	100
US 59_ATL_TY D_TRM 310	5.6	18.7	22	-	36.8	58.6	93.4	99.1	100
US 59_ATL_TY D_SHELBY CO LINE	5.9	18.3	21.4	-	37.6	56.5	91.8	99	100
US 271_ATL_CMHB-F_CAMP	5.4	15.2	17.6	21.1	25.3	40.3	97.2	100	100
IH 35 TOM Mix_AUS	6.6	10.2	13	17.3	24.1	56.3	100	100	100
RM 3238_AUS_TOM	8.7	14.2	21.1	30.2	47.5	79.4	99.6	100	-
US71_AUS_TOM	6.5	10.7	12.9	16	21	47.3	99.3	100	-
IH10_BMT_SMA-D	8.4	11.1	14.6	15.6	18.1	26.3	65.5	88.1	100
SH 82_BMT_SMA-D	8.8	13.1	15.9	18.5	24.2	30.2	66.5	85.9	100
SL 207_BMT_TY D	4	14.5	26.5	-	40.5	67.9	98.6	100	100
US 69_BMT_PFC	1.6	-	-	-	5.4	14.9	54.3	83	100
US 90_BMT_SMA-D	8.1	11.1	13.8	18	23	28.7	65.1	89	100
IH 45_BRY_TY C	2.8	10.4	15.5	-	35.4	61.3	80.4	-	100
IH 45_BRY_PFC	2	-	-	-	3.1	4.7	45.4	88.9	100
SH 6_BRY_NEW PFC	1.8	-	-	-	3.9	7.7	45.7	81	100
SH 6_BRY_OLD PFC	1.8	-	-	-	3.9	7.7	45.7	81	100
IH 35_LRD_SMA_WEBB	10.1	-	-	-	22.5	30.3	70.1	93.1	100
IH 35_LRD_SMA-C_LASALLE	8	10.7	12.7	15.5	19.8	21.3	47.8	87.8	100
US 59_LFK_PFC_Nacodoches	1.9	-	-	-	3.7	9.5	52.7	80.5	100
SH 7_LFK_TY D_Houston	4.9	14.8	20.8	-	32.6	51.9	78.4	-	100
IH 20_ODA_SP-C_Martin	7.6	12.4	16.1	21.9	30.7	55.7	87	98.5	100
IH 20_ODA_SP-D_Midland_2012	7.8	12.9	17	23.4	34.7	56.5	90.6	99.2	100
IH 20_ODA_SP-D_Midland_2013	7.7	13.7	17.9	24.4	34.1	55.5	90.5	99.2	100
IH 10_SAT_SMA-D_BEXAR	8.1	11.9	13.1	15.5	19	24.1	54.9	86.2	100
IH 10_SAT_TY C_BEXAR	5.2	17.4	24.5	-	39.6	53.9	80.6	-	100
IH 37_SAT_PFC_BEXAR	2	-	-	-	2.8	8.7	52	83	100
IH 10_YKM_TY D_AUSTIN	3.6	17.4	27	-	38.7	61.3	96.2	100	100

SH 36_YKM_TY D_AUSTIN	3.3	13.5	22	-	38.3	60.5	91.1	99.9	100
US 77_PHR_TY D_Kennedy	4.6	16.9	24.4	-	44.6	61.4	89.1	98.8	100
US 281_PHR_TY D_Hidalgo	4.9	20	26.3	-	42.1	64.4	90.4	98.5	100

Section ID	Sieve Size, Cumulative Passing %						
	No. 200	No. 80	No. 40	No. 10	No.4	3/8"	1/2"
SH 6 Bwp 2-1, Wp 2-1 Middle	3.3	8.1	13.5	34.9	58.3	82	99.7
SH 6 Bwp 2-1 Bottom	4.4	19.0	30.1	45.9	69.4	98.4	100
US 385_ODA_CMHB-F	5.6	8	11.3	21.7	49.4	98.9	100
IH 20_ODA_PFC_2004	5.6	8	11.3	21.7	49.4	98.9	100

Table A-2 Aggregate Texture and Angularity Data

Section ID	Texture			Angularity		
	BMD	AMD105	AMD180	BMD	AMD105	AMD180
IH 30_ATL_SMA_	212.865	146.956	139.730	2711.048	2103.727	2031.181
US 59_ATL_CMHB-F_FM 2792	338.796	245.080	223.442	3042.002	2326.436	2295.421
US 59_ATL_TY D_TRM 310	340.293	231.230	223.177	3053.064	2415.128	2312.008
US 59_ATL_TY D_SHELBY CO LINE	340.098	235.487	223.212	3051.622	2412.691	2309.846
US 271_ATL_CMHB-F_CAMP	355.781	211.213	187.858	2485.036	1935.100	1906.148
IH 35 TOM Mix_AUS	329.621	244.752		2628.379	1831.138	
RM 3238_AUS_TOM	331.297	250.479		2649.302	1814.856	
US71_AUS_TOM	329.565	244.562		2627.683	1831.680	
IH10_BMT_SMA-D	315.475	297.725		3017.425	2657.225	
SH 82_BMT_SMA-D	377.775	261.721		3090.563	2656.750	
SL 207_BMT_TY D	253.704	201.486	189.059	2652.508	1951.370	1922.113
US 69_BMT_PFC	259.897	215.728		2646.732	2271.563	
US 90_BMT_SMA-D	273.437	200.993		2637.083	1865.109	
IH 45_BRY_TY C	283.627	202.653		2711.190	2041.385	
IH 45_BRY_PFC	193.050	132.300		2712.175	1622.375	
SH 6_BRY_NEW PFC	331.112	249.844		2646.984	1816.660	
SH 6_BRY_OLD PFC	331.112	249.844		2646.984	1816.660	
IH 35_LRD_SMA_WEBB	240.897	187.361		2721.731	1751.527	
IH 35_LRD_SMA-C_LASALLE	444.207	245.921		2872.847	1983.396	
US 59_LFK_PFC_Nacodoches	347.048	249.150	227.080	3086.559	2442.439	2342.207
SH 7_LFK_TY D_Houston	300.203	240.824		2863.631	2191.003	
IH 20_ODA_SP-C_Martin	366.900	252.524	245.190	2743.733	1917.715	1807.820
IH 20_ODA_SP-D_Midland_2012	342.062	239.151	225.472	2733.780	1884.024	1756.817
IH 20_ODA_SP-D_Midland_2013	342.113	239.193	225.512	2733.800	1884.093	1756.922
US 385_ODA_CMHB-F	427.542	309.266		2768.035	1999.970	
IH 20_ODA_PFC_2004	427.542	309.266		2768.035	1999.970	
IH 10_SAT_SMA-D_BEXAR	277.855	191.877	173.304	2596.041	1794.027	1535.405
IH 10_SAT_TY C_BEXAR	202.321	144.655	135.983	2659.633	1754.349	1625.360
IH 37_SAT_PFC_BEXAR	278.050	238.885	232.119	2653.709	1750.563	1553.372
IH 10_YKM_TY D_AUSTIN	263.446	105.022	84.846	2652.319	1602.676	1394.093
SH 36_YKM_TY D_AUSTIN	118.595	75.3504	68.607	2772.539	1623.814	1565.969
US 77_PHR_TY D_Kennedy	309.350	213		2902.400	2685.675	
US 281_PHR_TY D_Hidalgo	298.826	197.464	185.798	2804.579	2638.757	2620.220
SH 6 Bwp 2-1, Wp 2-1 Middle	313.753	259.750		3203.438	2677.501	
SH 6 Bwp 2-1 Bottom	313.753	259.750		3203.438	2677.501	

Table A-3 Traffic Data

State	Section ID	Design Lane factor for AADT	Design Lane factor for Truck	Average AADT	Avg % Truck Traffic
Atlanta	IH 30_ATL_SMA_	0.7	0.8	13860	37
	US 59_ATL_CMHB-F_FM 2792	0.7	0.9	4478	16.2
	US 59_ATL_TY D_TRM 310	0.7	0.9	5202	15.2
	US 59_ATL_TY D_SHELBY CO LINE	0.7	0.9	6572	22.2
	US 271_ATL_CMHB-F_CAMP	0.4	0.45	13268	15.2
Austin	IH 35 TOM Mix_AUS	0.4	0.5	28317	27.1
	RM 3238_AUS_TOM	0.5	0.5	4540	4.4
	US71_AUS_TOM	0.7	0.9	20500	6.3
Beaumont	IH10_BMT_SMA-D	0.7	0.8	22700	22.5
	SH 82_BMT_SMA-D	0.4	0.45	7764	18.8
	SL 207_BMT_TY D	0.5	0.5	4860	11.9
	US 69_BMT_PFC	0.6	0.8	28164	8.8
	US 90_BMT_SMA-D	0.4	0.45	3928	10.7
Bryan	IH 45_BRY_TY C	0.7	0.8	13150	34
	IH 45_BRY_PFC	0.7	0.8	13150	34
	SH 6_BRY_NEW PFC	0.7	0.9	12860	14
	SH 6_BRY_OLD PFC	0.7	0.9	12120	15
Laredo	IH 35_LRD_SMA_WEBB	0.4	0.5	11400	24
	IH 35_LRD_SMA-C_LASALLE	0.8	0.9	6700	28
Lufkin	US 59_LFK_PFC_Nacodoches	0.8	0.9	13970	22.6
Odessa	IH 20_ODA_SP-C_Martin	0.8	0.9	7614	37.6
	IH 20_ODA_SP-D_Midland_2012	0.8	0.9	7480	37.4
	IH 20_ODA_SP-D_Midland_2013	0.7	0.8	16430	27.4
	US 385_ODA_CMHB-F	0.8	0.9	3642	12.8
San Antonio	IH 10_SAT_SMA-D_BEXAR	0.7	0.8	25330	18.8
	IH 10_SAT_TY C_BEXAR	0.7	0.9	25180	11.7
	IH 37_SAT_PFC_BEXAR	0.7	0.9	13380	21.4
YKM	IH 10_YKM_TY D_AUSTIN	0.7	0.8	20000	25
	SH 36_YKM_TY D_AUSTIN	0.5	0.5	5500	18
PHARR	US 77_PHR_TY D_Kennedy	0.8	0.9	4700	27
	US 281_PHR_TY D_Hidalgo	0.8	0.9	11313	28

A-4 CTMeter Data

Table A-4-1 Beaumont CTMeter Data

CTM, (mm)	Beaumont				
	IH-10	LP-207	SH-82 SMA	US-69	US-90
WP1	0.77	0.67	0.50	1.63	1.02
WP2	0.97	0.69	0.59	1.70	0.98
WP3	0.79	0.68	-	1.58	-
WP4	0.8	0.61	-	1.68	-
BWP1	-	-	-	-	-
BWP2	-	-	-	-	-
BWP3	-	-	-	-	-
BWP4	-	-	-	-	-
Shoulder1	0.6	0.53	0.99	2.77	0.85
Shoulder2	-	-	0.89	-	-
Shoulder3	0.76	0.50	-	2.20	-
Shoulder4	-	-	-	-	-

Table A-4-2 Odessa CTMeter Data

CTM, (mm)	Odessa			
	I-20_Midland_SPD12	I-20_Martin_PFC	I-20_Martin_SPC	I-20_Midland_2013
WP1	0.70	1.61	0.74	0.76
WP2	0.73	1.61	0.77	0.66
WP3	0.71	-	0.70	0.65
WP4	-	-	-	-
BWP1	-	-	0.65	0.82
BWP2	-	-	-	-
BWP3	-	-	-	-
BWP4	-	-	0.65	0.73
Shoulder1	0.8	1.61	-	-
Shoulder2	-	1.57	-	-
Shoulder3	-	-	-	-
Shoulder4	0.65	-	-	-

Table A-4-3 Atlanta CTMeter Data

CTM, (mm)	Atlanta				
	IH-30-ATL	US-59-Panola-CMHBF	US-59-Panola-FM999	US-59-Panola-TRM311	US-271-ATL
WP1	0.61	0.68	0.38	0.52	0.81
WP2	0.68	0.6	0.35	0.53	0.73
WP3	0.71	0.7	0.34	0.6	0.77
WP4	0.71	0.64	0.31	0.59	-
BWP1	0.66	-	-	-	0.71
BWP2	-	-	-	-	-
BWP3	0.79	-	-	-	0.7
BWP4	-	-	-	-	-
Shoulder1	-	0.67	0.69	0.5	0.66
Shoulder2	-	-	-	-	-
Shoulder3	-	0.62	0.56	0.44	0.52
Shoulder4	-	-	-	-	-

Table A-4-4 Pharr and San Antonio CTMeter Data

CTM, (mm)	Pharr		San Antonio				
	US-77-Ken	US-281-TyD	I-10-Bex-SMA	I-10-Bex-TyC	I-37-PFC	US-90-Uvalde	US-281-ATS
WP1	0.73	0.7	0.81	0.57	1.65	0.39	0.52
WP2	0.69	0.64	0.64	0.58	1.58	0.35	0.46
WP3	0.73	0.62	0.76	0.54	1.78	0.33	-
WP4	-	-	-	-	-	-	-
BWP1	-	-	0.93	0.63	1.74	-	2.43
BWP2	-	-	-	-	-	-	2.63
BWP3	-	-	0.63	0.5	1.86	-	-
BWP4	-	-	-	-	-	-	-
Shoulder1	0.33	0.6	-	0.4	-	0.36	-
Shoulder2	-	-	-	-	-	-	-
Shoulder3	0.34	0.58	-	-	-	0.4	-
Shoulder4	-	-	-	-	-	-	-

Table A-4-5 Laredo CTMeter Data

CTM, (mm)	Laredo			
	IH-35-LRD-LAS-NB	IH-35-LRD-LAS-SB	IH-35-LRD-NP-COT-S	IH-35-LRD-LRD-Webb
WP1	0.42	0.48	0.27	1.2
WP2	0.44	0.47	0.24	1.1
WP3	-	0.47	-	1.25
WP4	-	-	-	1.02
BWP1	0.46	-	1.03	-
BWP2	0.51	-	1.07	-
BWP3	-	-	-	-
BWP4	-	-	-	-
Shoulder1	-	0.94	1.19	0.83
Shoulder2	-	-	1.1	-
Shoulder3	-	0.96	-	0.98
Shoulder4	-	-	-	-

Table A-4-6 Lufkin, Houston, and YKM CTMeter Data

CTM, (mm)	Lufkin		Houston	YKM	
	SH7-LFK	US-59-Noco	SH-6	IH-10	SH-36-HMA
WP1	0.62	1.76	1.55	0.45	0.63
WP2	0.6	1.71	1.60	0.45	0.69
WP3	0.61	1.79	1.42	0.36	0.59
WP4	0.55	-	1.74	0.39	0.56
BWP1	0	1.86	-	-	-
BWP2	-	-	-	-	-
BWP3	-	1.81	-	-	-
BWP4	-	-	-	-	-
Shoulder1	0.66	-	1.96	0.71	0.56
Shoulder2	-	-	-	-	-
Shoulder3	0.8	-	2.13	0.64	0.54
Shoulder4	-	-	-	-	-

Table A-4-7 Austin CTMeter Data

CTM, (mm)	Austin		
	FM3328	I35-Austin	SH-71
WP1	0.58	0.82	0.8
WP2	0.51	0.77	0.74
WP3	0.47	0.78	0.83
WP4	-	-	-
BWP1	-	0.84	-
BWP2	-	-	-
BWP3	-	-	-
BWP4	-	-	-
Shoulder1	0.45	-	0.97
Shoulder2	0.43	0.8	0.75
Shoulder3	-	-	-
Shoulder4	-	-	-

Table A-4-8 Bryan CTMeter Data

CTM, (mm)	Bryan			
	IH45-PFC	IH45-TYC	SH6-PFC-new	SH6-PFC-old
WP1	1.30	1	1.80	1.54
WP2	1.21	0.91	1.53	1.71
WP3	-	-	-	-
WP4	-	-	-	-
BWP1	1.59	0.97	2.14	1.89
BWP2	1.59	0.86	1.85	1.87
BWP3	-	-	-	-
BWP4	-	-	-	-
Shoulder1	-	-	-	-
Shoulder2	-	-	-	-
Shoulder3	-	-	-	-
Shoulder4	-	-	-	-

A-5 DFT Data

Table A-5-1 Beaumont DFT Data

DFT at 20 km/hr	Beaumont				
	IH-10	LP-207	SH-82 SMA	US-69	US-90
WP1	0.42	0.50	0.52	0.61	0.53
WP2	0.40	0.54	0.52	0.40	0.54
WP3	0.42	0.55	-	0.38	-
WP4	0.42	0.56	-	0.36	-
BWP1	-	-	-	-	-
BWP2	-	-	-	-	-
BWP3	-	-	-	-	-
BWP4	-	-	-	-	-
Shoulder1	0.7	0.71	0.69	0.49	0.63
Shoulder2	-	-	0.69	-	-
Shoulder3	0.605	0.68	-	0.46	-
Shoulder4	-	-	-	-	-

Table A-5-2 Odessa DFT Data

DFT at 20 km/hr	Odessa			
	I-20_Midland_SPD12	I-20_Martin_PFC	I-20_Martin_SPC	I-20_Midland_2013
WP1	0.53	0.55	0.39	0.49
WP2	0.52	0.57	0.40	0.48
WP3	0.53	-	0.37	0.48
WP4	-	-	-	-
BWP1	-	-	0.49	0.61
BWP2	-	-	-	-
BWP3	-	-	-	-
BWP4	-	-	0.50	0.6
Shoulder1	0.73	0.68	-	-
Shoulder2	-	0.72	-	-
Shoulder3	-	-	-	-
Shoulder4	0.75	-	-	-

Table A-5-3 Atlanta DFT Data

DFT at 20 km/hr	Atlanta				
	IH-30-ATL	US-59-Panola-CMHBF	US-59-Panola-FM999	US-59-Panola-TRM311	US-271-ATL
WP1	0.73	0.49	0.57	0.535	0.71
WP2	0.73	0.51	0.60	0.54	0.71
WP3	0.73	0.53	0.56	0.55	0.73
WP4	0.73	0.54	0.57	0.53	-
BWP1	0.78	-	-	-	0.76
BWP2	-	-	-	-	-
BWP3	0.78	-	-	-	0.73
BWP4	-	-	-	-	-
Shoulder1	-	0.66	0.785	0.72	0.77
Shoulder2	-	-	-	-	-
Shoulder3	-	0.71	0.79	0.74	0.85
Shoulder4	-	-	-	-	-

Table A-5-4 Pharr and San Antonio DFT Data

DFT at 20 km/hr	Pharr		San Antonio				
	US-77-Ken	US-281-TyD	I-10-Bex-SMA	I-10-Bex-TyC	I-37-PFC	US-90-Uvalde	US-281-ATS
WP1	0.47	0.44	0.46	0.49	0.39	-	0.31
WP2	0.46	0.43	0.43	0.48	0.38	0.58	0.28
WP3	0.45	0.43	0.47	0.46	0.4	0.58	-
WP4	-	-	-	-	-	-	-
BWP1	-	-	0.45	0.45	0.31	-	0.60
BWP2	-	-	-	-	-	-	0.63
BWP3	-	-	0.42	0.44	0.33	-	-
BWP4	-	-	-	-	-	-	-
Shoulder1	0.62	0.57	-	0.69	-	0.73	-
Shoulder2	-	-	-	-	-	-	-
Shoulder3	0.61	0.54	-	-	-	0.75	-
Shoulder4	-	-	-	-	-	-	-

Table A-5-5 Laredo DFT Data

DFT at 20 km/hr	Laredo			
	IH-35-LRD-LAS-NB	IH-35-LRD-LAS-SB	IH-35-LRD-NP-COT-S	IH-35-LRD-LRD-Webb
WP1	0.39	0.37	0.205	0.43
WP2	0.40	0.37	0.225	0.44
WP3	-	0.36	-	0.40
WP4	-	0.36	-	0.46
BWP1	0.43	-	-	-
BWP2	0.42	-	0.54	-
BWP3	-	-	-	-
BWP4	-	-	-	-
Shoulder1	-	0.57	0.61	0.62
Shoulder2	-	-	0.62	-
Shoulder3	-	0.54	-	0.63
Shoulder4	-	-	-	-

Table A-5-6 Lufkin, Houston, and YKM DFT Data

DFT at 20 km/hr	Lufkin		Houston	YKM	
	SH7-LFK	US-59-Noco	SH-6	IH-10	SH-36-HMA
WP1	0.63	0.45	0.41	0.40	0.29
WP2	-	0.4	0.44	0.41	0.33
WP3	0.61	0.43	0.41	0.40	0.30
WP4	0.59	-	0.40	0.41	0.29
BWP1	-	0.53	-	-	-
BWP2	-	-	-	-	-
BWP3	-	0.46	-	-	-
BWP4	-	-	-	-	-
Shoulder1	0.74	-	0.40	0.59	0.61
Shoulder2	-	-	-	-	-
Shoulder3	0.76	-	0.45	0.64	0.63
Shoulder4	-	-	-	-	-

Table A-5-7 Austin DFT Data

DFT at 20 km/hr	Austin		
	FM3328	I35-Austin	SH-71
WP1	0.64	0.49	0.49
WP2	0.65	0.44	0.50
WP3	0.65	0.49	0.51
WP4	-	-	-
BWP1	-	-	-
BWP2	-	0.56	-
BWP3	-	-	-
BWP4	-	-	-
Shoulder1	0.84	-	0.62
Shoulder2	0.86	0.57	0.63
Shoulder3	-	-	-
Shoulder4	-	-	-

Table A-5-8 Bryan DFT Data

DFT at 20 km/hr	Bryan			
	IH45-PFC	IH45-TYC	SH6-PFC-new	SH6-PFC-old
WP1	0.35	0.34	0.31	0.36
WP2	0.33	0.34	0.29	0.35
WP3	-	-	-	-
WP4	-	-	-	-
BWP1	0.41	0.37	0.37	0.45
BWP2	0.39	0.33	0.33	0.44
BWP3	-	-	-	-
BWP4	-	-	-	-
Shoulder1	-	-	-	-
Shoulder2	-	-	-	-
Shoulder3	-	-	-	-
Shoulder4	-	-	-	-

Appendix B – Sealcoat

Table B-1 Aggregate Gradation (Cumulative % Retained)

Sieve Size	Cumulative Retained (%)		
	Grade 3	Grade 4	Grade 5
1``	-	-	-
7/8 ``	-	-	-
3/4 ``	0	-	-
5/8 ``	0-2	0	-
1/2 ``	20-40	0-5	0
3/8``	80-100	20-40	0-5
1/4 ``	95-100	-	-
No.4	-	95-100	50-80
No.8	99-100	98-100	98-100

Table B-2 Aggregate Texture and Angularity Data

Section ID	Texture			Angularity		
	BMD	AMD105	AMD180	BMD	AMD105	AMD180
US 77_PHR_GR3_Cameron	499.365	227.121	213.534	2926.364	1945.145	1735.848
US 281_PHR_GR3_Hidalgo	581.650	326.500		2589.625	1569.775	
US 281_PHR_GR3_Brooke_TRM 752	499.365	227.121	213.534	2926.364	1945.145	1735.848
US 281_PHR_GR3_Brooke_TRM 722	581.650	326.500		2589.625	1569.775	
US 377_FTW_GR3_Hood	219.709	125.641	105.146	2676.475	1702.489	1496.160
US 377_FTW_GR3_Tarrant	219.709	125.641	105.146	2676.475	1702.489	1496.160
SH 199_FTW_GR3_Parker	195.125	116		2649.700	1646.050	
US 67_BWD_GR4_Coleman	219.709	125.641	105.146	2676.475	1702.489	1496.160
US 67_BWD_GR4_Brown	219.709	125.641	105.146	2676.475	1702.489	1496.160
US 183_BWD_GR4_Eastland	249.449	125.035	116.680	2738.360	1693.279	1518.136
US 377_BWD_GR4_Brown	219.709	125.641	105.146	2676.475	1702.489	1496.160
US 90_SAT_GR4_Bexar	147.835	90.971	83.988	2646.301	2214.888	1922.761
FM 1518_GR3_Bexar	266.692	238.899	233.901	2664.419	1728.358	1552.914
SH 16_SAT_GR4_Atascosa_TRM 626	462.408	434.028	424.305	3144.438	1972.419	1940.779
SH 16_SAT_GR 4_Atascosa_TRM 642	581.650	326.500		2589.625	1569.775	
SH 36_YKM_GR 3_Austin	156.480	88.002	79.740	2648.315	1815.372	1749.992
US 59_LFK_GR3_Angelina	558.637	446.350		2957.900	2113.900	
US 69_LFK_GR4_Angelina	283.537	236.412		1974.913	1347.463	
US 287_LFK_GR4_Trinity	283.537	236.412		1974.913	1347.463	
FM 2213_LFK_GR5_San Augustine	283.537	236.412		1974.913	1347.463	
US 59_LFK_GR4_Shelby	266.692	238.899	233.901	2664.419	1728.358	1552.914
LP 338_ODA_GR4_Ector	427.542	309.266	293.333	2768.035	1999.971	1932.344
US 385_ODA_GR4_Crane	172.532	100.092	90.883	2665.842	1654.067	1408.696
US 385_ODA_GR4_Ector	172.532	100.092	90.883	2665.842	1654.067	1408.696
SH 82_BMT_GR4_Jefferson	283.537	236.412		1974.913	1347.463	
FM 365_BMT_GR4_Jefferson	283.537	236.412		1974.913	1347.463	
FM 105_BMT_GR4_Orange	283.537	236.412		1974.913	1347.463	
US 80_ATL-GR4_Harrison	283.537	236.412		1974.913	1347.463	
US 59_ATL_GR3_Cass_RG_TRM238	191.247	165.049	159.389	2691.062	2288.818	2230.886
SH 77_ATL_GR4_Cass_TRM 745_SS	244.489	156.482	152.577	2579.935	1931.762	1787.538
SH 77_ATL_GR4_Cass_TRM 720_RG	166.072	132.860	120.722	2905.053	2391.690	2358.177

Table B-3 Traffic Data

State	Section ID	Design Lane factor for AADT	Design Lane factor for Truck	Average AADT	Avg % Truck Traffic
Pharr	US 77_PHR_GR3_Cameron	0.8	0.9	8500	22
	US 281_PHR_GR3_Hidalgo	0.8	0.9	8482	29
	US 281_PHR_GR3_Brooke_TRM 752	0.8	0.9	6000	34
	US 281_PHR_GR3_Brooke_TRM 722	0.8	0.9	7336	32
Dallas-FW	US 377_FTW_GR3_Hood	0.8	0.9	10923	9.2
	US 377_FTW_GR3_Tarrant	0.8	0.9	13055	7.5
	SH 199_FTW_GR3_Parker	0.5	0.5	5822	18.2
Brownwood	US 67_BWD_GR4_Coleman	0.4	0.45	5665	13.5
	US 67_BWD_GR4_Brown	0.4	0.45	5846	13.5
	US 183_BWD_GR4_Eastland	0.5	0.5	2395	15.8
	US 377_BWD_GR4_Brown	0.4	0.45	13186	7.8
San Antonio	US 90_SAT_GR4_Bexar	0.7	0.9	24357	3.6
	FM 1518_GR3_Bexar	0.5	0.5	2854	19.7
	SH 16_SAT_GR4_Atascosa_TRM 626	0.8	0.9	4532	13.8
	SH 16_SAT_GR 4_Atascosa_TRM 642	0.5	0.5	9000	21.3
YKM	SH 36_YKM_GR 3_Austin	0.5	0.5	5500	18
Lufkin	US 59_LFK_GR3_Angelina	0.7	0.8	11760	28.2
	US 69_LFK_GR4_Angelina	0.4	0.45	12888	13.3
	US 287_LFK_GR4_Trinity	0.5	0.5	1746	28.1
	FM 2213_LFK_GR5_San Augustine	0.5	0.5	500	13.5
	US 59_LFK_GR4_Shelby	0.4	0.45	10250	34.2
Odessa	LP 338_ODA_GR4_Ector	0.5	0.5	4171	27
	US 385_ODA_GR4_Crane	0.8	0.9	2484	15.5
	US 385_ODA_GR4_Ector	0.8	0.9	3929	12
Beaumont	SH 82_BMT_GR4_Jefferson	0.5	0.5	1877	11
	FM 365_BMT_GR4_Jefferson	0.5	0.5	3820	7
	FM 105_BMT_GR4_Orange	0.8	0.45	13264	5.6
Atlanta	US 80_ATL-GR4_Harrison	0.5	0.5	3464	7.7
	US 59_ATL_GR3_Cass_RG_TRM238	0.8	0.9	8826	21
	SH 77_ATL_GR4_Cass_TRM 745_SS	0.5	0.5	2935	12
	SH 77_ATL_GR4_Cass_TRM 720_RG	0.8	0.9	1193	19

B-4 CTMeter Data

Table B-4-1 Beaumont and Odessa CTMeter Data

CTM, (mm)	Beaumont			Odessa			
	FM-105	FM-365	SH-82 Seal Coat	LP_338_ Seal Coat	US_385_C MHBF	US_385_Sea lCoat_Ector	US_385_Seal Coat_Crane
WP1	2.38	2.62	1.18	0.81	0.89	0.72	1.55
WP2	2.42	2.54	1.20	0.94	0.78	0.96	1.53
WP3	-	2.61	-	0.96	0.74	0.83	-
WP4	-	2.42	-	-	-	-	-
BWP1	2.46	3.12	2.28	1.72	-	1.51	2.14
BWP2	2.42	-	2.1	-	-	-	2.26
BWP3	-	3	-	-	-	-	-
BWP4	-	-	-	1.96	-	1.56	-
Shoulder1	-	-	-	-	0.77	-	2.97
Shoulder2	-	-	-	-	-	-	-
Shoulder3	-	-	-	-	-	-	-
Shoulder4	-	-	-	-	0.85	-	-

Table B-4-2 Atlanta CTMeter Data

CTM, (mm)	Atlanta			
	SH-77-Atlanta	SH-77-Cass-Gravel	US-59-Cass	US-80-Harrison
WP1	1.31	2.57	1.8	2.03
WP2	1.33	2.44	2.03	1.9
WP3	1.53	-	1.9	1.9
WP4	1.26	-	-	-
BWP1	-	2.79	-	-
BWP2	-	2.81	-	-
BWP3	-	-	-	-
BWP4	-	-	-	-
Shoulder1	3.26	-	3.13	2.49
Shoulder2	-	-	-	-
Shoulder3	2.39	-	3.38	2.61
Shoulder4	-	-	-	-

Table B-4-3 Pharr CTMeter Data

CTM, (mm)	Pharr			
	US-77-Camer	US-281-Haidalgo-SealCoat	US-281-Brook-742	US-281-718
WP1	1.9	0.62	0.81	0.45
WP2	2.27	1.57	0.8	0.51
WP3	2	0.7	0.8	0.48
WP4	1.79	-	-	-
BWP1	2.42	2.33	1.84	-
BWP2	-	-	-	-
BWP3	2.27	2.37	1.61	1.27
BWP4	-	-	-	-
Shoulder1	-	-	-	-
Shoulder2	-	-	-	-
Shoulder3	-	-	-	-
Shoulder4	-	-	-	-

Table B-4-4 San Antonio CTMeter Data

CTM, (mm)	San Antonio				
	FM-1518	US-90-Seal Coat	SH-16-McMullen	SH-16-ATS-TRM642	SH-16-ATS-TRM626
WP1	2.31	2.48	1.42	1.05	1.29
WP2	2.04	2.25	1.35	1.22	1.73
WP3	-	-	-	-	-
WP4	-	-	-	-	-
BWP1	2.81	3	-	2.49	2.72
BWP2	-	2.37	-	2.14	2.82
BWP3	-	-	-	-	-
BWP4	-	-	-	-	-
Shoulder1	-	-	2.93	-	-
Shoulder2	-	-	2.98	-	-
Shoulder3	-	-	-	-	-
Shoulder4	-	-	-	-	-

Table B-4-5 YKM and Brownwood CTMeter Data

CTM, (mm)	YKM	Brownwood			
	SH-36-SealCoat	US67-Brown	US67-Coleman	US183-Eastland	US377-Brown
WP1	1.37	1.15	0.82	1.45	1.89
WP2	1.24	1.01	0.71	1.48	1.96
WP3	-	-	-	-	-
WP4	-	-	-	-	-
BWP1	-	1.96	-	1.71	-
BWP2	-	1.9	-	1.68	-
BWP3	-	-	-	-	-
BWP4	-	-	-	-	-
Shoulder1	3.48	2.38	2.05	-	2.68
Shoulder2	-	-	-	-	-
Shoulder3	-	-	-	-	-
Shoulder4	-	-	-	-	-

Table B-4-6 Dallas-FW CTMeter Data

CTM, (mm)	Dallas-FW		
	SH 199-Parker	US 377-Hood	US 377-Tarrant
WP1	2.65	-	2.23
WP2	2.14	2.49	0.48
WP3	-	-	2.38
WP4	-	-	-
BWP1	2.92	-	-
BWP2	2.69	-	-
BWP3	-	-	-
BWP4	-	-	-
Shoulder1	-	2.9	3.21
Shoulder2	-	3	3.41
Shoulder3	-	-	-
Shoulder4	-	-	-

Table B-4-7 Lufkin CTMeter Data

CTM, (mm)	Lufkin				
	Lufkin-FM2213	US 59-Shelby	US-59-LFK-ANG	US-69-LFK-ANG	Grovton-287
WP1	1.53	1.62	1.97	1.15	2.78
WP2	1.65	1.42	2	1.12	2.82
WP3	-	1.43	1.96	1.64	2.86
WP4	-	-	1.93	1.74	-
BWP1	1.93	2.24	-	-	3.09
BWP2	2.02	2.20	-	-	-
BWP3	-	-	-	-	3.26
BWP4	-	-	-	-	-
Shoulder1	-	-	2.83	2.88	-
Shoulder2	-	-	-	-	-
Shoulder3	-	-	2.53	3.33	-
Shoulder4	-	-	-	-	-

B-5 DFT Data

Table B-5-1 Beaumont and Odessa DFT Data

DFT at 20 km/hr	Beaumont			Odessa			
	FM-105	FM-365	SH-82 Seal Coat	LP_338_Seal Coat	US_385_CMHBF	US_385_SealCoat_Ector	US_385_Seal Coat_Crane
WP1	0.93	0.88	0.98	0.44	0.54	0.2	0.35
WP2	0.84	-	0.98	0.50	0.54	0.26	0.35
WP3	-	0.83	-	0.50	0.54	0.25	-
WP4	-	0.87	-	-	-	-	-
BWP1	0.91	0.42	0.90	0.55	-	0.35	0.45
BWP2	0.84	-	0.93	-	-	-	0.43
BWP3	-	0.80	-	-	-	-	-
BWP4	-	-	-	0.56	-	0.34	-
Shoulder1	-	-	-	-	0.69	-	0.64
Shoulder2	-	-	-	-	-	-	-
Shoulder3	-	-	-	-	-	-	-
Shoulder4	-	-	-	-	0.69	-	-

Table B-5-2 Atlanta DFT Data

DFT at 20 km/hr	Atlanta			
	SH-77-Atlanta	SH-77-Cass-Gravel	US-59-Cass	US-80-Harrison
WP1	0.72	0.63	0.56	0.98
WP2	0.71	0.61	0.60	0.965
WP3	-	-	0.57	0.99
WP4	0.78	-	-	-
BWP1	-	0.69	-	-
BWP2	-	0.64	-	-
BWP3	-	-	-	-
BWP4	-	-	-	-
Shoulder1	0.96	-	0.79	0.97
Shoulder2	-	-	-	-
Shoulder3	0.84	-	0.73	0.98
Shoulder4	-	-	-	-

Table B-5-3 Pharr DFT Data

DFT at 20 km/hr	Pharr			
	US-77-Camer	US-281-Haidalgo-SealCoat	US-281-Brook-742	US-281-718
WP1	0.31	0.28	0.24	0.25
WP2	0.28	0.30	0.27	0.28
WP3	0.29	0.33	0.25	0.26
WP4	0.30	-	-	-
BWP1	0.31	0.58	0.27	0.55
BWP2	-	-	-	-
BWP3	0.36	0.58	0.26	0.51
BWP4	-	-	-	-
Shoulder1	-	-	-	-
Shoulder2	-	-	-	-
Shoulder3	-	-	-	-
Shoulder4	-	-	-	-

Table B-5-4 San Antonio DFT Data

DFT at 20 km/hr	San Antonio				
	FM-1518	US-90-Seal Coat	SH-16-McMullen	SH-16-ATS-TRM642	SH-16-ATS-TRM626
WP1	0.69	0.39	0.47	0.56	0.53
WP2	0.66	0.34	0.49	0.57	0.53
WP3	-	-	-	-	-
WP4	-	-	-	-	-
BWP1	0.75	0.41	-	0.69	0.65
BWP2	-	0.43	-	0.71	0.61
BWP3	-	-	-	-	-
BWP4	-	-	-	-	-
Shoulder1	-	-	0.67	-	-
Shoulder2	-	-	0.63	-	-
Shoulder3	-	-	-	-	-
Shoulder4	-	-	-	-	-

Table B-5-5 YKM and Brownwood DFT Data

DFT at 20 km/hr	YKM	Brownwood			
	SH-36-SealCoat	US67-Brown	US67-Coleman	US183-Eastland	US377-Brown
WP1	0.44	0.19	0.23	0.32	0.22
WP2	0.41	0.18	0.19	0.22	0.26
WP3	-	-	-	-	-
WP4	-	-	-	-	-
BWP1	-	0.24	-	0.31	-
BWP2	-	-	-	0.32	-
BWP3	-	-	-	-	-
BWP4	-	-	-	-	-
Shoulder1	0.74	0.41	0.31	-	-
Shoulder2	-	-	-	-	-
Shoulder3	-	-	-	-	-
Shoulder4	-	-	-	-	-

Table B-5-6 Dallas-FW DFT Data

DFT at 20 km/hr	Dallas-FW		
	SH 199-Parker	US 377-Hood	US 377-Tarrant
WP1	0.27	0.25	0.22
WP2	0.25	0.24	0.16
WP3	-	-	0.24
WP4	-	-	-
BWP1	0.39	-	-
BWP2	0.30	-	-
BWP3	-	-	-
BWP4	-	-	-
Shoulder1	-	0.59	-
Shoulder2	-	-	0.51
Shoulder3	-	-	-
Shoulder4	-	-	-

Table B-5-7 Lufkin DFT Data

DFT at 20 km/hr	Lufkin				
	Lufkin-FM2213	US 59-Shelby	US-59-LFK-ANG	US-69-LFK-ANG	Grovton-287
WP1	-	0.59	-	0.86	0.72
WP2	0.86	0.58	0.31	0.87	-
WP3	-	0.55	0.31	0.88	0.41
WP4	-	-	0.31	0.89	-
BWP1	-	0.65	-	-	0.71
BWP2	0.81	0.66	-	-	-
BWP3	-	-	-	-	0.79
BWP4	-	-	-	-	-
Shoulder1	-	-	0.45	0.83	-
Shoulder2	-	-	-	0	-
Shoulder3	-	-	0.56	0.83	-
Shoulder4	-	-	-	-	-